

GeoPlanet: Earth and Planetary Sciences

Tymon Zielinski
Ksenia Pazdro
Agata Dragan-Górska
Agata Weydmann *Editors*

Insights on Environmental Changes

Where the World is Heading

 Springer

GeoPlanet: Earth and Planetary Sciences

Editor-in-chief

Paweł Rowiński

Series editors

Marek Banaszkiewicz

Janusz Pempkowiak

Marek Lewandowski

Marek Sarna

For further volumes:

<http://www.springer.com/series/8821>

Tymon Zielinski · Ksenia Pazdro
Agata Dragan-Górska · Agata Weydmann
Editors

Insights on Environmental Changes

Where the World is Heading

 Springer

Editors

Tymon Zielinski
Air-Sea Interactions
Institute of Oceanology, Polish Academy
of Sciences
Sopot
Poland

Agata Dragan-Górska
Physics
Institute of Oceanology, Polish Academy
of Sciences
Sopot
Poland

Ksenia Pazdro
Chemistry
Institute of Oceanology, Polish Academy
of Sciences
Sopot
Poland

Agata Weydmann
Ecology
Institute of Oceanology, Polish Academy
of Sciences
Sopot
Poland

The GeoPlanet: Earth and Planetary Sciences Book Series is in part a continuation of Monographic Volumes of Publications of the Institute of Geophysics, Polish Academy of Sciences, the journal published since 1962 (<http://pub.igf.edu.pl/index.php>).

ISSN 2190-5193

ISSN 2190-5207 (electronic)

ISBN 978-3-319-03682-3

ISBN 978-3-319-03683-0 (eBook)

DOI 10.1007/978-3-319-03683-0

Springer Cham Heidelberg New York Dordrecht London

Library of Congress Control Number: 2013958390

© Springer International Publishing Switzerland 2014

This work is subject to copyright. All rights are reserved by the Publisher, whether the whole or part of the material is concerned, specifically the rights of translation, reprinting, reuse of illustrations, recitation, broadcasting, reproduction on microfilms or in any other physical way, and transmission or information storage and retrieval, electronic adaptation, computer software, or by similar or dissimilar methodology now known or hereafter developed. Exempted from this legal reservation are brief excerpts in connection with reviews or scholarly analysis or material supplied specifically for the purpose of being entered and executed on a computer system, for exclusive use by the purchaser of the work. Duplication of this publication or parts thereof is permitted only under the provisions of the Copyright Law of the Publisher's location, in its current version, and permission for use must always be obtained from Springer. Permissions for use may be obtained through RightsLink at the Copyright Clearance Center. Violations are liable to prosecution under the respective Copyright Law.

The use of general descriptive names, registered names, trademarks, service marks, etc. in this publication does not imply, even in the absence of a specific statement, that such names are exempt from the relevant protective laws and regulations and therefore free for general use.

While the advice and information in this book are believed to be true and accurate at the date of publication, neither the authors nor the editors nor the publisher can accept any legal responsibility for any errors or omissions that may be made. The publisher makes no warranty, express or implied, with respect to the material contained herein.

Printed on acid-free paper

Springer is part of Springer Science+Business Media (www.springer.com)

Series Editors

- Geophysics: Paweł Rowiński
Editor-in-Chief
Institute of Geophysics
Polish Academy of Sciences
ul. Ks. Janusza 64
01-452 Warszawa, Poland
p.rowinski@igf.edu.pl
- Space Sciences: Marek Banaszekiewicz
Space Research Centre
Polish Academy of Sciences
ul. Bartycka 18A
00-716 Warszawa, Poland
- Oceanology: Janusz Pempkowiak
Institute of Oceanology
Polish Academy of Sciences
Powstańców Warszawy 55
81-712 Sopot, Poland
- Geology: Marek Lewandowski
Institute of Geological Sciences
Polish Academy of Sciences
ul. Twarda 51/55
00-818 Warszawa, Poland
- Astronomy: Marek Sarna
Nicolaus Copernicus Astronomical Centre
Polish Academy of Sciences
ul. Bartycka 18
00-716 Warszawa, Poland
sarna@camk.edu.pl

Managing Editor

Anna Dziembowska

Institute of Geophysics, Polish Academy of Sciences

Advisory Board

Robert Anczkiewicz

Research Centre in Kraków
Institute of Geological Sciences
Kraków, Poland

Aleksander Brzeziński

Space Research Centre
Polish Academy of Sciences
Warszawa, Poland

Javier Cuadros

Department of Mineralogy
Natural History Museum
London, UK

Jerzy Dera

Institute of Oceanology
Polish Academy of Sciences
Sopot, Poland

Evgeni Fedorovich

School of Meteorology
University of Oklahoma
Norman, USA

Wolfgang Franke

Geologisch-Paläntologisches Institut
Johann Wolfgang Goethe-Universität
Frankfurt/Main, Germany

Bertrand Fritz

Ecole et Observatoire des
Sciences de la Terre
Laboratoire d'Hydrologie et de
Géochimie de Strasbourg
Université de Strasbourg et CNRS
Strasbourg, France

Truls Johannessen

Geophysical Institute
University of Bergen
Bergen, Norway

Michael A. Kaminski

Department of Earth Sciences
University College London
London, UK

Andrzej Kijko

Aon Benfield
Natural Hazards Research Centre
University of Pretoria
Pretoria, South Africa

Francois Leblanc

Laboratoire Atmospheres, Milieux
Observations Spatiales, CNRS/IPSL
Paris, France

Kon-Kee Liu

Institute of Hydrological and Oceanic
Sciences
National Central University Jhongli
Jhongli, Taiwan

Teresa Madeyska

Research Centre in Warsaw
Institute of Geological Sciences
Warszawa, Poland

Stanisław Massel

Institute of Oceanology
Polish Academy of Sciences
Sopot, Polska

Antonio Meloni

Instituto Nazionale di Geofisica
Rome, Italy

Evangelos Papathanassiou

Hellenic Centre for Marine Research
Anavissos, Greece

Kaja Pietsch

AGH University of Science
and Technology
Kraków, Poland

Dušan Plašienka

Prírodovedecká fakulta, UK
Univerzita Komenského
Bratislava, Slovakia

Barbara Popielawska

Space Research Centre
Polish Academy of Sciences
Warszawa, Poland

Tilman Spohn

Deutsches Zentrum für Luftund
Raumfahrt in der Helmholtz
Gemeinschaft
Institut für Planetenforschung
Berlin, Germany

Krzysztof Stasiewicz

Swedish Institute of Space Physics
Uppsala, Sweden

Roman Teisseyre

Earth's Interior Dynamics Lab
Institute of Geophysics
Polish Academy of Sciences
Warszawa, Poland

Jacek Tronczynski

Laboratory of Biogeochemistry
of Organic Contaminants
IFREMER DCN_BE
Nantes, France

Steve Wallis

School of the Built Environment
Heriot-Watt University
Riccarton, Edinburgh
Scotland, UK

Wacław M. Zuberek

Department of Applied Geology
University of Silesia
Sosnowiec, Poland

Contents

The Influence of Matrix Effects on Trace Analysis of Pharmaceutical Residues in Aqueous Environmental Samples	1
Marta Borecka, Anna Białk-Bielińska, Grzegorz Siedlewicz, Piotr Stepnowski and Ksenia Pazdro	
Valles Marineris: A Place Full of Answers	17
O. Kromuszczyńska, M. Makowska and K. Dębniak	
Determination of Tetracyclines Residues in the Gulf of Gdańsk (Southern Baltic Sea) Sediments Using a Tandem Solid-Phase Extraction with Liquid Chromatography Coupled with Tandem Mass Spectrometry	33
Grzegorz Siedlewicz, Ksenia Pazdro, Marta Borecka, Kinga Kornowska, Anna Białk-Bielińska and Piotr Stepnowski	
A Modern Approach to Aerosol Studies Over the Baltic Sea	49
A. Strzalkowska, P. Makuch, O. Zawadzka and P. Pakszys	
Water in the Deepest Crater of Mars	65
Natalia Zalewska	
Application of an Object Classification Method for Determining the Spatial Distribution of Sea Bottom Structures and Their Cover Using Images from a Side Scan Sonar	77
Paulina Pakszys	
The Role of Extreme Events in the Development of the Coastline in the Darlowko Area	95
Małgorzata Merchel	
Attenuation of Groundwater Flow Due to Irregular Waves in Permeable Sea Bottom	109
Anna Przyborska	

Ocean Acidification: Environmental Issue and Its Impact on Marine Life	127
Agnieszka Cichowska and Alicja Kosakowska	
Allelopathic Influence of Cyanobacteria <i>Microcystis aeruginosa</i> on Green Algae <i>Chlorella vulgaris</i>	141
Adam Źak and Alicja Kosakowska	

The Influence of Matrix Effects on Trace Analysis of Pharmaceutical Residues in Aqueous Environmental Samples

Marta Borecka, Anna Białk-Bielińska, Grzegorz Siedlewicz,
Piotr Stepnowski and Ksenia Pazdro

Abstract Pharmaceuticals are a class of emerging environmental contaminants. They are manufactured to be biologically active and to be persistent against biodegradation. This makes them more risky for the environment, as they can have negative impact on living organisms. However, still there are many problems in reliable analysis of these compounds due to low amounts and complexity of the environmental samples. The technique widely used for this purpose is liquid chromatography coupled with tandem mass spectrometry. One of the main drawbacks of this technique is the change in ionization efficiency—phenomenon known as the matrix effect. Matrix effects heavily influence both qualitative and quantitative analyses. Therefore, it also has impact on the quality of the obtained results. Thus the main aim of the present study was to investigate the influence of six different aqueous environmental matrices on the solid-phase extraction efficiency and the final determination of twelve selected sulfonamides by LC-MS/MS technique. The obtained results showed that both were strongly affected by the matrix composition. The more complicated the matrix was, the greater influence was observed (matrix effects in tap water were in the range from 8.77 to -16.49% and in wastewater influents from -63.67 to -97.43%). Extraction efficiency of selected drugs decreased from 94.9 to 41.5 % for tap water samples to from 31.6 to 0 % for wastewater influents. Thus, it is of high significance to use an approach to correct effects caused by matrix components. The proper calculation of the real concentrations of pharmaceuticals in the environment is required for determining the consequent risk to living organisms.

M. Borecka (✉) · A. Białk-Bielińska · P. Stepnowski
Department of Environmental Analysis, Faculty of Chemistry, University of Gdańsk,
ul. Wita Stwosza 63, 80-952 Gdańsk, Poland
e-mail: mborecka@chem.univ.gda.pl

G. Siedlewicz · K. Pazdro
Institute of Oceanology, Polish Academy of Sciences, ul. Powstańców Warszawy 55,
81-712 Sopot, Poland

Keywords Antibiotic residues • Aqueous environmental samples • LC-MS/MS
Matrix effects • Extraction efficiency

1 Introduction

Interest in the presence of pharmaceutical residues in the environment has increased significantly over the last decade. These compounds comprise one of the few groups of chemicals specifically designed to act on living cells, which presents a special risk when these contaminants enter, persist and disseminate in the environment. Pharmaceuticals have been detected throughout the world, especially in wastewater, surface water, groundwater, marine water and also drinking water. The concentrations of these compounds in the water are low—in the range from ng L^{-1} to $\mu\text{g L}^{-1}$ (Daughton and Ternes 1999; Halling-Sørensen et al. 1998). There exists very well documented evidence that some drugs may affect microorganisms and wild life in severe and unexpected ways. Aquatic organisms are particularly important targets, as they are exposed over their whole life time (Carlsson et al. 2006; Santos et al. 2010).

Since pharmaceutical residues have been widely recognized as new emerging pollutants and simultaneously occur in extremely low concentrations, there has been increasing interest in the development of more selective and sensitive methods for their monitoring in the environment (Buchberger 2011; Kostopoulou and Nikolaou 2008; Kot-Wasik et al. 2007). The number of papers on analysis of drugs in water is significant, but still there are many problems related to the improvements in analytical procedures. These problems could cause inaccurate quantification when analyzing real samples.

Liquid chromatography coupled with tandem mass spectrometry, due to its high sensitivity and selectivity, is one of the most popular and appropriate techniques for trace analysis of pharmaceutical residues (Antignac et al. 2005). However, in the case of very complex matrices (like environmental samples), this technique is highly susceptible to the influence of co-extracted components. This has been widely reported in literature (Renew and Huang 2004; Klopfer et al. 2005; Hao et al. 2007; Lacey et al. 2008; Madureira et al. 2009; Marín et al. 2009). Unfortunately, little is known about the influence of sample matrix complexity on results through the determination of matrix effects and also extraction efficiency.

It should be noticed that matrix effects are unseen in the chromatogram but they have vast impact on methods accuracy and sensitivity because coeluting substances can affect analyte ionization process leading to a signal increase (enhancement) or signal decrease (suppression) (Taylor 2005). This phenomenon was first described by Tang and Kebarle (1993). The authors examined how the signal of the analyte ion recorded with the mass spectrometer depended on the concentration of the analyte ion in the solution and also how this signal was susceptible to the presence of ions of other compounds in the studied solution. They showed that as

the concentrations of other compounds increased the electrospray responses of the analytes decreased. Many authors have studied this phenomenon, but its exact mechanism is still unknown (King et al. 2000; Truffelli et al. 2010). There are different mechanisms proposed in literature to explain the suppression or the enhancement of the signal, e.g., it probably originates from the competition between an analyte and the coeluting, undetected matrix components (Taylor 2005).

Matrix effects are caused by compounds which can be subdivided into two groups: endogenous components (naturally occurring in environmental samples and still present after sample pre-treatment or extraction) and exogenous components (introduced during sample collection or during the pre-treatment/extraction processes or reagents added to the mobile phase to improve chromatographic resolution) (Hall et al. 2012). Different substances can be able to induce matrix effects. Potential ion suppressors are ionic species (inorganic electrolytes, salts), polar compounds (phenols, arylsulfonates) and organic molecules (like carbohydrates, amines, urea, lipids and peptides) (Gosetti et al. 2010; Hall et al. 2012). This applies especially to those compounds or metabolites which chemical structure is similar to the target analyte, as well as to the compounds which are present in analyzed samples extracts at high concentrations (Marín et al. 2009; Gosetti et al. 2010). The physicochemical properties of the analytes can also influence the degree of enhancement or suppression of their ionization. Bonfiglio et al. (1999) reported that highly polar compounds generally appeared to be affected to a greater ion suppression than less polar molecules.

Environmental matrices represent high sample composition variability and it is difficult to find samples that have the same composition, even if the samples belong to the same type of matrices (Marín et al. 2009). Therefore, the main aim of the present study was to investigate the influence of different aqueous environmental matrices on the solid-phase extraction efficiency and final determination of twelve selected pharmaceuticals (described in Table 1) using LC-MS/MS technique. The estimation of extraction efficiency and matrix effects leads to better measurement reliability and renders data from inter-laboratory studies comparable. A detailed study was carried out on six different water samples (tap, lake, river and sea water, effluent and influent wastewater).

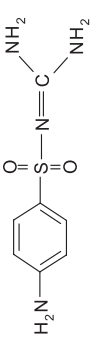
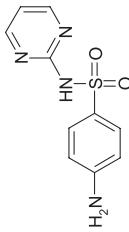
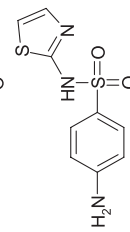
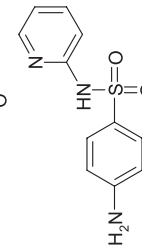
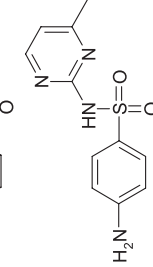
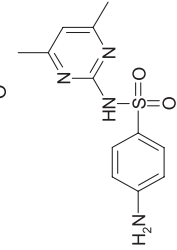
2 Materials and Methods

2.1 Chemicals

Sulfamethazine and sulfapyridine were purchased from Serva (Weissensberg, Germany). All other standards (Table 1) were obtained from Sigma–Aldrich (Steinheim, Germany).

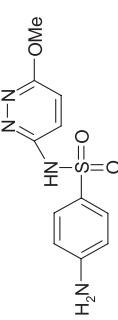
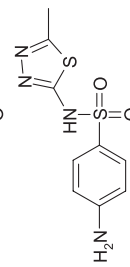
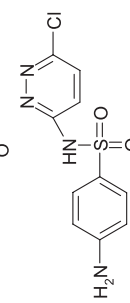
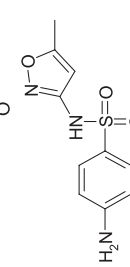
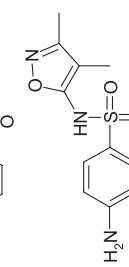
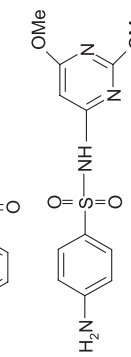
Methanol (MeOH) and acetonitrile (ACN) of HPLC grade were obtained from POCH S.A. (Gliwice, Poland). Acetonitrile (LC–MS Chromasolv®) was purchased from Sigma–Aldrich (Steinheim, Germany). Deionized water was

Table 1 Characteristic of studied pharmaceuticals

Name	CAS number	Chemical structure	Molecular weight (g mol ⁻¹)	pK _a
Sulfaguanidine	68-67-0		214.2	11.3
Sulfadiazine	68-35-9		250.3	6.5
Sulfathiazole	72-14-0		255.3	7.1
Sulfapyridine	144-83-2		249.2	8.4
Sulfamerazine	127-79-7		264.3	8.0
Sulfamethazine	57-68-1		278.3	7.4

(continued)

Table 1 continued

Name	CAS number	Chemical structure	Molecular weight (g mol ⁻¹)	pK _a
Sulfamethoxypyridazine	80-35-3		280.3	7.2
Sulfamethiazole	144-82-1		270.3	5.5
Sulfachloropyridazine	80-32-0		284.7	5.5
Sulfamethoxazole	723-46-6		253.3	5.7
Sulfisoxazole	127-69-5		267.3	5.0
Sulfadimethoxine	122-11-2		310.3	5.9

produced by the HYDROLAB System (Gdańsk, Poland). Ammonium acetate (NH_4Ac) and acetic acid (AcH) both of analytical reagent grade were purchased from Chempur (Piekary Śląskie, Poland).

Standard stock solutions of each compound were prepared by dissolving 50 mg in 100 mL of methanol obtaining a final concentration of $500 \mu\text{g mL}^{-1}$. All standards were stored in the dark at -18°C . The stock solutions were mixed and diluted with methanol to prepare working solution ($20 \mu\text{g mL}^{-1}$). To prepare calibration curves, working solution was diluted with mobile phase A to a proper concentration.

2.2 Sample Collection and Storage

The experiments were conducted with the use of tap, lake, river and sea water, as well as effluent and influent wastewater. Drinking water was collected from the tap of a private home in Gdańsk. Lake water was collected from the lake Fiszewo ($54^\circ 6' \text{ N}$, $17^\circ 42' \text{ E}$). River water was taken from river Wda ($54^\circ 04' \text{ N}$, $17^\circ 40' \text{ E}$). Sea water was collected from the Gulf of Gdańsk (Baltic Sea) close to the mouth of the Vistula ($54^\circ 22' \text{ N}$, $18^\circ 57' \text{ E}$). Wastewater samples were obtained from a wastewater treatment plant located in Gdańsk ("Gdańsk-Wschód" Saur Neptun Gdańsk).

Samples were collected in glass bottles pre-rinsed with ultrapure water. Immediately after collection the samples were filtered through $0.45 \mu\text{m}$ glass fiber filters (Macherey—Nagel) and then stored at 4°C in the dark until analysis.

2.3 Solid Phase Extraction Procedure

The solid phase extractions were performed with the use of Strata-X Polymeric Reversed Phase cartridges (3 mL/200 mg, Phenomenex Inc.). The cartridge was sequentially preconditioned with 3 mL MeOH, 6 mL ACN:MeOH (50:50, v/v), 6 mL H_2O :MeOH (95:5, v/v) and 10 mL deionized water. Each of 500 mL sample was transferred through the cartridge at the rate of 5 mL min^{-1} . After sample loading, the cartridge was rinsed with 3 mL H_2O :ACN (95:5, v/v) and then dried under the vacuum for 10 min. Sulfonamides were eluted with 6 mL MeOH:ACN (50:50, v/v). The obtained extracts were evaporated to dryness under a stream of nitrogen and reconstituted in 1 mL mobile phase A and analyzed by LC-MS/MS.

2.4 LC-ESI-Tandem MS Analysis

Chromatographic separation of analytes was performed using an Agilent 1,200 Series LC system (Agilent Technologies Inc., Santa Clara, USA) equipped with

Gemini C₁₈ column (150 × 4.6 mm, 5 μm pore size) (Phenomenex Inc., Torrance, CA). Mobile phase A consisted of H₂O:ACN (90:10, v/v, 1 mM NH₄Ac/AcH, pH 3.5) and mobile phase B was 100 % ACN. The flow rate was 0.3 mL min⁻¹. The gradient programme started with 0 % of mobile phase B, which was increased to 64 % within 32 min. The injection volume was 50 μL and the analytical wavelength was 270 nm. The LC flow was directly introduced into the mass spectrometer. The mass spectrometric measurements were carried out on an HCT Ultra ion trap mass spectrometer (Bruker Daltonics, Bremen, Germany) equipped with an electrospray ionization source (ESI). For data acquisition EsquireControl software was used. The source temperature was 300 °C. Nitrogen was employed as the nebulizer gas (30 psi) and the dry gas (10 L min⁻¹). Helium (99.999 %) was used as the collision gas in the ion trap. Analyses were performed in the positive mode. Ions were acquired in multiple reaction monitoring mode. The optimized MS/MS conditions for the compounds are shown in Table 2.

2.5 Quantitative Determination of Matrix Effects and Extraction Efficiency

The determination of matrix effects was based on post-extraction addition technique. This technique involves extraction of two sets of samples—one set contains the analyte added to an extracted matrix (post-extraction sample), and the other contains the analyte in the mobile phase. Matrix effects (ME) and extraction efficiency (EE) were calculated by the use of the strategy applied by Caban et al. (2012) with the Eqs. (1)–(2) shown below:

$$ME (\%) = \left(\frac{B - D}{A} - 1 \right) \times 100 \quad (1)$$

$$EE (\%) = \left(\frac{C - D}{B - D} \right) \times 100 \quad (2)$$

where: *A* is the peak area of the analyte(s) recorded for the standard solution, *B* is the peak area of the analyte(s) recorded for the sample spiked with the target compound(s) after extraction, and *C* is the peak area of the analyte(s) recorded for the sample spiked with the target compound(s) before extraction, whereas *D* denotes peak area of the analyte(s) recorded for a non-spiked sample. All samples were spiked at the same concentration of 1 μg mL⁻¹ for each analyte. ME value of 0 % indicate that there is no matrix effect. A negative (–) value indicates matrix suppression and a positive (+) value indicates matrix enhancement.

More information on evaluation of ME and EE of developed analytical methods was presented by Caban et al. (2012).

Table 2 Precursor and product ions used for the MS/MS detection of the pharmaceuticals

Retention time (min)	Compound	Precursor ion with isolation width	Product ions	Fragmentation amplitude (V)
9.4	Sulfaguanidine	215 ± 2.0	156	0.55
			173	0.50
			122	0.55
17.9	Sulfadiazine	251 ± 0.8	156	0.75
			174	0.55
			108	0.75
18.5	Sulfathiazole	256 ± 2.0	156	0.55
			108	0.60
			92	0.65
19.0	Sulfapyridine	250 ± 0.9	156	0.50
			184	0.60
			108	0.55
19.9	Sulfamerazine	265 ± 2.0	190	0.65
			174	0.60
			156	0.55
21.5	Sulfamethazine	279 ± 1.9	204	0.60
			124	0.55
			156	0.55
21.9	Sulfamethoxypyridazine	281 ± 1.9	156	0.45
			126	0.55
			188	0.50
22.0	Sulfamethiazole	271 ± 2.0	156	0.60
			108	0.70
			92	0.60
25.1	Sulfachloropyridazine	285 ± 2.0	156	0.75
			108	0.60
			92	0.75
26.4	Sulfamethoxazole	254 ± 2.0	156	0.65
			188	0.65
			147	0.50
27.3	Sulfisoxazole	268 ± 2.0	156	0.70
			113	0.65
			108	0.65
28.9	Sulfadimethoxine	311 ± 2.0	156	0.60
			245	0.60
			218	0.65

3 Results and Discussion

3.1 Influence of Matrix Components on Final Determination by LC-MS/MS

Matrix effects from the six water samples mentioned above (tap, lake, river and sea water, effluent and influent wastewater) were evaluated for the twelve selected sulfonamides. To estimate the degree of ion suppression or enhancement, Eq. (1) was used. Figure 1 gives an overview of the obtained results.

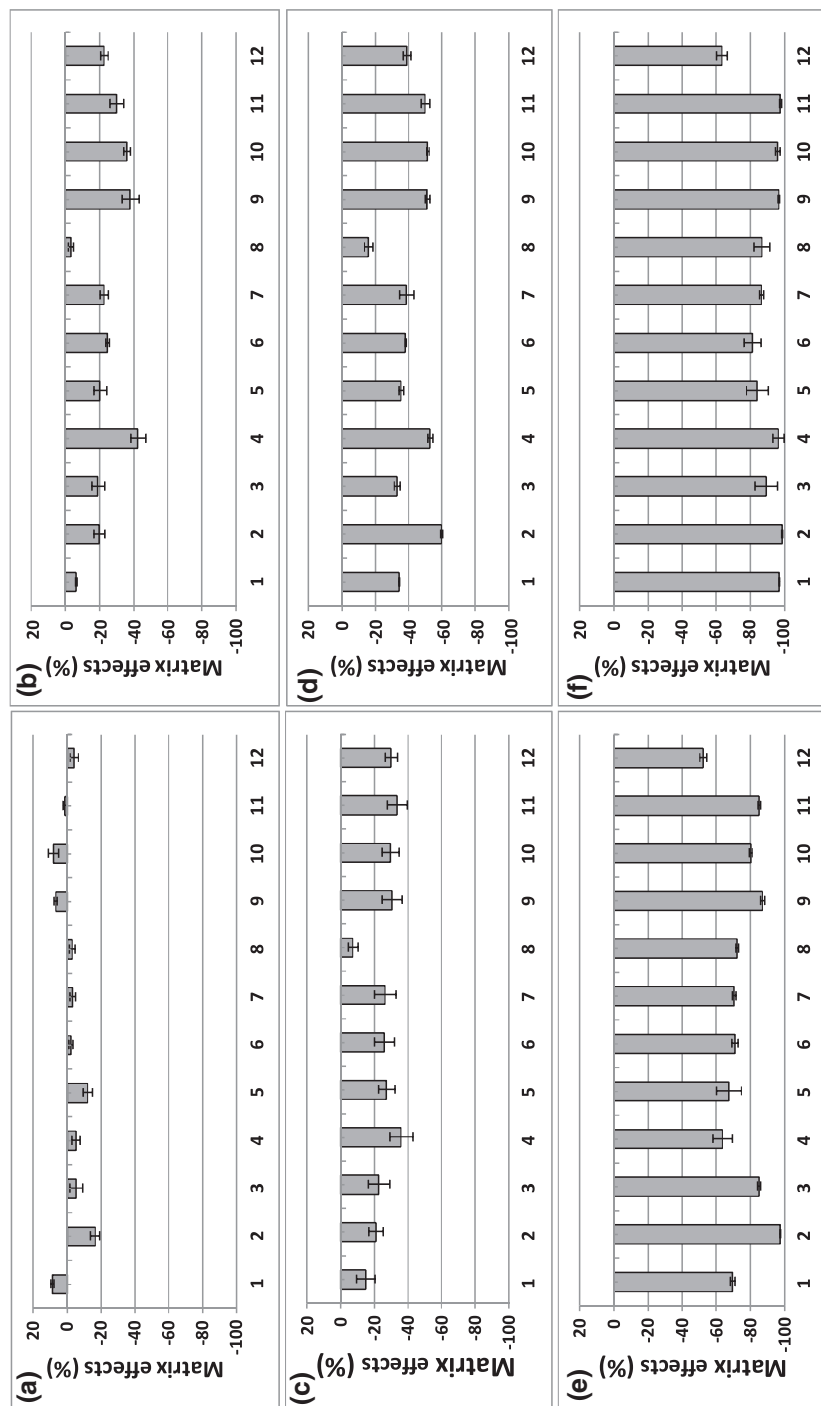


Fig. 1 Matrix effects in: **a** tap water, **b** lake water, **c** river water, **d** sea water, **e** effluent wastewater, **f** influent wastewater (*1* sulfaguandine; *2* sulfadiazine; *3* sulfathiazole; *4* sulfapyridine; *5* sulfamerazine; *6* sulfamethazine; *7* sulfamethoxypyridazine; *8* sulfachloropyridazine; *9* sulfachloropyridazine; *10* sulfamethoxazole; *11* sulfisoxazole; *12* sulfadimethoxine)

For most of the studied samples (analyzed by LC-MS/MS technique), matrix composition caused signal suppression of target analytes. This effect was observed especially in the case of wastewater samples (both in influent and effluent wastewater). Signal enhancement has been observed only in tap water analysis for sulfaguanidine, sulfachloropyridazine, sulfamethoxazole and sulfoxazole. The results are consistent with the literature (Petrović et al. 2005; Vieno et al. 2006; Ye et al. 2007; Kasprzyk-Hordern et al. 2008a, b), according to which in LC-ESI-MS/MS technique the most frequently observed phenomenon is ion suppression. It has been also shown that atmospheric pressure chemical ionization (APCI) is less prone to matrix effects than ESI, for specific compounds. Therefore, the problem of matrix effects can be solved by changing the ionization source (if possible, as there are some limitations—the analytes must be thermally stable and readily ionized by this technique) (Taylor 2005).

The lowest values of ME were determined for analysis of tap water samples (from 8.77 to -16.49%). The results obtained in lake water (signal suppression from -2.96 to -42.42%) and river water (signal suppression from -7.23 to -35.94%) were similar. In surface waters humic substances (humic and fulvic acids) represent the major components of dissolved organic matter and they are responsible for the matrix interferences that generally impair the detection of the target compounds (Madureira et al. 2009). Slightly higher values of ME were measured in the marine water samples (from -15.77 to 59.57%). Seawaters contain important amounts of salts: if the salts remain in the final extract, they may impair ionization process in ESI technique.

As it was expected, the highest signal suppression was observed in influent wastewater and ranges from -81.14 to -98.46% . Slightly lower signal reduction was observed in wastewater effluents (from -63.67 to -97.43%) in comparison with influents. This is not a surprise as analyzed wastewater samples contain very high amounts of organic and also inorganic matter that are recognized as enhancers of ME.

The obtained results demonstrated that the chemical nature of the analytes interferes also on the matrix effect. This statement is in accordance with the published work (Hall et al. 2012). The ion suppression differed between analytes. It may be the result, for example, of their different polarity. As it was mentioned in the introduction, that there is a difference between the ion suppression which depends on the polarity of the analyzed compound (Bonfiglio et al. 1999).

On the base of the obtained results, the following relation can be noted—the more complicated the matrix, the greater the degree of suppression. Other authors had the same observations (Renew and Huang 2004; Lacey et al. 2008; Madureira et al. 2009). Therefore, as the environmental samples have high matrix composition variability, the matrix effects must be evaluated with every sample set analysis in order to avoid erroneous quantifications (Madureira et al. 2009).

However, the comparison of the obtained results with the literature data is very difficult, due to the fact that there are different methods of calculating matrix effects (as there is no consensus on how they should be evaluated)

(Taylor 2005; Marín et al. 2009). In many cases, it is still an overlooked aspect of method validation. This parameter should be evaluated with each set of samples analyzed.

The overall greater signal suppression in the wastewater samples also shows that the wastewater organic matter exerts a strong matrix effect. This phenomenon may be caused by several reasons. Steen et al. (1999) demonstrated that co-extracted organic materials (humic acids) cause signal suppression in ESI-MS detection as they may reduce ionization efficiency of the analytes by taking up some of the limited number of excess charged sites on the surfaces of electrosprayed droplets. Schmitt-Kopplin et al. (1999) showed that antibiotics may sorb to organic matters in the samples. Therefore, the concentrations of freely dissolved antibiotics is lower and thus more difficult to detect.

The range of signal decrease in wastewater samples were highly evident and exceeded the accepted level. The possible strategy to remove or minimize it is the modification of the sample extraction methodology. For this reason, an alternative sample preparation or sample cleanup step is required.

Caban et al. (2012), who developed a procedure for extracting β -blockers and β -antagonists from wastewaters using solid-phase extraction technique, used at washing step hexane to remove the non-selectively non-polar substances present in the samples. The use of hexane was also reported by Jones-Lepp and Stevens (2007). Another approach can be the use of tandem solid-phase extraction procedure. Renew and Huang (2004) developed the SPE method for the determination of fluoroquinolone, sulfonamide and trimethoprim antibiotics in wastewater samples in which an anion-exchange cartridge and a HLB cartridge were used in tandem to reduce organic matter interference. Acidification of samples pH 2.5 prior to extraction yielded predominantly neutral sulfonamides and cationic fluoroquinolones and trimethoprim. As a result, the neutral and cationic antibiotics were not retained in the anion-exchange cartridges while some of the highly negatively-charged natural organic matter were.

3.2 *Extraction Efficiency*

Strata-X cartridges were used due to their selectivity for polar compounds. It is one of the most commonly used type of cartridges for the extraction of pharmaceuticals from environmental samples. Efficiency and robustness on extraction procedure were tested for six different water samples. The values of matrix effects were taken into account in assessing the effectiveness of the extraction of selected drugs as described in Sect. 2.3—Eq. (2).

One of the problems frequently encountered in extracting organic contaminants from environmental samples is matrix interference due to their high complexity. It affects not only detection, as it was fully described in Sect. 3.1., but it could also result in the reduction of extraction efficiency. The results of EE for each matrix are presented in Fig. 2.

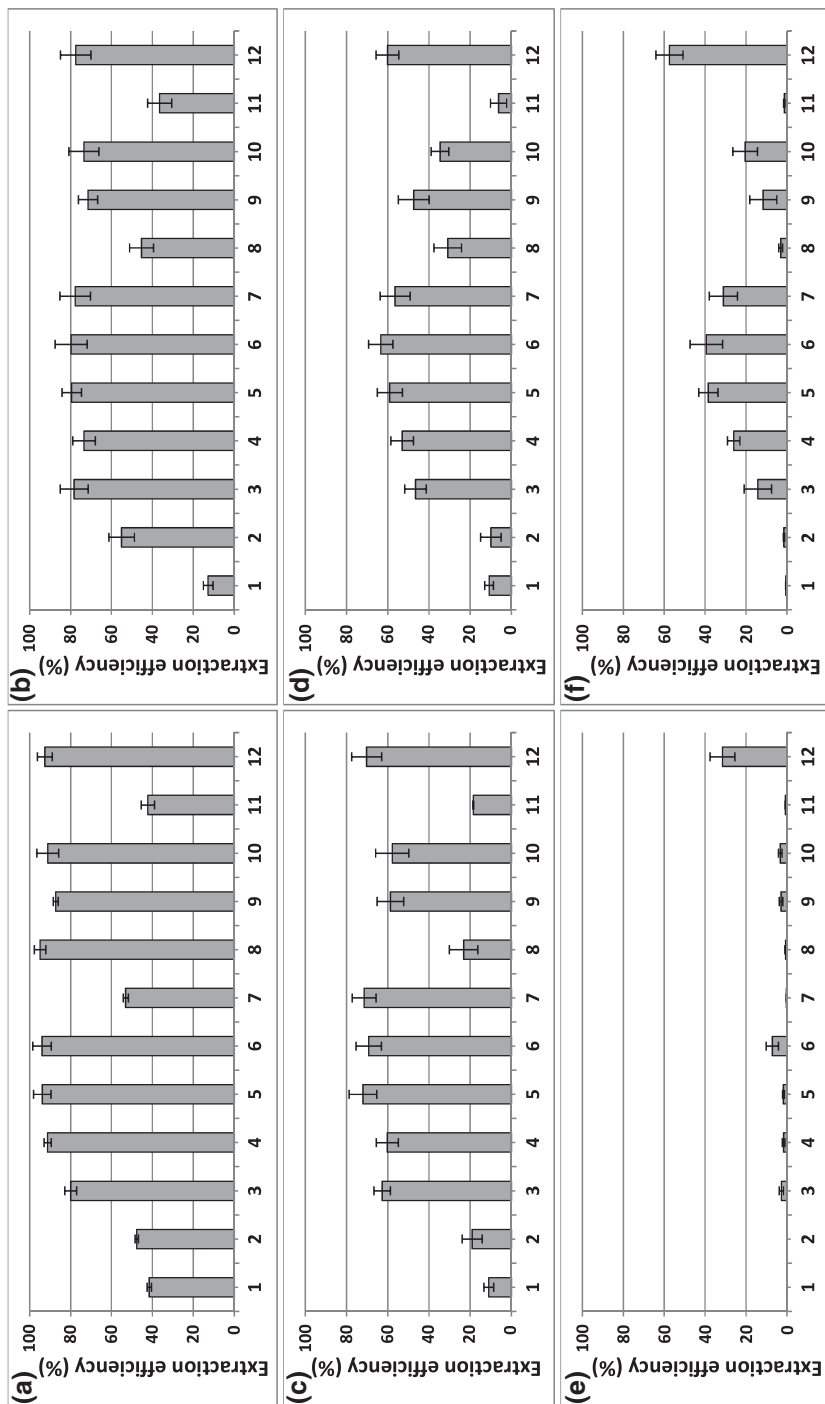


Fig. 2 Extraction efficiency: **a** tap water, **b** lake water, **c** river water, **d** sea water, **e** effluent wastewater, **f** influent wastewater (*I* sulfaguandine; 2 sulfafadiazine; 3 sulfathiazole; 4 sulfapyridine; 5 sulfamerazine; 6 sulfamerazine; 7 sulfamethoxyipyridazine; 8 sulfamethiazole; 9 sulfachloropyridazine; 10 sulfamethoxazole; 11 sulfisoxazole; 12 sulfadimethoxine)

The EE achieved for all target compounds were mostly higher than 50 %. However, some substances such as sulfaguanidine, sulfadiazine, sulfamethiazole and sulfisoxazole showed lower extraction efficiency. This could be mainly attributed to the fact that the chosen conditions were not appropriate for those compounds.

Sulfaguanidine is characterized by the $pK_a = 11.3$ which differs from the pK_a values of other selected drugs. Babić et al. (2006) used solid phase extraction and HPLC technique for the determination of veterinary pharmaceuticals (including three sulfonamides: sulfamethazine, sulfadiazine and sulfaguanidine) in wastewater. The obtained recoveries were ranged from 68.3 to 97.9 %—only for sulfaguanidine low recovery was achieved (11.2 %). Low EE obtained for sulfadiazine, sulfamethiazole and sulfisoxazole may also appear as the result of low breakthrough volume. This statement has been confirmed using lower river water sample volume (250 mL instead of 500 mL) for the extraction. The obtained EE values for sulfadiazine, sulfamethiazole and sulfisoxazole were 62, 73 and 51 % respectively.

The highest EE—in the range of 41.5–94.9 %—was achieved for tap water samples. It is due to the fact that the tested matrix does not contain interferences which could affect significantly the solid-phase extraction procedure.

The extraction efficiency of selected drugs from the rest of the analyzed samples decreased in the following order: lake water, river water, sea water, effluent wastewater and influent wastewater. The obtained EE (except of the compounds described above) were in the range from 40 to 80 %—with the exception of wastewater samples where the extraction efficiency was lower than 40 % (only for sulfadimethoxine the EE from wastewater influent was equal to 57 %). These values were decreasing with the increasing amounts of organic and also inorganic matter in the analyzed samples.

River and lake waters contain a large amount of organic compounds (like humic and fulvic acids). Humic substances have properties typical of weak anionic electrolytes, which may affect the sorption efficiency of SPE cartridges. This could be related to SPE retention competition between these anions and sulfonamides in anionic form (Białk-Bielińska et al. 2011). The pH finally applied in this study was 7.0, hence sulfonamides could be present in anionic form (see Table 1).

The sea water may contain high amounts of organic substances (in particular in the case of coastal samples) and most of all high concentrations of inorganic salts. High salinity, due to the retention competition between seawater anions (chlorides, bromides, sulfates, phosphates) and sulfonamides in anionic form, may affect the extraction efficiency. These compound may cause that there is considerably lower surface area of the sorbent available, which significantly disrupts the SPE-procedure (Białk-Bielińska et al. 2011).

The results obtained for lake river and sea water samples analysis were similar to those presented in literature (Kleywegt et al. 2011; Wang et al. 2011). The extraction efficiency of selected drugs from influent and effluent wastewater matrices were much lower in comparison with the literature (Vanderford and Snyder 2006; Kasprzyk-Hordern et al. 2008b; Lacey et al. 2008). Therefore, the presented procedure should be further elaborated. Hence, a higher mass of sorbent is required

to process a similar volume of sample, or lower sample volume should be used. Another approach can be the use of tandem solid-phase extraction (as described in Sect. 3.1.).

4 Summary

The study demonstrated that the impact of matrix complexity on the results of sulfonamides analysis by SPE and LC-ESI-MS/MS was significant. The results show the following regularity—the more complicated the matrix is, the more the quality of final result is affected. Thus, it is of high significance to use a plausible approach to correct these effects, in order to avoid inaccurate quantification (by overestimation or underestimation) when analyzing real samples. This parameter should be evaluated with each set of samples analyzed. The use of the method proposed in this study (the post-extraction addition technique) has also some disadvantages (time-consuming and higher costs of the analysis), however this technique ensures that the obtained concentration values are reliable. It is necessary to assess the ecotoxicological risk of the presence of pharmaceuticals residues in aquatic environment in the credible way.

Acknowledgments The authors would like to acknowledge the financial support of the Polish Ministry of Science and Higher Education under grant DS 30-8110-D195-13.

References

- Antignac JP, De Wasch K, Monteau F, De Brabander H, Andre F, Le Bizec B (2005) The ion suppression phenomenon in liquid chromatography–mass spectrometry and its consequences in the field of residue analysis. *Anal Chim Acta* 529:129–136
- Babić S, Ašperger D, Mutavdžić D, Horvat AJM, Kaštelan-Macan M (2006) Solid phase extraction and HPLC determination of veterinary pharmaceuticals in wastewater. *Talanta* 70:732–738
- Białk-Bielińska A, Siedlewicz G, Pazdro K, Fabiańska A, Stepnowski P, Kumirska J (2011) A very fast and simple method for the determination of sulfonamide residues in seawaters. *Anal Meth* 3:1371–1378
- Bonfiglio R, King RC, Olah TV, Merkle K (1999) The effects of sample preparation methods on variability of the electrospray ionization response for model drug compounds. *Rapid Commun Mass Spectrom* 13:1775–1785
- Buchberger WW (2011) Current approaches to trace analysis of pharmaceuticals and personal care products in the environment. *J Chrom A* 1218:603–618
- Caban M, Migowska N, Stepnowski P, Kwiatkowski M, Kumirska J (2012) Matrix effects and recovery calculations in analyses of pharmaceuticals based on the determination of β -blockers and β -agonists in environmental samples. *J Chrom A* 1258:117–127
- Carlsson C, Johansson AK, Alvan G, Bergman K, Kühler T (2006) Are pharmaceuticals potent environmental pollutants? Part I: environmental risk assessments of selected active pharmaceutical ingredients. *Sci Total Environ* 364:67–87
- Daughton CG, Ternes TA (1999) Pharmaceuticals and personal care products in the environment: agents of subtle change? *Environ Health Perspect* 107:907–938

- Gosetti F, Mazzucco E, Zampieri D, Gennaro MC (2010) Review. Signal suppression/enhancement in high-performance liquid chromatography tandem mass spectrometry. *J Chrom A* 1217:3929–3937
- Hall TG, Smukste I, Bresciano KR, Wang Y, McKearn D, Savage RE (2012) Identifying and overcoming matrix effects in drug discovery and development. Tandem mass spectrometry—applications and principles. In: J Prasain (ed) ISBN: 978-953-51-0141-3, InTech, doi:10.5772/32108
- Halling-Sørensen B, Nors Nielsen S, Lanzky PF, Ingerslev F, Holten Liitzhøfl HC, Jørgensen SE (1998) Occurrence, fate and effects of pharmaceutical substances in the environment—a review. *Chemosphere* 36:357–393
- Hao C, Zhao X, Yang P (2007) GC-MS and HPLC-MS analysis of bioactive pharmaceuticals and personal-care products in environmental matrices. *TrAC* 26:569–580
- Jones-Lepp TL, Stevens R (2007) Pharmaceuticals and personal care products in biosolids/sewage sludge: the interface between analytical chemistry and regulation. *Anal Bioanal Chem* 387:1173–1183
- Kasprzyk-Hordern B, Dinsdale RM, Guwy AJ (2008a) The effect of signal suppression and mobile phase composition on the simultaneous analysis of multiple classes of acidic/neutral pharmaceuticals and personal care products in surface water by solid-phase extraction and ultra performance liquid chromatography–negative electrospray tandem mass spectrometry. *Talanta* 74:1299–1312
- Kasprzyk-Hordern B, Dinsdale RM, Guwy AJ (2008b) The occurrence of pharmaceuticals, personal care products, endocrine disruptors and illicit drugs in surface water in South Wales, UK. *Water Res* 42:3498–3518
- King R, Bonfiglio R, Fernandez-Metzler C, Miller-Stein C, Olah T (2000) Mechanistic investigation of ionization suppression in electrospray ionization. *J Am Soc Mass Spectrom* 11:942–950
- Kleywegt S, Pileggi V, Yang P, Hao C, Zhao X, Rocks C, Thach S, Cheung P, Whitehead B (2011) Pharmaceuticals, hormones and bisphenol A in untreated source and finished drinking water in Ontario, Canada—occurrence and treatment efficiency. *Sci Total Environ* 409:1481–1488
- Kloepfer A, Quintana JB, Reemtsma T (2005) Operational options to reduce matrix effects in liquid chromatography–electrospray ionization-mass spectrometry analysis of aqueous environmental samples. *J Chrom A* 1067:153–160
- Kostopoulou M, Nikolaou A (2008) Analytical problems and the need for sample preparation in the determination of pharmaceuticals and their metabolites in aqueous environmental matrices. *Trac-Trend Anal Chem* 27:1023–1035
- Kot-Wasik A, Dębska J, Namieśnik J (2007) Analytical techniques in studies of the environmental fate of pharmaceuticals and personal-care products. *Trac-Trend Anal Chem* 26:557–568
- Lacey C, McMahon G, Bones J, Barron L, Morrissey A, Tobin JM (2008) An LC–MS method for the determination of pharmaceutical compounds in wastewater treatment plant influent and effluent samples. *Talanta* 75:1089–1097
- Madureira TV, Barreiro JC, Rocha MJ, Cass QB, Tiritan ME (2009) Pharmaceutical trace analysis in aqueous environmental matrices by liquid chromatography–ion trap tandem mass spectrometry. *J Chrom A* 1216:7033–7704
- Marín JM, Gracia-Lor E, Sancho JV, López FJ, Hernández F (2009) Application of ultra-high-pressure liquid chromatography–tandem mass spectrometry to the determination of multi-class pesticides in environmental and wastewater samples. Study of matrix effects. *J Chrom A* 1216:1410–1420
- Petrović M, Hernando MD, Díaz-Cruz MS, Barceló D (2005) Liquid chromatography–tandem mass spectrometry for the analysis of pharmaceutical residues in environmental samples: a review. *J Chrom A* 1067:1–14
- Renew JE, Huang CH (2004) Simultaneous determination of fluoroquinolone, sulfonamide, and trimethoprim antibiotics in wastewater using tandem solid phase extraction and liquid chromatography–electrospray mass spectrometry. *J Chrom A* 1042:113–121

- Santos LHMLM, Araujo AN, Fachini A, Pena A, Delerue-Matos C, Montenegro MCBSM (2010) Review. Ecotoxicological aspects related to the presence of pharmaceuticals in the aquatic environment. *J Hazard Mater* 175:45–95
- Schmitt-Kopplin Ph, Burhenne J, Freitag D, Spiteller M, Kettrup A (1999) Development of capillary electrophoresis methods for the analysis of fluoroquinolones and application to the study of the influence of humic substances on their photodegradation in aqueous phase. *J Chrom A* 837:253–265
- Steen RJCA, Hogenboom AC, Leonards PEG, Peerboom RAL, Cofino WP, Brinkman UATH (1999) Ultra-trace-level determination of polar pesticides and their transformation products in surface and estuarine water samples using column liquid chromatography–electrospray tandem mass spectrometry. *J Chrom A* 857:157–166
- Tang L, Kebarle P (1993) Dependence of ion intensity in electrospray mass spectrometry on the concentration of the analytes in the electrosprayed solution. *Anal Chem* 65:3654–3668
- Taylor PJ (2005) Matrix effects: the Achilles heel of quantitative high-performance liquid chromatography–electrospray–tandem mass spectrometry. *Clin Chem* 38:328–334
- Trufelli H, Palma P, Famigliani G, Cappiello A (2010) An overview of matrix effects in liquid chromatography–mass spectrometry. *Mass Spectrom Rev* 30:491–509
- Vanderford BJ, Snyder SA (2006) Analysis of pharmaceuticals in water by isotope dilution liquid chromatography/tandem mass spectrometry. *Environ Sci Technol* 40:7312–7320
- Vieno NM, Tuhkanen T, Kronberg L (2006) Analysis of neutral and basic pharmaceuticals in sewage treatment plants and in recipient rivers using solid phase extraction and liquid chromatography–tandem mass spectrometry detection. *J Chrom A* 1134:101–111
- Wang C, Shi H, Adams CD, Gamagedara S, Stayton I, Timmons T, Ma Y (2011) Investigation of pharmaceuticals in Missouri natural and drinking water using high performance liquid chromatography–tandem mass spectrometry. *Water Res* 45:1818–1828
- Ye Z, Weinberg HS, Meyer MT (2007) Trace analysis of trimethoprim and sulfonamide, macrolide, quinolone, and tetracycline antibiotics in chlorinated drinking water using liquid chromatography electrospray tandem mass spectrometry. *Anal Chem* 79:1135–1144

Valles Marineris: A Place Full of Answers

O. Kromuszczyńska, M. Makowska and K. Dębniak

Abstract Valles Marineris (VM), a great canyon complex on Mars, the largest in Solar System, is an object of our research reported in this paper. There are three major aims of our work. (1) The first purpose is to create a multilayered map of the VM region using ArcGIS software and ISIS Planetary Image Processing Software. It will be the first detailed and complex synthesis of this canyon system. The second part of our investigation consists of two approaches to understand a phenomenon called Deep-Seated Gravitational Spreading (DSGS)—a slope deformation mechanism. (2) Observations and interpretations of DSGS features in Valles Marineris in comparison to terrestrial ones are one way to gain knowledge about this phenomenon. (3) Another method of the DSGS studies is to create a numerical model in the Martian and terrestrial conditions. Preliminary results show that the main factors causing DSGS are the slope angle and the angle of internal friction. The size of DSGS features on Mars is at least one order of magnitude larger than the terrestrial equivalents. The height of fault offsets in the Martian example varies from 50 to 1,000 m, while on Earth it rarely exceeds 25 m.

1 Introduction

One of the most spectacular places on Mars is Valles Marineris (VM; Fig. 1a)—the largest canyon complex in the Solar System. It is located in the equatorial region of the planet, covering a surface area of 650 by 2,000 km (Sharp 1973; Blasius et al. 1977; Schultz and Lin 2001; Peulvast et al. 2001), and characterized by depths exceeding 10 km.

O. Kromuszczyńska (✉) · M. Makowska · K. Dębniak
WROONA Group, Institute of Geological Sciences, Polish Academy of Sciences,
Research Centre in Wrocław, Podwale St. 75, 50-449 Wrocław, Poland
e-mail: okromuszczyńska@twarda.pan.pl

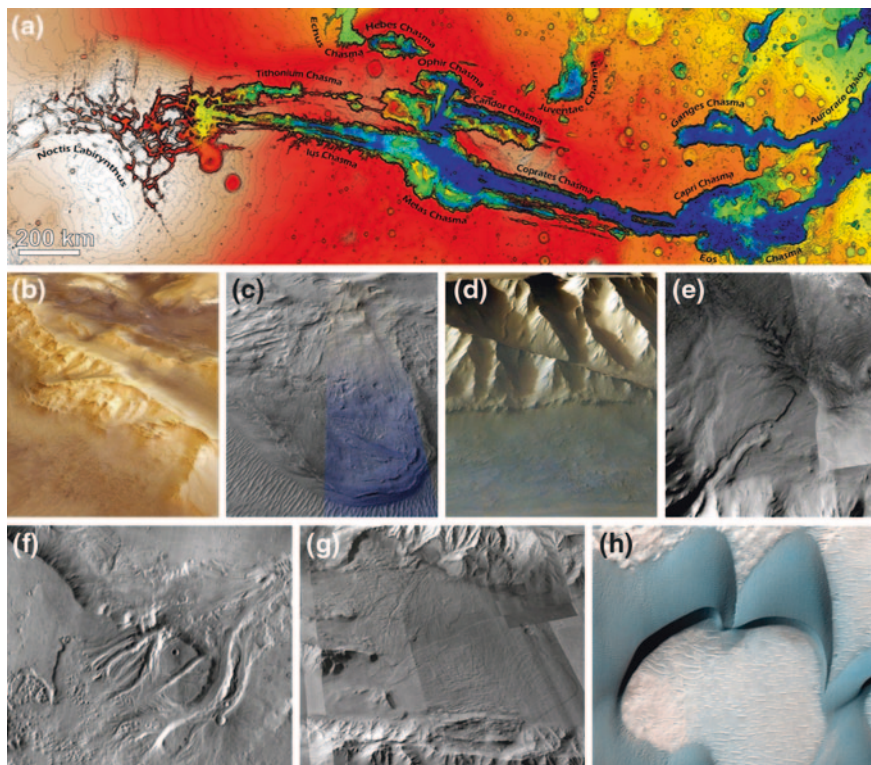


Fig. 1 Valles Marineris and effects of numerous processes occurring in the canyon complex, **a** VM general view; **b** faults, tectonic processes, **c** rock glacier, **d** triline, mark maximum glacier elevation, **e** river system, **f** outflow channels, fluvial processes, **g** landslides, mass wasting processes, and **h** dunes, eolian processes

The VM size, which is a reflection of a geological process variety occurring in the area, constitutes the canyon system as an object of interest for scientists. Owing to the complex presence in the Martian crust, it is possible to study past and current processes taking place in the region, because the canyon system allows human investigation to penetrate for several kilometers into the planet subsurface. The walls and floor of the canyons are a perfect record of the geological history of Mars, and carry information about its internal structure.

Despite many local interpretations of the VM origin and development prepared by other researches, a detailed regional map for the entire system does not still exist. A map presenting VM as an entirety—as a structure with a documented geological history, occurring processes and features produced by these processes, is needed. For that reason we make an effort in the first part of our investigation to create this desired cartographic paper.

To investigate the processes occurring on another planet, one has to assume that they act similarly to those known on Earth. Therefore, it is important to find on Earth

and Mars similar structures in order to explain the mechanisms of their formation. One of the phenomena occurring in the VM is a deep-seated gravitational spreading—a mass movement, involving gravitational propagation of topographic ridges, caused by the slope instability. The analogue for this phenomenon has been found in the Polish and Slovakian Tatra Mountains. In the second part of our studies we compare the effects of this phenomenon on Earth and Mars and conduct its numerical modeling.

2 Geological History of Valles Marineris

The Martian history started 4.6 billion years ago (Ga) and has been divided into three major periods on the basis of stratigraphic relationships and the impact crater density (Scott and Tanaka 1986; Greeley and Guest 1987; Tanaka and Scott 1987). Noachian is the oldest period, and it dates terrains created before 3.7 Ga. The middle part of the history, between 3.7 and 3.0 Ga, is called Hesperian, whereas the youngest is the Amazonian Period (3.0 Ga—present). The most probable genesis of Valles Marineris took place during the earliest times of the Mars development (Tanaka et al. 2012).

Valles Marineris is known for humanity for over 40 years. Between 1962 and 1973, Mariners, the American robotic interplanetary probes, were sent into interplanetary space to investigate terrestrial planets—Mercury, Venus, and Mars. The canyon name originates from the Mariner 9 mission, during which the first photography of Valles Marineris was taken in 1971, revealing the structure (Hartman 2003). Despite the fact that through all these years VM has been the target in numerous investigations and studies (for example: Dohm et al. 2009; Peulvast and Masson 1993; Williams et al. 2003; Quantin et al. 2004), there are still a lot of questions regarding its origin and development, lacking in clear answers. A number of hypotheses about the VM genesis has been created. It is associated with salt tectonics by some researchers (Montgomery et al. 2009), whereas others proposed collapse as a way to initiate surface fracturing (Rodriguez et al. 2006; McKenzie and Nimmo 1999). Mantle plume development related to central uplift has also been proposed (Dohm et al. 2009). The largest group of scientists seems to favor rifting induced by dike emplacement (Tanaka and Golombek 1989) as a process responsible for the VM creation. It is certain that processes related to the Valles Marineris origin and evolution are complex and enigmatic.

Valles Marineris situated in the Tharsis Plateau region, south of the Martian equator, is the most spectacular structure in the Solar System. It is a trough complex with the wall height up to 11 km and the length exceeding 4,000 km, covering an area of $650 \times 2,000$ km (Carr and Head 2010). Valles Marineris is composed of interconnected, elongated, deep depressions called chasmata (singular: chasma), from the west: Tithonium and Ius, Ophir, Candor, Melas, Coprates, Eos, Capri, Ganges which constitute the main part of the structure (Mège and Bourgeois 2011; Peulvast et al. 2001). In contrary, three chasmata (Echus, Hebes, and Juventae) are localized hundreds of kilometers north of the main system, separated by plateau—they are the deepest depressions in Valles Marineris (Scott and Tanaka 1986). The system continues westward into Noctis Labyrinthus, a structure of

tectonic origin composed of grabens (Warner et al. 2012). Ius Chasma is located in the western part of Valles Marineris and directly connected to Noctis Labyrinthus. The chasma is characterized by a simple axial shape, composed of two parallel grabens separated by the Geryon Montes ridge. Walls of the canyon are layered and 8–11 km deep (Bibring and Erard 2001). Tithonium Chasma, located north of Ius Chasma, reveals similarity in shape to Ius Chasma and is also connected to Noctis Labyrinthus. The canyon south walls are structured in a spur-and-gully morphology, whereas north walls are eroded. The Tithonium Chasma depth is similar to the depth described in Ius Chasma (Quantin et al. 2004). Ius Chasma is connected to Melas Chasma, a huge canyon of irregular shape, situated in the central part of Valles Marineris. This chasma is considered as a potential area of paleolakes due to the dense valley networks in the highlands surrounding the canyon (Metz et al. 2009). Well-developed spurs and gullies, as well as triangular faces morphstructures are observed on the canyon walls (Dromart et al. 2007). Melas Chasma is linked on the northern border with Candor Chasma, i.a. by a residual part of plateau which is slowly converted into a narrow ridge separated in the middle part. Interior Layered Deposits (ILDs) can be distinguished on the Candor Chasma floor (Michalski and Niles 2011). ILDs are formed by sedimentary (Nedell et al. 1987; Malin and Edgett 2000; Rossi et al. 2007) or volcanic (Chapman and Tanaka 2001; Hynes et al. 2002) processes in the early Martian history and they are characterized by the presence of hydrated sulfate minerals and finely crystalline ferric oxides (Murchie et al. 2009). The eastern part of Valles Marineris is occupied by Coprates Chasma, adjacent from the west to Melas Chasma. The canyon shape is similar to Ius Chasma, i.e., elongated and composed of two parallel grabens separated by a massif. Spur-and-gully morphology and layers can be observed on the southern walls of the massif. In addition, the massif is compositionally and structurally similar to the chasma walls (Beyer and McEwen 2005).

Owing to the incredible canyon depth, it is possible to observe complexity of geological processes inside, like: aeolian, fluvial, mass wasting, periglacial, and tectonic. Current aeolian activity is the most dynamic process on Mars. Numerous depositional and erosional landforms, like dunes, ripples, yardangs, wind tails, and dust devils are present (Fig. 1h) (Silvestro et al. 2011). Aeolian processes play the main role in the landscape changing by removal and redeposit of the material. However, Mars was a much more dynamic planet in the past, and evidences of ancient fluvial erosion on the Martian surface, manifested in the form of valley networks (Fig. 1e) and outflow channels (Fig. 1f) can be found (Fasset and Head III 2005). Mass wasting processes can be also observed on the Martian surface, including landslides as the most common phenomenon. The spectacular landslides are found in Coprates Chasma (Fig. 1g) (Quantin et al. 2004). In addition, periglacial landforms, like polygon patterns, stone circles, and collapsed pits, are common in Valles Marineris (Fig. 1c, d) (Johnsson et al. 2012). Moreover, very intensive tectonic processes creating faults, uphill-facing scarps, and double crests were present in the early Martian history, but tectonic structures observed today are mostly remnants of the original features driven by the gravity (Fig. 1b) (Rossi et al. 2008).

2.1 *Creating a Map*

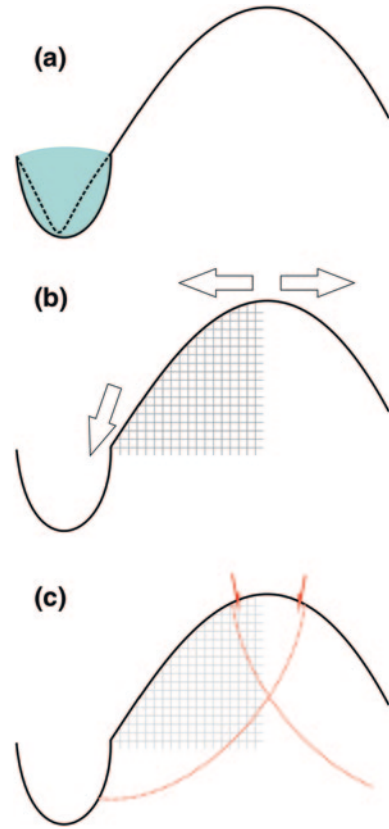
The discussion on the geological history is still open. There is an enormous amount of data, letting us better understand the geological processes occurred on Mars. However the knowledge of this subject is not sufficient. Many investigations have been performed in the VM area, but their spatial and topical variety makes past and present conditions in the canyon system hard to understand. The planetological exploration of VM has reached the point where synthesis and correlation of previous works has to be done. The summary can become a framework for the new insight in the canyon history, and at the same time the answer for most significant questions of tectonic, fluvial, glacial, and climatic processes occurred in the VM region. The synthesis will be composed of a multilayered GIS map, which is based on data obtained from several Martian missions: Mars Global Surveyor (1996–2006; MGS), Mars Odyssey (2001–present; MO), Mars Express (2003–2014; MEx), and Mars Reconnaissance Orbiter (2005–2010; MRO). The datasets from these missions (MGS–MOLA, MO–THEMIS night IR, MEx–HRSC and MRO–CTX visible, HiRISE) will be used to create mosaic necessary to impose other thematic layers. The basic layer for the map production consists of CTX images processed and merged into a mosaic by USGS ISIS Planetary Image Processing Software. Several description layers and one interpretation layer will be created using ArcGIS software.

3 Deep-Seated Gravitational Spreading

Deep-Seated Gravitational Spreading (DSGS), also called Deep-Seated Gravitational Slope Deformations (for instance: Bachmann et al. 2009) or Sackung (for instance: Zischinsky 1966) is a very slow deformation of topographic ridges with diagnostic features such as crestal grabens, indicating ridge-top splitting, and uphill-facing normal faults scarps on ridge flanks (Mège and Bourgeois 2011; Beck 1968; Savage and Varnes 1987; Hutchinson 1988; Agliardi et al. 2001; Kinakin and Stead 2005). This phenomenon is observed in formerly glaciated mountains all over the Earth, in many different lithologies and geochemical characteristics (Bachmann et al. 2009; Zischinsky 1966; Hippolyte et al. 2006; Jarman 2006; Kobayashi 1956; Reitner and Linner 2009). Uphill-facing normal faults scarps and crestal grabens were also found on walls and internal ridges of VM (Mège and Bourgeois 2011; Kromuszczyńska et al. 2012; Bourgeois et al. 2011), indicating that DSGS also occurred in this Martian structure.

DSGS is one of mass wasting processes, which triggering factors remain still unclear, but most frequent explanation of the onset of DSGS is glacial debuttressing following removal of mountain glaciers (Mège and Bourgeois 2011; Jarman 2006; Pánek et al. 2011; McCalpin and Irvine 1995; Ballantyne 2002; Agliardi et al. 2009; Hippolyte et al. 2009; Kellerer-Pirklbauer et al. 2010). Mountain valleys are changed by glaciers from V-shaped to U-shaped, causing removal of the

Fig. 2 Schematic occurrence of the DSGS phenomenon; description in the text



rock mass from slope toes (Fig. 2a, b). During glaciation and later deglaciation, the climate favors fracturing and damage of rocks constituting a slope (Fig. 2b). After a glacier removal, without a support from slope toes, the slope becomes unstable in the lower part and a large shearing stress is produced. The remaining mass of rocks in the upper part of the slope is too large (Fig. 2b), so it is pulled down by the gravity. The consequence is an extensive stress formation in the top of the slope, and the subsequent normal faults appearance (Fig. 2c). Eventually, uphill-facing scarps and crestal grabens are produced. The shearing stress in slope toes causes basal slope bulging.

3.1 DSGS Observations in Valles Marineris (Mars) and Tatra Mountains (Earth)

In order to compare the scale of DSGS on Mars and Earth, the deformations must be quantified. Vertical offset of uphill-facing normal fault scarps, as diagnostic features of DSGS, were used for the quantification and comparison.

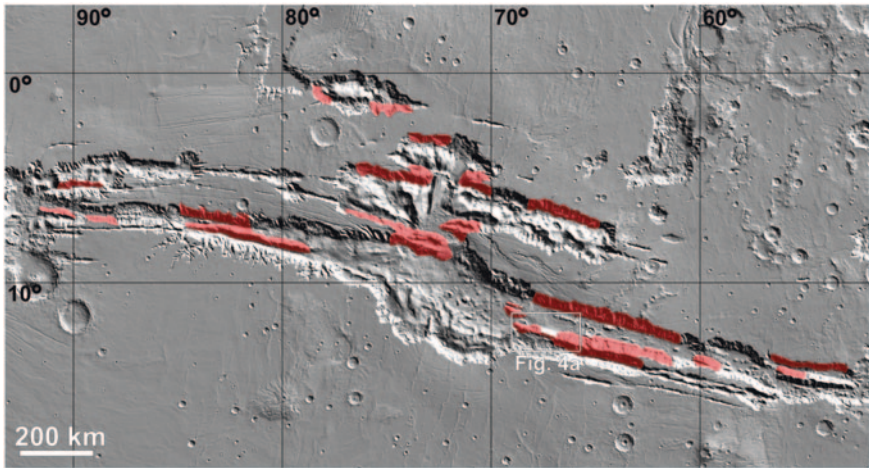


Fig. 3 Location of major DSGS sites in VM and Fig. 4a

Observations on Mars are done using the appropriate orbital datasets (especially Mars Odyssey/Themis, MRO/CTX, MRO/HiRISE, and MGS/MOLA from NASA, and Mars Express/HRSC from ESA).

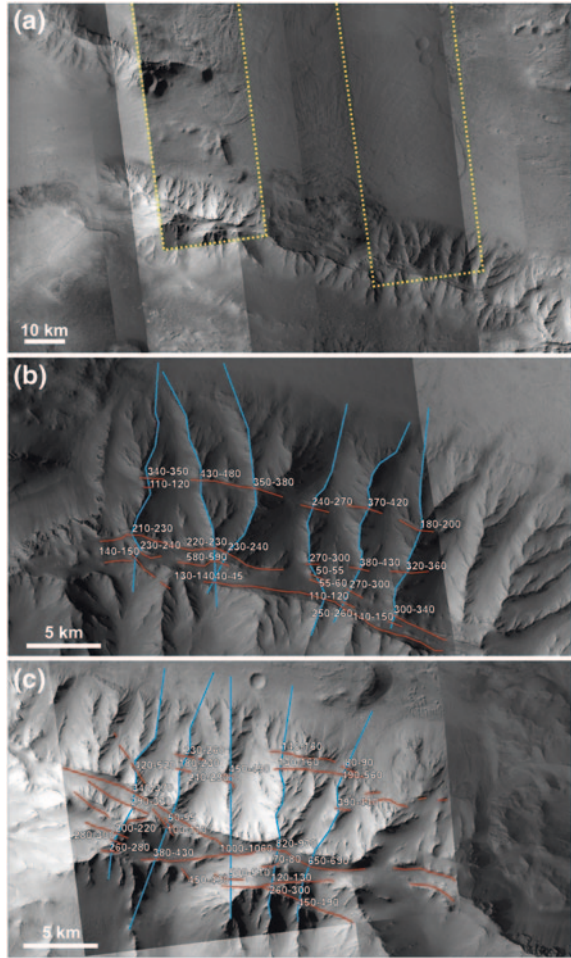
DSGS has been identified in many places in VM (Fig. 3). Uphill-facing scarps cut across the primary spur-and-gully morphology of chasmata walls, as well as slopes of internal ridges.

An example of the DSGS occurrence in VM is a topographic ridge in Coprates Chasma (Fig. 4a). Digital Elevation Models (DEMs) obtained from the MRO/CTX image correlation allowed to determine the vertical offset of uphill-facing faults located on the Coprates Chasma central topographic ridge. Two DEMs from Coprates Chasma orientated North–South were examined. The DEMs are located on Eastern and Western side of the enormous landslide formed by the ridge collapse (Fig. 4a). The DEMs' grid spacing is 30 m and the estimated vertical accuracy is 15 m.

The DEMs cover only the northern slope of the ridge, so this area has become the study site. Eleven profiles were created and analyzed. Uphill-facing normal fault scarps within DEMs were mapped and height of their offsets was measured. The height and geometry of scarps, both visible on profiles obtained from DEMs, do not represent the initial state of the fault. Both characteristics have been changed by erosional and accumulative processes. However, fault offsets can be retrieved on the basis of assumptions involving an angle of inclination of the fault surface (fault dip angle). The typical dip angle of many normal faults in extensional regime on Earth is 60–70° (Gudmundsson 1992; Acocella et al. 2003); therefore, assumed dip angles are also in this range.

The profile analyses of normal fault vertical offsets on the Coprates northern slope revealed two conclusions: (1) the fault offset in the eastern part of Coprates

Fig. 4 **a** Investigated ridge in Coprates Chasma, *yellow lines* boundaries of DEMs, **b** values of vertical offsets of normal faults in East part of investigated area, *blue lines* profiles, *red lines* mapped faults, and **c** values of vertical offsets of normal faults in West part of investigated area, *blue lines* profiles, *red lines* mapped faults



ridge is ranged between 40 and 830 m, with the average value of ~ 280 m (Fig. 4b) and (2) the Western part is characterized by a fault offset in a range between 50 and 1,000 m, and the average value ~ 320 m (Fig. 4c).

The historic and most famous terrestrial examples of DSGS have been found in the Tatra Mountains (Drecki and Zyszkowska 2008; Jahn 1964; Mahr 1977; Nemcok 1972; Nemčok and Baliak 1977). These examples were taken under consideration during this research.

In order to quantify deformations in the Tatra Mountains we conducted field work, including: accurate measurements of the length, width, and depth of fault scarps, identification of the type of failure initiation mode (shear/tensile), and examination of their distribution along ridge slope.

Length, width, and depth were measured using the Wide Area Differential GPS technique (WADGPS), an improved differential GPS technique requiring a single

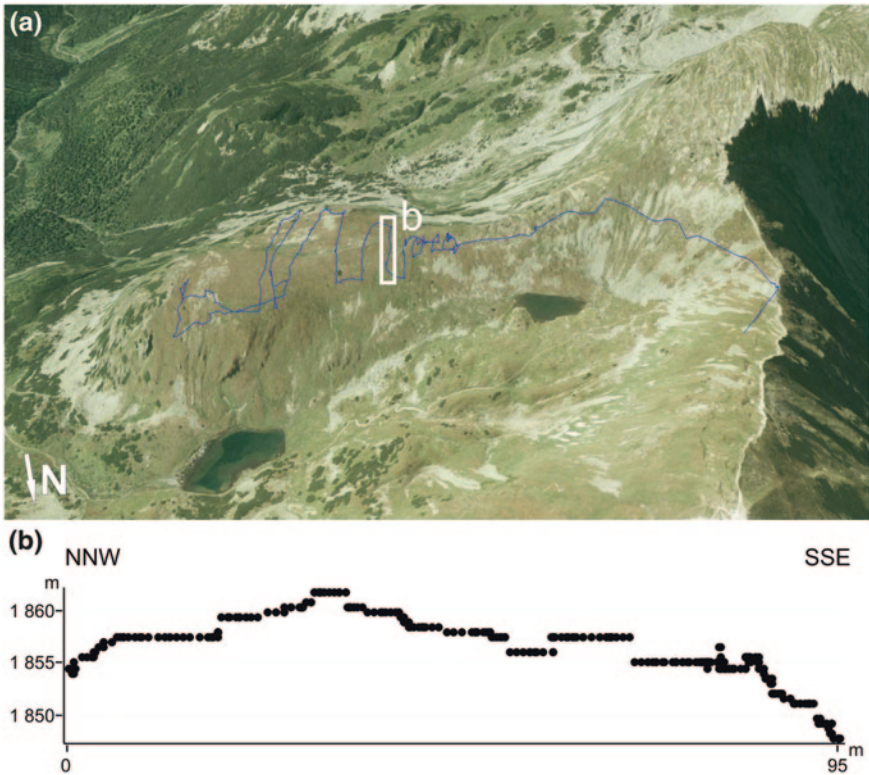


Fig. 5 a Location of investigation site and profiles path in Ostrý Roháč area, b example of profile from Ostrý Roháč area

device having the Wide Area Augmentation System capability. Garmin GPSmap 62 s was used. For short distances and for double check of GPS results, a classical retractable tape measurement or/and a laser tape were performed. The laser tape is a Makita 60 m LD060P, of 1.5 mm accuracy for the investigated distances.

One of the sites studied in the Tatra Mountains is a ridge located east of Ostrý Roháč (Fig. 5a), close to the Polish–Slovakian border. DSGS appears as uphill-facing normal faults at the top of the topographic ridge. The ridge-top and slopes are intensely deformed, some scarps are up to 5–10 m high (Fig. 5b), indicating that DSGS has been extremely active in that location since the last glaciation.

The Tatra Mountains’ investigations succeeded in the conclusion that vertical offsets of terrestrial normal faults created by DSGS rarely exceed 15–25 m, with mean values in the range of 5–12 m. It is consistent with the literature studies (see supplementary table in Mège and Bourgeois 2011). Although the Martian DSGS examples share many common features with the ones in the Tatra Mountains, there is a significant difference in terms of size of both terrestrial and Martian DSGS.

Table 1 Values of the slope inclination and the angle of internal friction

	Slope inclination [$^{\circ}$] α	
	45	45
Angle of internal friction [$^{\circ}$] φ	40	40
	30	30
	20	20
	10	10

3.2 DSGS Numerical Modeling

The triggering mechanism of DSGS is still not well understood. Any conventional methods to specify the details of that process are not sufficient to determine them. In order to gain profound knowledge about an influence of such factors as erosional activity of glaciers, regional isostatic activity, and presence of layered deposits on triggering mechanism, a preliminary modelling were conducted.

2D modeling of a DSGS process is performed using the finite element code ADELI (Hassani 1994), software devoted to solve quasi-static termo-mechanical behavior of the lithosphere at geological time scales (Savage et al. 2007). Experiments are performed using the idea of objective derivative. Space is discretized by using linear elements and the time estimation is obtained from the finite method based on the Dynamic Relaxation Method (Savage et al. 2007). The shape and size of the model (Fig. 6) were selected according to the results of physical and numerical modeling of massif fracturing during a Deep-Seated Gravitational Slope Deformation (Bachmann et al. 2009).

The boundary conditions are imposed at horizontal border of the model; vertical borders are not fixed (Fig. 6). The model provides 20 time-steps, corresponding to one million years. At the beginning, the model is elastically equilibrated under the Martian gravity (Bouissou et al. 2012). The parameter value of deformation modulus $E^* = 20$ GPa was used according to the experimental data (Schultz 1995). The value of deformation modulus is related to Geomechanics Rock Mass Rating (RMR) (Bieniawski 1978) of rock mass, system based on measurable parameters of the rock mass (uniaxial compressive strength, discontinuity characteristics, rock quality designation RQD). The deformation modulus of the rock mass is smaller than the corresponding Young's modulus for intact rock due to the influence of discontinuities in the rock mass weakening. The Poisson ratio (ν) and density (ρ) are 0.23 (Chemenda et al. 2009) and $2,800 \text{ kg/m}^3$ (Merrien-Soukatchoff et al. 2001), respectively. The cohesion value obtained from RocLab, a free software for analysis of rock mass strength, was constant, $c = 8.4 \text{ MPa}$ (Rocscience 2007). The internal friction angle and slope inclination were variable (Table 1).

Results were displayed using xadeli software. Arrows shown in Figs. 7 and 8 indicate the displacement direction. Outcome for the slope angle $= 45^{\circ}$ and very low angle of internal friction $= 10^{\circ}$ (Fig. 7a, b) show that plastic strain accumulation occurs inside the model and evolves with time until the complete collapse at the time-step 20. The generated failure surface is curved with a very steep dip angle.

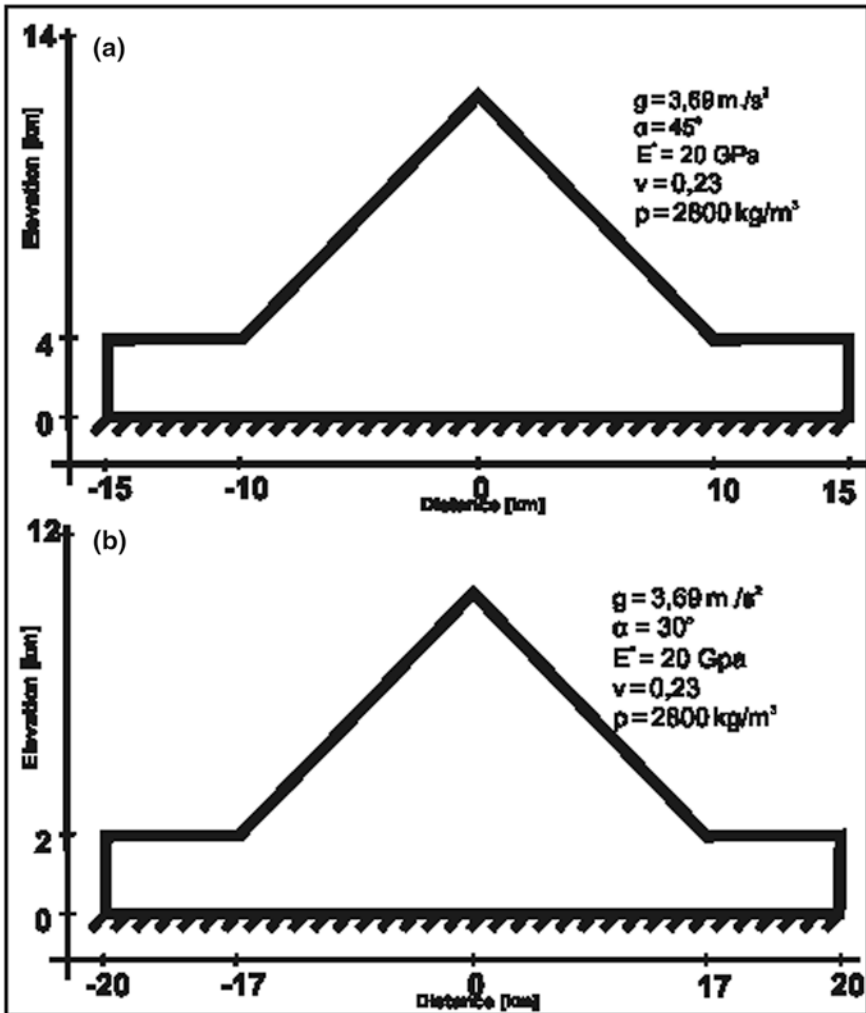


Fig. 6 Shape of the model, boundary condition and mechanical characteristic of the numerical model. g gravity acceleration, slope inclination, E^* deformation modulus, ν Poisson ratio, ρ density, a slope inclination 45° , b slope inclination 30°

The angle of internal friction was changed to 20° (Fig. 7c, d). Similar results were obtained, but it was possible to reach the time-step 20 without collapse. The plastic deformation was evolving slowly. Results from the experiment with a very high angle of internal friction of 30° and 40° (Fig. 7e, f), as predicted, do not generate failure surface and plastic strain were cumulated at the toe of the slope. The second experiment was conducted by setting the angle of slope inclination $\alpha = 30^\circ$ (Fig. 8). Results with $\alpha = 30^\circ$ and the angle of internal friction $\varphi = 10^\circ$ show analogous effects as obtained for the 45° slope inclination and the same value of internal friction angle (Fig. 8a, b).

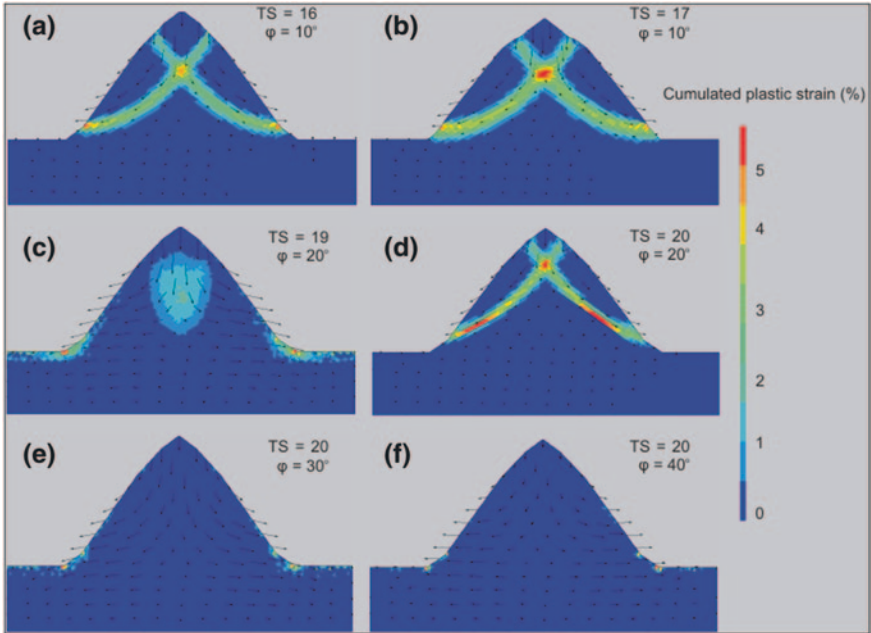


Fig. 7 Stages of the failure with the slope inclination of 45°. *TS* time-step, φ angle of internal friction

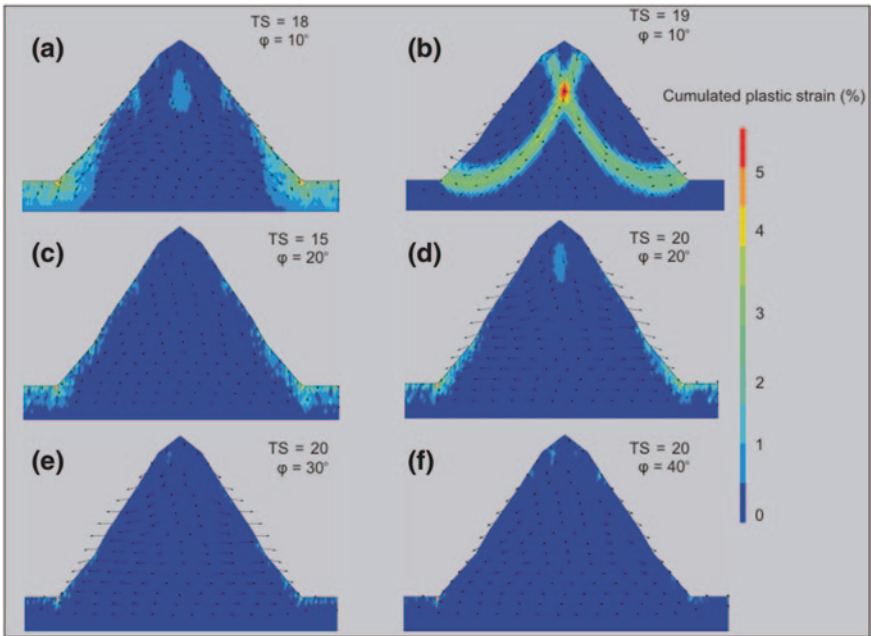


Fig. 8 Stages of the failure with the slope inclination of 30°. *TS* time-step, φ angle of internal friction

The failure occurred at the time-step 19 and the system collapsed during the next time-step. The plastic strain accumulation occurs inside the model, generating a similarly curved failure surface. Different results were obtained due to the implementation of the 20° angle of internal friction (Fig. 8c, d). It can be observed that at the time-step 19 a small accumulation of plastic strain appears inside the model near the crest of the ridge without any well-developed failure surface. In the case of the internal friction angle of 30° and 40° , an insignificant plastic deformation is observed at the toe of the slope (Fig. 8e, f).

The preliminary studies of the DSGS mechanism using 2-D finite element code ADELI were conducted in this paper. The results show that the main factors in slope stability are the slope angle and the angle of internal friction. Another significant factor is a proper shape of the initial slope.

4 Conclusions

The most spectacular Martian canyon complex, Valles Marineris, is a unique structure in the entire Solar System. No other place can give us such a detailed and precise access into the planet's interior and its history. Nowhere else, full profiles up to 11 km can be found. Mars is a planet of terrestrial type and many processes and phenomena which occurred there in the past and are ongoing today are very similar to those on Earth. All information obtained from VM can be used to answer many questions, not only about the Red Planet, but also about the past, present, and future of Earth. One of common phenomena is Deep-Seated Gravitational Spreading whose diagnostic features are present on Mars and Earth. In both cases it has been interpreted to be a postglacial process. The size of DSGS features on Mars is at least one order of magnitude larger than the terrestrial equivalents. The height of fault offsets in the Martian example varies from 50 to 1,000 m, while on Earth it rarely exceeds 25 m. The difference of size between Martian and terrestrial DSGS features is due to topographic gradient which is one order of magnitude higher on Mars than on Earth. Numerical modeling results determine the angle of slope and the angle of internal friction as the main factors responsible for slope deformations by DSGS. The future model shape will be more constrained by using the limit analysis method.

The greatest problem with the enormous quantity of data hidden in VM is the lack of access to it. The topography of canyon system prevents rovers operating on Mars to get inside, so all the data currently available for us are datasets from satellites. Most of them (i.a. CTX, HiRISE, HRSC, MOLA, and THEMIS datasets) will be incorporated to produce first detailed map of the VM region and the interpretation of its geological history.

We hope that future Martian exploration missions will allow to get the access inside the VM canyon complex and obtain surficial data from the through floor and walls. That will certainly bring answers to a great number of questions about the Martian history and evolution.

Acknowledgments Work presented in this paper is financed by Foundation for Polish Science, project TEAM 2011-7/9 Mars: another planet to approach geoscience issues. Authors would like to thank Daniel Mège and colleagues from WROONA Group for their help and support.

References

- Acocella V, Korne T, Salvini F (2003) Formation of normal faults along the axial zone of the Ethiopian Rift. *J Struct Geol* 25:503–513
- Agliardi F, Crosta G, Zanchi A (2001) Structural constraints on deep-seated slope deformation kinematics. *Eng Geol* 59:83–102
- Agliardi F, Crosta GB, Zanchi A, Ravazzi C (2009) Onset and timing of deep-seated gravitational slope deformations in the eastern Alps, Italy. *Geomorphology* 103:113–129
- Bachmann D, Bouissou S, Chemenda A (2009) Analysis of massif fracturing during deep-seated gravitational slope deformation by physical and numerical modeling. *Geomorphology* 103:130–135
- Ballantyne C (2002) Paraglacial geomorphology. *Quatern Sci Rev* 21:1935–2017
- Beck AC (1968) Gravity faulting as a mechanism of topographic adjustment. *N Z J Geol. Geophys.* 11:191–199
- Beyer RA, McEwen AS (2005) Layering stratigraphy of eastern Coprates and northern Capri Chasma, Mars. *Icarus* 179
- Bibring JP, Erard S (2001) The Martian surface composition. *Space Sci Rev* 96:293–316
- Bieniawski ZT (1978) Determining rock mass deformability—Experience from case histories. *Int J Rock Mech Min Sci* 15:237–247
- Blasius KR, Cutts JA, Guest JE, Masursky H (1977) Geology of the Valles Marineris: first analysis of imaging from the Viking 1 Orbiter primary mission. *J Geophys Res* 82:4067–4091
- Bouissou S, Darnault R, Chemenda A, Rolland Y (2012) Evolution of gravity-driven rock slope failure and associated fracturing: geological analysis and numerical modelling. *Tectonophysics*
- Bourgeois O, Mège D, Gourronc M, Bultel B, Massé M, Le Deit L (2011) Extensive glaciation of Valles Marineris (Mars) revealed by sacking, trimlines and ablation tills. In: Abstract of the EPSC-DPS joint meeting, Nantes, France, EPSC-DPS2011-255
- Carr MH, Head JH III (2010) Geologic history of Mars. *Earth Planet Sci Lett* 294:185–203
- Chapman MG, Tanaka KL (2001) Interior trough deposits on Mars: subice volcanoes? *J Geophys Res* 106(E5):10,087–010,100
- Chemenda A, Bois T, Bouissou S, Tric E, Bachmann D (2009) Numerical modelling of the gravity-induced destabilization of a slope: the example of the La Clapiere landslide, southern France. *Geomorphology*
- Dohm JM, Williams J-P, Anderson RC, Ruiz J, McGuire PC, Komatsu G, Davila AF, Ferris JC, Schulze-Makuch D, Baker VR, Boynton WV, Fairén AG, Hare TM, Miyamoto H, Tanaka KL, Wheelock SJ (2009) New evidence for a magmatic influence on the origin of Valles Marineris, Mars. *J Volcanol Geoth Res* 185:12–27
- Drecki I, Żyszkowska J (2008). Evaluation of cartographic resources in researching landforms in high mountains. In: Case study of double ridges in the Polish part of the Tatra Mountains. 6th ICA mountain cartography workshop, mountain mapping and visualisation, pp. 23–32
- Dromart G, Quantin C, Broucke O (2007) Stratigraphic architectures spotted in southern Melas Chasma, Valles Marineris. *Mars. Geology* 35:363–366
- Fasset CI, Head III JW (2005) Fluvial sedimentary deposits on Mars: ancient deltas in crater lake in the Nili Fossae region. *J Geophys Lett* 32(14)
- Greeley R, Guest JE (1987) Geologic map of eastern equatorial region of Mars. *U.S. Geol Surv Misc Geol Invest Map I-1802-B*, 1:15000000 scale
- Gudmundsson A (1992) Formation and growth of normal faults at the divergent plate boundary in Iceland. *Terra Nova* 4:464–471
- Hartman WK (2003) A traveler's guide to Mars. Chapter 29: Valles Marineris. Workman Publishing, New York
- Hassani R (1994) Modélisation numérique de la déformation des systèmes géologique. Ph. D Thesis, Université de Montpellier 2, France
- Hippolyte J-C, Brocard G, Tardy M, Nicoud G, Bourlès D, Braucher R, Ménard G, Souffaché B (2006) The recent fault scarps of the western Alps (France): tectonic surface ruptures or gravitational sacking scarps? A combined mapping, geomorphic, levelling, and ¹⁰Be dating approach. *Tectonophysics* 418:255–276

- Hippolyte JC, Bourlès D, Braucher R, Carcaillet J, Léanni L, Arnold M, Aumaitre G (2009) Cosmogenic ^{10}Be dating of a sacking and its faulted rock glaciers, in the Alps of Savoy (France). *Geomorphology* 108:312–320
- Hutchinson JN (1988) General Report: morphological and geotechnical parameters of landslides in relation to geology and hydrogeology. In: Proceedings of the 5th International Symposium on Landslides, Lausanne, vol 1. Balkema, Rotterdam pp 3–35
- Hynek BM, Arvidson RE, Phillips RJ (2002) Geologic setting and origin of Terra Meridiani hematite deposit on Mars. *J Geophys Res* 107(E10):5088
- Jahn A (1964) Slope morphological features resulting from gravitation. *Zeitschrift Geomorph. Suppl* 5:59–72
- Jarman D (2006) Large rock slope failures in the Highlands of Scotland: characterisation, causes and spatial distribution. *Eng Geol* 83:161–182
- Johnsson A, Reiss D, Hauber E, Zanetti M, Hiesinger H, Johansson L, Olvmo M (2012) Periglacial mass-wasting landforms on Mars suggestive of transient liquid water in the recent past: insight from solifluction lobes on Svalbard. *Icarus* n218(1)
- Kellerer-Pirklbauer A, Proske H, Strasser V (2010) Paraglacial slope adjustment since the end of the Last Glacial Maximum and its long-lasting effects on secondary mass wasting processes: Hauser Kaibling, Austria. *Geomorphology* 120:65–76
- Kinakin D, Stead D (2005) Analysis of the distributions of stress in natural ridge forms: implications for the deformation mechanisms of rock slopes and the formation of sacking. *Geomorphology* 65:85–100
- Kobayashi K (1956) Periglacial morphology of Japan. *Biuletyn Periglacialny* 4:15–36
- Kromuszczynska O, Mège D, Gurgurewicz J (2012) Giant sacking scarps in Valles Marineris. In: Abstract of the Lunar and planetary science conference 43. Lunar and Planetary Institute, Houston 1161.pdf
- Mahr T (1977) Deep-reaching gravitational deformations of high mountain slopes. *Bull Int Assoc Eng Geol* 16:121–127
- Malin MC, Edgett KS (2000) Sedimentary rocks of Early Mars. *Science* 290(12):1927–1937
- McCalpin JP, Irvine JR (1995) Sackungen at the Aspen Highlands Ski Area, Pitkin County, Colorado. *Environ Eng Geosci* 1:277–290
- McKenzie D, Nimmo F (1999) The generation of Martian floods by the melting of ground ice above dykes. *Nature* 397:231–233
- Mège D, Bourgeois O (2011) Equatorial glaciations on Mars revealed by gravitational collapse of Valles Marineris wallslopes. *Earth Planet Sci Lett* 310:182–191
- Merrien-Soukatchoff V, Quenot X, Guglielmi Y (2001) Modélisation par éléments distincts du phénomène de fauchage gravitaire. Application au glissement de La Clapière (Saint-Etienne-de-Tinée, Alpes-Maritimes). *Rev Fr Geotech* 95(96):133–142
- Metz JM, Grotzinger JP, Mohrig D, Milliken R, Prather B, Pirmez C, McEwen AS, Weitz CM (2009) Sublacustrine depositional fans in southwest Melas Chasma. *J Geophys Res* 114(E10):E10002
- Michalski JR, Niles PB (2011) Origin of martian interior layered deposits (ILDs) by atmospherically driven processes. In: abstract American Geophysical Union, Fall Meeting 2011
- Montgomery DR, Som SM, Jackson MPA, Schreiber BC, Gillespie AR, Adams JB (2009) Continental-scale salt tectonics on Mars and the origin of Valles Marineris and associated outflow channels. *GSA* 121:117–133
- Murchie S, Roach L, Seelos F, Milliken R, Mustard J, Arvidson R, Wiseman S, Lichtenberg K, Andrews-Hanna J, Bishop J, Bibring JP, Parente M, Morris R (2009) Evidence for the origin of layered deposits in Candor Chasma, Mars, from mineral composition and hydrologic modeling. *J Geophys Res* 114
- Nedell SS, Squyres SW, Andersen CW (1987) Origin and evolution of the layered deposits in the Valles Marineris, Mars. *Icarus* 70(3):409–414
- Nemčok A (1972) Gravitational slope deformation in high mountains. In: Proceedings of the 24th international geology congress, 13: pp. 132–141
- Nemčok A, Baliak F (1977) Gravitational deformations in Mesozoic rocks of the Carpathian mountain ranges. *Bull Int Assoc Eng Geol* 16:109–111

- Pánek T, Tábořík P, Klimeš J, Komárková V, Hradecký J, Šťastný M (2011) Deep-seated gravitational slope deformations in the highest parts of the Czech Flysch Carpathians: Evolutionary model based on kinematic analysis, electrical imaging and trenching. *Geomorphology* 129:92–112
- Peulvast JP, Masson PL (1993) Erosion and tectonics in central Valles Marineris (Mars): a new morpho-structural model. *Earth Moon Planet* 61:191–217
- Peulvast J-P, Mège D, Chiciak J, Costard F, Masson PL (2001a) Morphology, evolution and tectonics of Valles Marineris wallslopes (Mars). *Geomorphology* 37:329–352
- Peulvast J-P, Mège D, Chiciak J, Costard F, Masson PL (2001b) Morphology, evolution and tectonics of Valles Marineris wallslopes (Mars). *Geomorphology* 37:329–352
- Quantin C, Allemand P, Mangold N, Delacourt C (2004a) Ages of Valles Marineris (Mars) landslides and implications for canyon history. *Icarus* 172:555–572
- Quantin C, Allemand P, Mangold N, Delacourt C (2004b) Ages of Valles Marineris (Mars) landslides and implications for canyon history. *Icarus* 172:555–572
- Reitner JM, Linner M (2009) Formation and preservation of large scale toppling related to Alpine tectonic structures—Eastern Alps. *Aust J Earth Sci* 102:69–80
- Rocscience (2007) RocLab. Rocscience, Toronto, Ontario. <http://www.rocscience.com/highlights>
- Rodriguez JAP, Kargel J, Crown DA, Bleamaster LF, Tanaka KL, Baker V, Miyamoto H, Dohm JM, Sasaki S, Komatsu G (2006) Headward growth of chasmata by volatile outbursts, collapse, and drainage: evidence from Ganges chaos, Mars. *Geophy Res Lett* 33
- Rossi AP, Neukum G, Pondrelli M, Zegers T, Masson P, Hauber E, Ori GG, Fueten F, Oosthoek J, Chicarro A, Foing B (2007) The case for large-scale spring deposits on Mars: light-toned deposits in crater bulges. Valles Marineris and chaos, LPSC XXXVIII, Houston
- Rossi AP, Neukum G, Pondrelli M, Van Gasselt S, Zegers T, Hauber E, Chicarro A, Foing B (2008) Large-scale spring deposits on Mars? *J Geophys Res* 113(E08016):17
- Savage WZ, Varnes DJ (1987) Mechanics of gravitational spreading of steep-sided ridges (sackung). *Jaeg Bull.* 3(5):31–36
- Savage M, Tommasi A, Ellis S, Chery J (2007). Modeling strain and anisotropy along the Alpine fault, South Island, New Zealand. In: Okaya D, Stern T, Davey F (eds.) *Geotectonic Investigation of a modern continent–continent collisional orogen: the southern Alps*. American Geophysical Union, NZ
- Schultz RA (1995) Limits on strength and deformation properties of jointed basaltic rock masses. *Rock Mech Rock Eng* 28:1–15
- Schultz RA, Lin J (2001) Three-dimensional normal faulting models of the Valles Marineris, Mars, and geodynamic implications. *J Geophys Res* 106(B8):16549–16566
- Scott DH, Tanaka KL (1986) Geologic map of western equatorial region of Mars. U.S. Geol Surv Misc Geol Invest Map I-1802-A, 1:15000000 scale
- Sharp RP (1973) Mars: troughed terrain. *J Geophys Res* 78(20):4063–4072
- Silvestro S, Vaz DA, Fenton LK, Geissler PE (2011) Active aeolian processes on Mars: a regional study in Arabia and Meridiani Terrae. *J Geophys Res Lett* 38
- Tanaka KL, Golombek MP (1989) Martian tension fractures and the formation of grabens and collapse features at Valles Marineris. In: *Proceedings of the Lunar and Planetary science*, vol 19, 383–396
- Tanaka KL, Scott DH, (1987) Geologic map of the polar regions of Mars. U.S. Geol Surv Misc Geol Invest Map I-1802-C
- Tanaka KL, Rodriguez JAP, Fortezzo CM, Platz T, Michael G, Robbins S (2012) Geologic history of Valles Marineris, Mars, revisited. In: *Lunar and planetary science conference*, vol 43. Lunar and Planetary Institute, Houston, p 2, 2821.pdf
- Warner NH, Sowe M, Gupta S, Dumke A, Goddard K (2012) Connecting Valles Marineris to the northern plains: linkage by lake overspill and catastrophic flooding. In: *Proceedings of the 43rd Lunar and planetary science conference*, Houston, p 1237
- Williams J-P, Paige DA, Manning CE (2003) Layering in the wall rock of Valles Marineris: intrusive and extrusive magmatism. *Geophys Res Lett* 30(12):4
- Zischinsky U (1966) On the deformation of high slopes. In: *Proceedings of the 1st Congress International Society Rock Mechanics* 2, pp 179–185

Determination of Tetracyclines Residues in the Gulf of Gdańsk (Southern Baltic Sea) Sediments Using a Tandem Solid-Phase Extraction with Liquid Chromatography Coupled with Tandem Mass Spectrometry

Grzegorz Siedlewicz, Ksenia Pazdro, Marta Borecka, Kinga Kornowska, Anna Białk-Bielińska and Piotr Stepnowski

Abstract Pharmaceuticals are biologically active and relatively persistent substances which have been recently recognized as a continuing threat to the aquatic environment. Numerous adverse effects may arise for aquatic non-target organisms from the presence of pharmaceutical residues. One of the main pharmaceutical contaminants are antibiotics which are in the environment in considerable concentrations and can have negative biological effects to marine microorganisms. Despite of this, the knowledge on antibiotics occurrence, behaviour and fate in the Baltic Sea is very limited. This study presents the preliminary results on tetracycline and oxytetracycline residues occurrence in the sediments collected from the Gulf of Gdańsk (southern Baltic Sea). Among the antibiotics, tetracyclines are one of the most popular class used for human and animal therapy and for animal breeding. The method for tetracyclines residues determination was optimized, using two types of Baltic sediments (sandy and muddy) spiked at nine concentration levels (from 1 to 1,000 ng g⁻¹ d.w.) to achieve the best validation parameters. Acetonitrile and EDTA-McIlvaine extraction buffer solution (pH 4) (1:1) for extraction and tandem SPE technique with Discovery SAX and Oasis HLB cartridges for extracts clean-up were applied. Quantitative and qualitative

G. Siedlewicz (✉) · K. Pazdro
Institute of Oceanology, Polish Academy of Sciences, ul. Powstańców Warszawy 55,
81-712 Sopot, Poland
e-mail: gsiedlewicz@iopan.gda.pl

M. Borecka · K. Kornowska · A. Białk-Bielińska · P. Stepnowski
Department of Environmental Analysis, Faculty of Chemistry, University of Gdańsk, ul.
Sobieskiego 18, 80-952 Gdańsk, Poland

determination of analysed antibiotics was performed with the use of liquid chromatography tandem mass spectrometry (LC-MS/MS) with electrospray ionization source in the positive mode. The recoveries for target antibiotics ranged from 78.8 to 131.1 % for tetracycline and 75.5–114.8 % for oxytetracycline. The LOD values ranged from 1.5 to 3.5 ng g⁻¹ d.w. for tetracycline and from 1.2 to 2.2 ng g⁻¹ d.w. for oxytetracycline. The developed method was applied in the determination of tetracyclines in six sediments collected in 2012 during r/v “Oceania” cruises. Oxytetracycline was identified in four of analyzed samples at concentrations from 21 to 625 ng g⁻¹ d.w. Tetracycline was determined only in one sediment sample collected close to WWTP “Gdańsk Wschód” outlet (13.8 ng g⁻¹ d.w.). None of the target compounds was identified in the accumulation area—the Gdańsk Deep.

Keywords Tetracyclines residues • Sediments • SPE-LC-MS/MS • Baltic Sea

1 Introduction

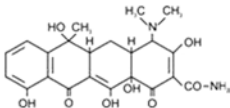
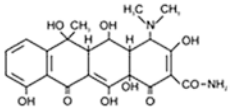
The use of pharmaceuticals is increasing worldwide. Among a wide variety of pharmaceuticals, antibiotics have been widely used to treat and prevent infectious diseases both in human and animals (Kümmerer 2008; Kemper 2008). These substances have been also often applied as growth promoters in livestock production, as feed additives in fish farm and to prevent crop damage induced by bacteria (Sarmah et al. 2006). The metabolism of antibiotics in the target organisms is incomplete, whereby they are excreted into environment via faeces or urines, and end up in the environment mainly through wastewaters effluents, surface runoff and the direct discharge from aquacultures (Sarmah et al. 2006). Continuous inputs of antibiotics have led to their important concentrations in the aquatic environment (Kümmerer 2008; Na et al. 2013). Although the major concern is associated with the development of resistance mechanisms in bacteria and its implications for human health, their sustained release to different environmental compartments and their bioactive properties also raise serious concerns about the toxicity of antibiotics to non-target aquatic organisms (Halling-Sørensen et al. 1998; Gonzalez-Pleiter et al. 2013). For this reason, the presence of pharmaceutical residues in aquatic environment, including marine ecosystems, is increasingly recognized as a potential environmental problem (Oskarsson et al. 2012). Antibiotics have been detected in many aquatic matrices, including drinking water, groundwater, river water (Hirsch et al. 1999; Sacher et al. 2001; Kümmerer 2008; Luo et al. 2011; Tamtam et al. 2008). Recent data show that contamination of the aquatic environment by antibiotics is not limited to freshwater ecosystems. The presence of selected antibiotics has been stated also in the case of marine waters (Gulkowska et al. 2007; Kümmerer 2008; Minh et al. 2009; Na et al. 2011; Thomas and Hilton 2004; Wille et al. 2010). However, otherwise to relatively large number of studies reporting the occurrence and fate of pharmaceutical residues in fresh waters environments, rather a few studies have investigated more extensively

the fate of antibiotics in sea waters. Moreover, only a few studies have been conducted on antibiotics residues in the marine sediment matrix (Yang et al. 2010; Zhou et al. 2011). Many of them are limited to the vicinity of aquacultures (e.g., Hektoen et al. 1995; Björklund et al. 1990; Lalumera et al. 2004; Ma et al. 2006). According to few available publications it was proved that antibiotics, especially tetracyclines, can be accumulated in sediments near the coast (Ma et al. 2006; Xu and Li 2010) and close to aquacultures (Hargrave et al. 2008; Lai and Hou 2008).

The lack of data is, in particular, visible in the Baltic Sea region. On the other hand, it is well known that natural features of the Baltic Sea, like water residence time of around 30 years, its shallowness and particularly large catchment area, make it susceptible to the accumulation of hazardous substances including new emerging contaminants (HELCOM 2010). This could be particularly true in the case of pharmaceuticals residues due to the fact that the Baltic Sea catchment area is home to about 85 million people and various branches of drugs industry, intensive farming and animal husbandry are located in the surrounding countries. However, there are only a few publications concerning pharmaceuticals occurrence in this area and are limited to water and fish (Beck et al. 2009; HELCOM 2010; Borecka et al. 2013; Vieno et al. 2007). The presence of selected sulfonamides and trimetoprim in the sediments from the Gulf of Gdańsk has been signalized quite recently (Siedlewicz et al. 2013). The presence of tetracyclines, one of the most popular antibiotic class in use, has not been reported as far in the Baltic Sea. Tetracyclines are a class of antibiotics characterized by a broad spectrum of activity, a relatively high degree of safety and low production costs, and are widely used both for growth promotion and therapeutic purposes in aquaculture and stockbreeding. 50 % of the veterinary antibiotics sold in France in 2004 were derived from tetracycline (Prado et al. 2009). Oxytetracycline was for many years of first choice as antibacterial agent in Norwegian fish farming (Hektoen et al. 1995). In Poland, oxytetracycline is the most popular drug of choice in the treatment of bacterial disease in fish (Harnisz et al. 2011). Antibiotics of this class are commonly used also in other Baltic countries (Schmidt et al. 2000). Residues of tetracyclines can persist for a long time, which makes them possible to reach and persist also in marine sediments (Wang et al. 2010). Existing data suggested long persistence of oxytetracycline in the environment.

Tetracyclines, like other pharmaceuticals, are present in the environment in low concentrations; this, together with the complexity of environmental matrices, makes their reliable determination difficult. Moreover, the use of method which is not precise and not accurate may implicate in overestimation or underestimation of the risk associated with presence of antibiotic residues in the marine environment. Extraction and clean-up efficiency are crucial steps in reliable antibiotics analysis in solid matrices. Various extraction methods for solid environmental matrices have been described (Blackwell et al. 2004; Lalumera et al. 2004). Tandem SPE method has been recently widely applied in extracts purification (Löffler and Ternes 2003; Halling-Sørensen et al. 2005; Yang et al. 2010). LC coupled to MS, particularly in tandem with MS has made impressive progress in the identification and quantitative determination of pharmaceutical residues in the environment (Nikolaou et al. 2007; Petrović et al. 2005; Borecka et al. 2013). However, still more methods have been described for determination of antibiotics, among them tetracyclines, in different water compartments than in marine sediments.

Table 1 Characteristics of the studied antibiotics

Name	CAS number	Chemical structure	Molecular weight (g mol ⁻¹)	pK _a	Log K _{ow}	Water solubility (mg L ⁻¹)
Tetracycline	60-54-8		444.4	3.30	-1.3	231
Oxytetracycline	79-57-2		460.4	3.27	-0.9	313

The latter is still more challenging due to the complexity of sediment matrix, interferences and longer sample preparation procedure.

The objectives of this work were (1) to develop an effective and sensitive method for tetracyclines (TCs) determination in the Baltic sediments and (2) to use the validated method to analyze these compounds in sediments samples collected from the Gulf of Gdańsk.

2 Materials and Methods

2.1 Reagents and Materials

Tetracycline and oxytetracycline were purchased from Sigma–Aldrich (Steinheim, Germany). The molecular structure and selected physicochemical properties of the tetracycline and oxytetracycline are shown in (Table 1). Separate standard stock solutions (100 mg L⁻¹) of individual compounds were prepared by dissolving an appropriate amount of each substance in methanol and stored in the dark at -18 °C. The stock solutions were mixed and diluted with methanol to prepare working solution (10 mg L⁻¹). To prepare calibration curves, working solution was diluted with water:acetonitrile 90:10 (v/v) to a proper concentration. All the solvents used were of HPLC grade and were obtained from Merck (Darmstadt, Germany). Ammonium acetate, acetic acid, citric acid, sodium acetate (all of analytical reagent grade) were purchased from POCH S.A. (Gliwice, Poland). Milli-Q water was prepared with a Mill-Q water purification system (Millipore, Germany).

2.2 Sediment Collection

Surface sediment samples were collected in 2012 from the Gulf of Gdańsk (southern Baltic Sea) during the cruises of r/v Oceania using Reineck or Niemistö corers. The location of sampling sites is shown in Fig. 1, while details



Fig. 1 Locations of sampling sites

Table 2 Location and characteristics of the sampling sites located in the Gulf of Gdańsk

Station number	Sampling site	Coordinates	Depth (m)	Sediment organic matter content (%)
1	Mouth of the Vistula, close to WWTP "Gdańsk Wschód" outlet	54°22,423 18°52,093	13	0.65
2	Mouth of the Vistula River	54°25,981 19°00,210	50	3.33
3	Central part of the Gulf of Gdańsk	54°29,317 18°56,660	64	15.30
4	Close to Hel Peninsula	54°32,717 18°46,304	52	9.97
5	Close to Gdynia Harbour	54°32,972 18°35,983	12	0.78
6	Gdańsk Deep	54°49,085 19°17,147	109	18.19
7	Outside Gulf of Gdańsk	54°55,088 18°29,985	30	0.45

of sampling sites and selected sediment characteristics are given in Table 2. The 0–5 cm layer of sediment was retrieved, frozen in pre-cleaned glass jars and transported to the laboratory, where the freeze-drying was carried out prior to chemical analyses.

2.3 Sediment Extraction

The extraction procedure of the collected sediment samples consisted of two steps: (a) extraction of the analytes from the sediment by sonification, and (b) enrichment and clean-up of the extract by SPE. The samples were extracted adopting the method described by Yang et al. (2010) and clean-up procedure was performed adopting the methods described by Blackwell et al. (2004) and Kołodziejka (2009).

In the case of the method development, before extraction 2.5 ml of working solution (10.0 mg L^{-1}) of the internal standard were spiked into the sediment to reach final concentration in sediment of $5 \mu\text{g g}^{-1}$ d.w. and kept in the dark at room temperature overnight to reach the equilibrium, then the excess of the solvent was evaporated at room temperature. Sediment blanks (sediment burned at $300 \text{ }^\circ\text{C}$ for 8 h) and laboratory blanks were analysed in parallel with the samples. Homogenized sediment samples of 5 g were weighed and placed into a 30-ml polypropylene centrifuge tubes, in which 10 ml of acetonitrile and 10 ml of EDTA-McIlvaine extraction buffer solution (pH 4) (1:1) (v/v) had been added. During the method development, different solutions of McIlvaine buffer or citric buffer were used to test extraction efficiency of tetracyclines from the spiked sediment. Finally, the extraction buffer consisted of a mixture (1:1 (v/v)) of 0.1 M Na_2EDTA and McIlvaine buffer. The McIlvaine buffer solution consisted of citric acid (0.2 M) and Na_2HPO_4 (0.4 M) in milli-Q water (3:2 v/v). Na_2EDTA was added to prevent the oxytetracycline from complexing with Ca^{2+} and Mg^{2+} ions and residual metals on the SPE cartridges (Lalumera et al. 2004). The samples were shaken for 1 min and placed in an ultrasonic bath for 20 min (water temperature $<30 \text{ }^\circ\text{C}$). The samples were then centrifuged for 10 min at 4,000 rpm (Sigma, Poland). Next, the supernatant was filtered through paper filter and collected in a glass flask. The extraction was repeated three times. The supernatants were combined and 1,440 ml of milli-Q water was added before clean-up step.

Discovery SAX (6 mL/500 mg; Sigma-Aldrich, Germany) and Oasis HLB (6 mL/500 mg; Waters, USA) cartridges were set up in tandem for clean-up of the aqueous sediment extracts. Different amounts of solvents for preconditioning were applied. Finally, each tandem column was preconditioned with 8 mL methanol and 8 mL of EDTA-McIlvaine diluted (20 times) extracting buffer solution. Each sediment extract was passed through the tandem cartridge at a flow rate of $\sim 6 \text{ mL min}^{-1}$ without allowing the cartridge to dry out. After sample loading the SAX cartridge was removed and the HLB was sequentially rinsed with 8 mL of diluted extracting buffer solution, 5 mL of 0.1 M sodium acetate, 8 mL of milli-Q water, 4 mL of 20 % methanol. Then the HLB cartridge was dried under vacuum for 20 min. The target compounds were eluted with 8 mL methanol. The methanol eluate was evaporated under gentle nitrogen stream to dryness and stored at $-18 \text{ }^\circ\text{C}$ until LC-MS/MS analysis. Just prior to the LC-MS/MS, the residue was reconstituted in 1 mL of mobile phase A, vortexed, centrifuged to remove particles and transferred to vials.

Table 3 Retention times, precursor and product ion masses used for LC-MS/MS analysis of tetracyclines

Compound	Retention time (min)	Precursor ion [M + H] ⁺ with isolation width	Product ions with isolation width	Fragmentation amplitude (V)
Tetracycline	7.6	445 ± 2.0	410 ^a ± 2.0 427 ± 2.0	0.80 0.90
Oxytetracycline	7.4	461 ± 2.0	426 ± 2.0 443 ^a ± 2.0	0.65 0.65

^aProduct ion used for quantification

2.4 LC-MS/MS Analysis

The LC separation was performed using an Agilent 1200 Series LC system (Agilent Technologies Inc., Santa Clara, USA) equipped with Gemini C18—110A column (150 × 4.6 mm, 5 μm pore size) (Phenomenex Inc., Torrance, CA). Mobile phase A consisted of H₂O:ACN (90:10, v/v, 1 mM NH₄Ac/AcH, pH 3.5) and mobile phase B was 100 % ACN. The flow rate was 0.3 mL min⁻¹. To optimize the chromatographic separation, a serial of preliminary experiments were performed to test different mobile phases gradients. The final gradient programme started with 18 % of mobile phase B, which was increased to 80 % within 15 min. The injection volume was 50 μL and the analytical wavelength was 359 nm. The LC flow was directly introduced into the mass spectrometer. The mass spectrometric measurements were carried out on an HCT Ultra ion trap mass spectrometer (Bruker Daltonics, Bremen, Germany) equipped with an electrospray ionization source. For data acquisition EsquireControl software was used. The source temperature was 350 °C. Nitrogen was employed as the nebulizer gas (30 psi) and the dry gas (10 L min⁻¹). Helium (99.999 %) was used as the collision gas in the ion trap. Analyses were performed in the positive mode for both compounds. Ions were acquired in multiple reaction monitoring mode. The optimized MS/MS conditions for the compounds are shown in Table 3.

2.5 Method Validation

The developed analytical procedure applying SPE-LC-MS/MS method was validated using sediment samples at nine spiking levels (1, 5, 10, 20, 50, 100, 200, 500, 1,000 ng g⁻¹ d.w. of sediment). Linearity, limits of detection (LODs), limits of quantification (LOQs) as well as precision and accuracy of the whole procedure were determined. The calibration curves were constructed by plotting peak area ratio (y) against analyte concentrations (x). Linearity was determined over a whole range of concentrations applied; however, for better accuracy of the results two concentration ranges were also applied (1–50 and 50–1,000 ng g⁻¹ d.w.). Each point was obtained as the average of five injections. The limits of detection

(LODs) of the method developed in this study for both analytes were evaluated by the measurement of 5 independent blank sediment samples fortified at the lowest acceptable concentration ($5 \text{ ng g}^{-1} \text{ d.w.}$). LODs were equal to three times standard deviation of the measured signals (Taverniers et al. 2004; Białk-Bielińska et al. 2009). The limits of quantification (LOQ) were calculated as three times the LOD values. The precision was determined by calculating the relative standard deviation (RSD) for the repeated measurements at each spiking level. Accuracy was calculated as agreement between the measured and known concentrations of each samples analyzed in the linearity ranges applied. The assessment of the influence of the matrix composition on the recovery of studied analytes was also performed. For this purpose, two types of sediments differing in granulometry and organic matter content were spiked with the same amount of tetracycline and oxytetracycline and analysed (station 7—outside the Gulf of Gdańsk; sandy sediment with low organic matter content; station 6—Gdańsk Deep—muddy sediment with high organic matter content).

3 Results and Discussion

3.1 Method Development

The method for tetracyclines residues determination was optimized to achieve the best validation parameters. Before elaboration of the most efficient extraction procedure, the optimum conditions for separation and detection should have been established. Chromatographic separation was achieved on Gemini C-18 column. Although complete separation is not necessary for selective MS-MS detection, it improves detectability and reduces the ion suppression effect (Białk-Bielińska et al. 2009). Therefore, different gradients of mobile phase were tested. Finally, the best separation was achieved applying the gradient programme started with 18 % of mobile phase B (acetonitrile), which was increased to 80 % within 15 min, resulting in relatively good separation of tetracycline and oxytetracycline. MS-MS detection parameters were optimized manually for each compound. After the best conditions for isolating the precursor ion had been determined, full scan MS/MSmode was used to record product ions from the standard solution of tetracyclines. For each compound, the fragmentation amplitude and isolation width were also optimized manually to increase the sensitivity and selectivity of the method and to select the two most intensive and characteristic fragmentation ions for qualitative analysis and one—of the highest intensity for quantitative analysis. Table 3 presents the results together with optimized fragmentation amplitude values for both compounds. 410 for tetracycline and 443 for oxytetracycline ions were selected as optimal quantification ions.

Extraction and SPE are the key steps in sample preparation; therefore, different solutions of McIlvaine buffer or citric buffer were used to test extraction efficiency of tetracyclines from the spiked sediment. A mixture of 0.1 M Na_2EDTA

and McIlvaine buffer (1:1 (v/v)) mixed with acetonitrile was finally chosen to be applied in further studies. Similarly different amounts of solvents were tested in clean-up procedure using tandem anion exchange cartridge (SAX) with a polymer cartridge (Oasis HLB) for preconditioning and elution. The recoveries for sediment at spiking level $5 \mu\text{g g}^{-1}$ d.w. were calculated. The detailed discussion of extraction and clean-up efficiency using different solvent will be presented elsewhere. The optimized solvent amounts applied finally in this study for extraction and SPE are listed in materials and methods.

Validation of the optimized method was performed using two sediments differing significantly in organic matter content and granulation. The results of the validation of the whole analytical procedure (SPE and LC-MS/MS) are presented in Table 4. The accuracy of the method was expressed as the mean recoveries of spiked analytes in sediment matrix. Recoveries were determined for 5 replicate samples at nine concentrations (1, 5, 10, 20, 50, 100, 200, 500, 1,000 ng g^{-1} d.w.). The sediments were fortified with antibiotics and subjected to the sample preparation procedure described above. The accuracy of the method was determined by assessing the agreement between the measured and known concentration of analyzed samples. Recoveries were calculated using an external calibration plot prepared for the sample matrix. At the lowest spiking level (1 ng g^{-1} d.w.) the recoveries increased enormously up to 320 % for tetracycline and 240 % for oxytetracycline. The main reason for the over-determinations was presumably an enhanced ionization due to the presence of matrix compounds. Such phenomena were also observed by Yang et al. (2010), reporting that sediment matrix components decreased signal responses of the sulfonamides, but increased signal responses of the tetracyclines, macrolides and fluorochinolones. The use of corresponding isotope-labeled internal standards of target compounds, if commercially available, would be a best choice to assess more precisely the matrix effects. Taking into account the aforementioned results, 5 ng g^{-1} d.w. was set as the lowest spiking acceptable concentration for LOD calculations. Produced average recoveries of tetracycline for remaining spiking levels ranged between 78.8 and 131.1 % for tetracycline and 75.5–114.8 % for oxytetracycline. The recoveries achieved in the present study were generally better than those reported by Yang et al. (2010) for the sediments from Pearl River in China spiked at the same levels (10, 50, 100 ng g^{-1}) and similar to those reported by Zhang et al. (2011). No tendency toward concentration-dependence was observed despite the wide concentration range. The same phenomena was reported by Jacobsen and Halling-Sørensen (2006) developing the method for tetracyclines, sulfonamides and tylosin determination in swine manure by LC-MS/MS. Furthermore, no tendency toward sediment type-dependence was demonstrated in this study. The recoveries for both type of sediments (sandy, poor in organic matter and muddy, rich in organic matter content) seem to satisfactory for applying this method to real samples analyses. Analyses of the blank samples, in which none of the analyzed compounds were detected, showed that the method also exhibited good selectivity.

The LOD values calculated as three times standard deviation of the measured signals blank sediment samples fortified at the lowest acceptable concentration

Table 4 Validation results for the entire analytical procedure applied to determine tetracycline and oxytetracycline in the Baltic sediments (SPE-LC-MS/MS)

Compound/matrix type	R ²	LOD (ng g ⁻¹ d.w.)	LOQ (ng g ⁻¹ d.w.)	Accuracy (%) Mean (RSD) n = 5					500 ng g ⁻¹ d.w.	1,000 ng g ⁻¹ d.w.
				10 ng g ⁻¹ d.w.	20 ng g ⁻¹ d.w.	50 ng g ⁻¹ d.w.	100 ng g ⁻¹ d.w.	200 ng g ⁻¹ d.w.		
Tetracycline/sandy sediment	0.98–0.99	1.51	4.54	131.1 (0.4)	81.6 (3.1)	96.1 (4.0)	113.5 (4.8)	86.4 (5.9)	109.5 (5.9)	98.5 (3.0)
Tetracycline/muddy sediment	0.98–0.99	3.52	10.55	99.1 (11.5)	92.1 (8.9)	122.4 (3.75)	91.6 (1.6)	78.8 (5.1)	108.2 (1.5)	98.8 (7.8)
Oxytetracycline/sandy sediment	0.99–1.00	2.16	6.49	98.9 (7.5)	92.0 (6.3)	101.4 (1.5)	107.7 (1.9)	75.5 (7.2)	110.2 (0.8)	98.3 (1.9)
Oxytetracycline/muddy sediment	0.98–1.00	1.23	3.70	114.8 (3.6)	96.9 (7.1)	96.0 (2.0)	88.8 (4.5)	99.1 (3.7)	105.1 (1.5)	98.9 (3.5)

n number of replicates

Table 5 Occurrence of tetracyclines residues in sediment samples collected from the Gulf of Gdańsk

Compound	Concentration (ng g ⁻¹ d.w.) (mean value ± SD) n = 3						
	Sampling station						
	1	2	3	4	5	6	7
Tetracycline	13.83 ± 3.00	n.d.	n.d.	n.d.	n.d.	n.d.	n.d.
Oxytetracycline	21.15 ± 0.03	435.3 ± 20.0	185.7 ± 6.1	625.2 ± 8.7	n.d.	n.d.	n.d.

n.d. not detected (below LOD)

ranged from 1.5 to 3.5 ng g⁻¹ d.w. for tetracycline and from 1.2 to 2.2 ng g⁻¹ d.w. for oxytetracycline. The corresponding LOQ values were 4.54–10.55 ng g⁻¹ d.w. for tetracycline and from 3.70 to 6.49 ng g⁻¹ d.w. for oxytetracycline. The linearity of the method was determined for both compounds. The calibration curves obtained for both compounds were linear over a wide range of concentrations from LOQ to 1,000 ng g⁻¹ d.w. with a determination coefficient (R²) > 0.988. The calibration curves were proved to be linear within the range of linear regression parameters of both matrix-matched and standard calibration curves. The precision of the proposed method was expressed by the RSD values [relative standard deviation (%)] of multiple (n = 5) analyses at each spiking concentration levels and was determined in the intraday tests. The results obtained in this study showed a narrow spread of the RSD values, indicating the reproducibility of the proposed method could be found satisfactory. Additionally, according to the U.S. EPA recommendations, the method is considered precise when RSD is less than or equal to 20 %. In the applied method, RSD values were in general well less 20 %.

The obtained results showed that an efficient and sensitive extraction and analytical method applying tandem SPE nad LC-MS/MS has been developed to determine tetracycline and oxytetracycline in the Baltic sediments. The use of a tandem anion exchange cartridge with a polymer cartridge for extracts clean-up was effective at removing most of interferences without significantly affecting the recovery of the studied compounds. The described method allows the determination of tetracycline and oxytetracycline in the Baltic sediments down to the lower ng g⁻¹ range with good precision and accuracy.

3.2 Sample Results

The applicability of the method to real samples was demonstrated by analyses of six surface sediment samples collected from the Gulf of Gdańsk. The results, expressed in ng g⁻¹ dry weight, are presented in Table 5. Among the two target compounds, oxytetracycline was detected at four locations and its concentration ranged from 21 to 625 ng g⁻¹ d.w. The highest concentration of 625 ng g⁻¹ d.w. was determined in the sediment collected at station located close to Hel Peninsula at 52 m depth. High amount of persistent, hydrophobic contaminants like polychlorinated biphenyls, lindane and polycyclic aromatic hydrocarbons were also noted at this location, situated near the Gdynia harbor

disposal site (Kowalkiewicz et al. 2013). The sediment was characterized by relatively high organic matter content (9.97 %). Tetracycline was detected only at one location—close to WWTP “Gdańsk Wschód” outlet. None of the analysed compound was detected in the Gdańsk Deep, accumulation area, where high concentrations of other contaminants were usually observed (Konat and Kowalewska 2001; Staniszevska et al. 2011; Beldowski and Pempkowiak 2003).

The comparison of the obtained data with the results reported for other marine ecosystems is rather difficult due to the lack of published data. In general, the tetracycline concentration measured close to WWTP “Gdańsk Wschód” outlet could be seen as similar to those observed in other examined coastal areas. The oxytetracycline concentrations observed in deeper parts of the Gulf of Gdańsk (except Gdańsk Deep) were similar or higher than those reported for river and marine sediments in other regions. Yang et al. (2010) found that the highest concentration of oxytetracycline was 335 ng g⁻¹ d.w. in the sediments of the Pearl River. In regards to marine sediments, oxytetracycline concentrations at the level of 400 ng g⁻¹ d.w. were reported by Capone et al. (1996) for sediments collected at the salmon mariculture facility in Puget Sound (Washington, USA). In contrast low ng g⁻¹ levels of oxytetracycline were observed by Lalumera et al. (2004) in sediment from seabass farm in Italian coastal waters. Na et al. (2013), studying the occurrence of 20 antibiotics in the coastal environment of Dalian (Yellow Sea), reported tetracycline level at low ng g⁻¹ d.w., whereas oxytetracycline was not detected in any sample despite its presence in seawater. The maximum concentrations of tetracycline measured by Liang et al. (2013) in Pearl River Estuary (South China Sea) sediment were in the range 2.64–6.62 ng g⁻¹ d.w. To our best knowledge, no data for European seas are available as far, except data reported by Lalumera et al. (2004).

These preliminary results demonstrated occurrence of oxytetracycline and into lesser extent tetracycline residues in the Gulf of Gdańsk sediments. However, a greater database is required to confirm this phenomenon for a larger area and to explain the environmental fate of the target compounds in this ecosystem. The differences in concentrations among the compounds and according to the sampling site could be attributed to many factors, such their local usage, distance from the source and physicochemical properties of target compounds. Tetracyclines may be quite persistent in marine environment under some conditions, with half-lives exceeding 400 days (Björklund et al. 1990; Capone et al. 1996; Hektoen et al. 1995). Some studies showed that tetracycline and oxytetracycline can be classified as non-biodegradable compounds (Capone et al. 1996; Prado et al. 2009). Sediment composition influencing sorption capacity as well as specific local hydrological and physicochemical conditions may also play an important role in tetracyclines transport, sorption and degradation processes. Sorption of TCs has been previously studied (Pouliquen and Bris 1996; Xu et al. 2009; Wang et al. 2010; Zhang et al. 2011). From these studies it follows that tetracyclines are effectively adsorbed onto marine sediments. Generally, cation exchange was proposed to be a primary mechanisms for tetracyclines sorption. Pouliquen and Bris (1996) showed that the sorption of tetracycline onto marine sediments increased with sediment content in organic matter. Wang et al. (2010) laboratory studies revealed that salinity (ionic strength) affected

sorption of tetracycline onto sediments. In general, sorption of tetracycline by sediment decreased with an increase in salinity. The main reason might be that the ionic competitors such as Cl^- and Na^+ could compete with (+0) and (+) species of tetracycline for interaction between sorbate and matrix surface. The increase of temperature led to decrease in tetracycline adsorption. According to Zhang et al. (2011), the presence of metallic ions greatly influences the sorption of tetracycline to soil and sediments, due to the formation of complexes between metallic ions and TC.

Consequently, the studies will be continued to establish more extensive database on tetracyclines spatial and temporal distribution in the southern Baltic Sea area and to explain this distribution pattern, taking into account the environmental conditions. Tetracyclines act as antimicrobials; therefore, their presence may influence several environmental processes carried by marine microorganisms. These microorganisms play a crucial role in nutrient cycling, organic matter mineralization and pollutant degradation (Ma et al. 2006; Yang et al. 2010). In eutrophicated seas like the Baltic Sea activity of microorganisms like heterotrophic bacteria is extremely important for nitrification and denitrification processes (Brettar et al. 2001). Thus, particular emphasis will be also placed on further investigations concerning the influence of identified compounds on bacterial communities living in the Baltic Sea sediments.

Acknowledgments This work was supported by the Polish Ministry of Science and Higher Education (project no. N N306 300536), National Science Centre (project no. DEC-2011/01/N/ST10/06977) and by the Institute of Oceanology of the Polish Academy of Sciences (statutory task no.II.2).

References

- Beck I-C, Brunh R, Gandrass J, Ruck W (2009) Estrogenic and pharmaceutical compounds—investigations in the German Baltic Sea. Publications of GKSS Research Centre. www.coast.gkss.de/internet/Poster-Iris-2.pdf. Accessed 05 July 2010 (2009)
- Beldowski J, Pempkowiak J (2003) Horizontal and vertical variabilities of mercury concentration and speciation in sediments of the Gdansk Basin, Southern Baltic Sea. *Chemosphere* 52:645–654
- Białk-Bielińska A, Kumirska J, Plavinskas R, Stepnowski P (2009) Optimization of multiple reaction monitoring mode for the trace analysis of veterinary sulfonamides by LC-MS/MS. *Talanta* 80:947–953
- Björklund H, Bondestam J, Bylund G (1990) Residues of oxytetracycline in wild fish and sediments from fish farms. *Aquaculture* 86:363–372
- Blackwell PA, Holtzen Ma, Halling-Sørensen B, Bocall A, Kay P (2004) Ultrasonic extraction of veterinary antibiotics from soil and pig slurry with SPE clean-up and LC-UV and fluorescence detection. *Talanta* 54:1058–1064
- Borecka M, Białk-Bielińska A, Siedlewicz G, Kornowska K, Kumirska J, Stepnowski P, Pązdro K (2013) A new approach for the estimation of expanded uncertainty of results of an analytical method developed for determining antibiotics in seawater solid-phase extraction disks and liquid chromatography coupled with tandem mass spectrometry technique. *J of Chromatogr A*. doi:10.1016/j.chroma.2013.07.018

- Brettar I, Moore ERB, Höfle MG (2001) Phylogeny and abundance of novel denitrifying bacteria isolated from the water column of the central Baltic Sea. *Microb Ecol* 42:295–305
- Capone DG, Weston DP, Miller V, Shoemaker C (1996) Antibacterial residues in marine sediments and invertebrates following chemotherapy in aquaculture. *Aquaculture* 145:55–75
- Gonzalez-Pleiter M, Gonzalo S, Rodea-Palomares I, Legane F, Rosal R, Boltes K, Marco E, Fernandez-Piñas F (2013) Toxicity of five antibiotics and their mixtures towards photosynthetic aquatic organisms: implications for environmental risk assessment. *Water Res* 47:2050–2064
- Gulkowska A, He Y, So MK, Yeung L, Giesy JP, Lam PK, Martin M, Richardson BJ (2007) The occurrence of selected antibiotics in Hong Kong coastal waters. *Mar Poll Bull* 54:1287–1306
- Halling-Sørensen B, Jacobsen AM, Jensen J, Sengelø VG, Vaclavik E, Ingerslev F (2005) Dissipation and effects of chlortetracycline and tylosin in two agricultural soils: a field-scale study in southern Denmark. *Environ Toxicol Chem* 24:802–810
- Halling-Sørensen B, Nors Nielsen S, Lanzky PF, Ingerslev F, Holten Liitzhøfl HC, Jørgensen SE (1998) Occurrence, fate and effects of pharmaceutical substances in the environment—a review. *Chemosphere* 36:357–393
- Hargrave BT, Doucette LI, Haya K, Friars FS, Armstrong SM (2008) A micro-dilution method for detecting oxytetracycline-resistant bacteria in marine sediments from salmon and mussel aquaculture sites and an urbanized harbour in Atlantic Canada. *Mar Pollut Bull* 56:1439–1445
- Harnisz M, Gołaś I, Pietruk M (2011) Tetracycline-resistant bacteria as indicators of antimicrobial resistance in protected waters—the example of the Drwęca River Nature Reserve (Poland). *Ecol Ind* 11:663–668
- Hektoen H, Berge J, Hormazabal V, Yndestad M (1995) Persistence of antibacterial agents in marine sediments. *Aquaculture* 133:175–184
- HELCOM (2010) Baltic Sea Environment Proceedings No. 120B Hazardous substances in the Baltic Sea—an integrated thematic assessment of hazardous substances in the Baltic Sea. <http://www.helcom.fi/stc/files/Publications/Proceedings/bsep120B.pdf>. Accessed 23 April 2013
- Hirsch R, Ternes T, Haberer K, Kratz KL (1999) Occurrence of antibiotics in the aquatic environment. *Sci Total Environ* 225(1–2):109–118
- Jacobsen AM, Halling-Sørensen B (2006) Multi-component analysis of tetracyclines, sulfonamides and tylosin in swine manure by liquid chromatography-tandem mass spectrometry. *Anal Bioanal Chem* 384:1164–1174
- Kemper N (2008) Veterinary antibiotics in the aquatic and terrestrial environment. *Ecol Ind* 8:1–13
- Kołodziejaska M (2009) Elaboration of a method for extraction, enrichment and quantitative determination of selected antibiotics applied in fish farms. M.Sc. thesis, University of Gdańsk, Chemistry Department, pp 92 (in polish)
- Konat J, Kowalewska G (2001) Polychlorinated biphenyls (PCBs) in sediments of the southern Baltic Sea—trends and fate. *Sci Total Environ* 280:1–15
- Kowalkiewicz Z, Pazdro K, Skauradzsun M, Jankowska D, Niemirydz E (2013) The influence of persistent organic pollutants (POPs) on the toxicity of sediments from the southern part of the Baltic Sea. In: Rosińska J, Neumann M (eds) *The functioning and protection of water ecosystems*. Adam Mickiewicz University, Poznań, pp 138–152
- Kümmerer K (2008) *Antibiotics in the environment*. In: Kümmerer K (ed) *Pharmaceuticals in the Environment*, 3rd edn. Springer, Berlin, pp 75–88
- Lalumera GM, Calamari D, Galli P, Castiglioni S, Crosa G, Fanelli R (2004) Preliminary investigation on the environmental occurrence and effects of antibiotics used in aquaculture in Italy. *Chemosphere* 54:661–668
- Lai HT, Hou JH (2008) Light and microbial effects on the transformation in four sulfonamides in eel pond water and sediment. *Aquaculture* 283:50–55
- Liang XM, Chen B, Xiangping N, Zhen S, Xiaoping H, Xiangdong L (2013) The distribution and partitioning of common antibiotics in water and sediment of the Pearl River Estuary, South China. *Chemosphere* 92:1410–1416
- Löffler D, Ternes (2003) Determination of acidic pharmaceuticals, antibiotics and ivermectin in river sediment using liquid chromatography–tandem mass spectrometry. *J Chromatogr A* 1021:133–144

- Luo Y, Xu L, Rysz M, Wang Y, Zhang H, Alvarez PJ (2011) Occurrence and transport of tetracycline, sulfonamide, quinolone, and macrolide antibiotics in the Haihe River Basin, China. *Environ Sci Technol* 45:1827–1833
- Ma D, Hu Y, Wang J, Ye S, Li A (2006) Effects of antibacterials use in aquaculture on biogeochemical processes in marine sediment. *Sci Total Environ* 367:273–277
- Minh TB, Leung HW, Loi I, Chan WH, So MK, Mao JQ, Choi D, Lam J, Zheng G, Martin M, Lee JH, Lam PK, Richardson BJ (2009) Antibiotics in the Hong Kong metropolitan area: ubiquitous distribution and fate in Victoria Harbour. *Mar Poll Bull* 58:1052–1062
- Na G, Gu J, Ge L, Zhang P, Wang Z, Liu C, Zhang L (2011) Detection of 36 antibiotics in coastal waters using high performance liquid chromatography–tandem mass spectrometry. *Chin J Oceanol Limnol* 29:1093–1102
- Na G, Fang X, Cai Y, Ge L, Zong H, Yuan X, Yao Z, Zhang Z (2013) Occurrence, distribution, and bioaccumulation of antibiotics in coastal environment of Dalian, China. *Mar Poll Bull* 69:233–237
- Nikolaou A, Meric S, Fatta D (2007) Review. Occurrence patterns of pharmaceuticals in water and wastewater environments. *Anal Bioanal Chem* 387:1225–1234
- Oskarsson H, Eriksson Wiklund A-K, Lindh K, Kumblad L (2012) Effect studies of human pharmaceuticals on *Fucus vesiculosus* and *Gammarus* spp. *Mar Environ Res* 74:1–8
- Petrović M, Hernando MD, Díaz-Cruz MS, Barceló D (2005) Liquid chromatography–tandem mass spectrometry for the analysis of pharmaceutical residues in environmental samples: a review. *J Chrom A* 1067:1–14
- Pouliquen H, Bris HL (1996) Sorption of oxolinic acid and oxytetracycline to marine sediments. *Chemosphere* 33:801–815
- Prado N, Ochoa J, Amrane A (2009) Biodegradation and biosorption of tetracycline and tylosin antibiotics in activated sludge system. *Process Biochem* 44:1302–1306
- Sacher F, Lange FT, Brauch HJ, Blankenhorn I (2001) Pharmaceuticals in groundwaters, analytical methods and results of a monitoring program in Baden-Württemberg, Germany. *J Chromatogr A* 938:199–210
- Sarmah A, Meyer M, Boxall B (2006) Review: a global perspective on the use, sales, exposure pathways, occurrence, fate and effects of veterinary antibiotics (VAs) in the environment. *Chemosphere* 65:725–759
- Schmidt AS, Bruun MS, Dalsgaard I, Pedersen K, Larsen JL (2000) Occurrence of antimicrobial resistance in fish-pathogenic and environmental bacteria associated with four Danish rainbow trout farms. *Appl Environ Microbiol* 66:4908–4915
- Siedlewicz G, Kotlarska E, Pazdro K (2013) Impact of antibiotic residues present in Baltic Sea sediments on the growth of sedimentary bacteria. Monographs book series Wrocław University of Technology Institute of Environmental Engineering, VII National Conference HYDROMICRO2013 Microorganisms–Human–Environment, accepted-in press
- Staniszewska M, Burska D, Sapota G, Bogdaniuk M, Borowiec K, Nosarzewska I, Bolałek J (2011) The relationship between the concentrations and distribution of organic pollutants and black carbon content in benthic sediments in the Gulf of Gdańsk, Baltic Sea. *Mar. Poll. Bull.* 62:1464–1475
- Tamtam F, Mercier F, Le Bot B, Eurin J, Dinh QT, Clement M, Chevreuil M (2008) Occurrence and fate of antibiotics in the Seine River in various hydrological conditions. *Sci Total Environ* 393:84–95
- Taverniers I, De Loose M, Bockstaele E (2004) Trends in quality in the analytical laboratory. II. Analytical method validation and quality assurance. *Trends Anal Chem* 23:535–551
- Thomas KV, Hilton MJ (2004) The occurrence of selected human pharmaceutical compounds in UK estuaries. *Mar Poll Bull* 49:436–444
- Vieno N, Tuhkanen T, Kronberg L (2007) Elimination of pharmaceuticals in sewage treatment plants in Finland. *Water Res* 41:1001–1012
- Wang J, Hu J, Zhang S (2010) Studies on the sorption of tetracycline onto clays and marine sediment from seawater. *J Colloid Interface Sci* 349:578–582
- Wille K, Noppe H, Verheyden K, Vanden Bussche J, De Wulf E, Van Caeter P, Janssen CR, De Brabander HF, Vanhaecke L (2010) Validation and application of an LC-MS/MS method for the simultaneous quantification of 13 pharmaceuticals in seawater. *Anal Bioanal Chem* 397:1797–1808

- Xu WH, Zhang G, Wai O, Zou SC, Li XD (2009) Transport and adsorption of antibiotics by marine sediments in a dynamic environment. *J Soils Sediments* 9:364–373
- Xu XR, Li XY (2010) Sorption and desorption of antibiotic tetracycline on marine sediments. *Chemosphere* 78:430–436
- Yang JF, Ying GG, Zhao JL, Tao R, Su HC, Chen F (2010) Simultaneous determination of four classes of antibiotics in sediments of the Pearl Rivers using RRLC–MS/MS. *Sci Total Environ* 408:424–432
- Zhang Z, Sun K, Gao B, Zhang G, Liu X, Zhao Y (2011) Adsorption of tetracycline on soil and sediment: effects of pH and the presence of Cu(II). *J Hazard Mater* 190:856–862
- Zhou L, Ying G, Zhao J, Yang J, Wang L, Yang B, Liu S (2011) Trends in the occurrence of human and veterinary antibiotics in the sediments of the Yellow River, Hai River and Liao River in northern China. *Environ Pollut* 159:188–1877

A Modern Approach to Aerosol Studies Over the Baltic Sea

A. Strzalkowska, P. Makuch, O. Zawadzka and P. Pakszys

Abstract Aerosols measured in coastal areas are significantly different from those over an open sea, both in terms of structure and physical properties. The aerosol composition and concentrations are generally uniform in the open sea area. In the case of coastal areas, the composition may be changed within a short period of time. Aerosols in coastal zone can be divided into three groups: the sea, a mixture of continental and maritime, and continental. This chapter describes the most representative day of a research campaign designed to characterize the optical properties of aerosols in the Baltic Sea (open sea and coastal areas). During the campaign, simultaneous measurements of aerosol optical depth were carried out at four stations around the Baltic Sea—Bornholm, Sopot, Preila and Liepaja, using the hand-held Microtops II sun photometers. The studies were supplemented with satellite data (MODIS) and the analysis of air mass back-trajectories at various altitudes and wind fields. Measurements were performed at four stations. Simultaneous measurements at these stations with use of Microtops sun photometer can provide important information on the aerosol optical depth (AOD) and hence on the radiation balance. Data obtained with Microtops complement well with those obtained from MODIS. Using wind field profiles we possibly detected sea surface impact on aerosol concentrations in Bornholm, where on 3 August 2011 the AOD was significantly greater, along with a strong onshore winds.

Keywords Aerosol • Baltic • Microtops • MODIS • AERONET • MAN

A. Strzalkowska (✉) · P. Makuch · P. Pakszys

Institute of Oceanology of the Polish Academy of Sciences, Sopot, Poland
e-mail: strzalkowska@iopan.gda.pl

O. Zawadzka

University of Warsaw, Warsaw, Poland

1 Introduction

Atmospheric aerosols are one of the most important components of Earth's atmosphere. According to the IPCC report, this is one of the basic "unknowns" in the climate research in the past decade (IPCC 2007). It is also a key issue in remote sensing measurements (Gao et al. 2000; Ruddick et al. 2000; Holton et al. 2003; Ichoku et al. 2004; Schroeder et al. 2007; Kratzer and Vinterhav 2010). Due to their direct (extinction of the Sun and Earth radiation) and indirect (participation in process of creation of clouds) effects on Earth's radiation balance aerosols influence both local and global climate (d'Almeida et al. 1991; Seinfeld and Pandis 1998; Kauffman et al. 2001; Chýlek et al. 2003; Stigebrandt and Gustafsson 2003; Satheesh and Moorthy 2005).

Aerosols effects strongly depend on particle optical properties. In order to describe these properties, two basic parameters are used: aerosol optical depth (AOD) and Ångström exponent. These properties strongly depend on the physical characteristics such as atmospheric humidity, wind direction and wind speed, which is an important factor affecting the production and transfer of aerosol particles in the atmosphere (Kastendeuch and Najjar 2003; Smirnov et al. 2003; Glantz et al. 2006).

The diversity of aerosol sources (natural and anthropogenic) and a relatively short lifetime are the main cause of spatial and temporal change of the particles composition. In connection with that, aerosol characterization and modeling are a real challenge, and it involves a strong emphasis on the development of remote sensing and ground-based photometric networks, which allow systematic and long-term measurements (Holben et al. 1998, 2001).

For many years, international projects, such as the Maritime Aerosol Network (MAN), which is a part of the NASA's AERONET Network, facilitated the creation of public databases. The data of these projects come from measurements made during research cruises, using Microtops sun photometers (Knobelspiess et al. 2004; Smirnov et al. 2003, 2009).

This chapter describes a modern approach to aerosol studies on a regional scale, such as the Baltic Sea area. We concentrate on both the open sea and coastal areas. As an example of the results we present the most representative day of a research campaign which took place in August 2011.

2 Marine Aerosols

The seas and oceans are among the largest natural sources of aerosol particles (Hobbs 2000). In the mid-1970s, it became clear that the knowledge of the optical properties of the marine aerosols is extremely poor. Experiments conducted on the sea and ocean territories started in 1980 because taking measurements in the different parts of oceans was often time-consuming and expensive venture.

Unfortunately, at that time measurement campaigns were not carried out systematically, experiments did not cover large areas and the accuracy of the measurement sometimes was poor or even unknown. However, the use of archival data enriches our understanding of the impact of aerosols on the climate over seas and oceans.

Marine aerosols can be divided into two types—one is the sea salt that enters the atmosphere due to the strong influence of wind on the sea surface. As a result, wind waves are formed and the particles are precipitated from the wave crests. Marine aerosols also can be generated by rainfalls or acoustic waves (Blanchard and Woodcock 1957; Blanchard 1963; Fitzgerald 1991). Sea salt particles are relatively large, i.e., above 2 μm in radius (Hobbs 2000). Emission of sea salt to the atmosphere strongly depends on the force, speed and direction of wind (Jacob et al. 1995). The second type of marine aerosol are dimethyl sulphide (DMS), which are emitted by phytoplankton into the atmosphere from the ocean surface. DMS is the largest source of biological aerosols and they oxidize to form methanesulfonic acid (MSA) and sulfate particles (Gabric et al. 2001, 2005).

The value of AOD in a clean environment oscillates around 0.01 for 500 nm (Porter et al. 2000) and in marine environment this value ranges between 0.06 and 0.08 (Smirnov et al. 2002). Greater values of AOD may result from long-range transport of aerosols from other areas. Especially in coastal areas such values can be greater than the clean condition ones (open oceans territory) due to the fact that in such regions winds may advect continental type or local emission particles into the study area.

2.1 Aerosols over the Baltic Sea

Despite strong focus on research and development of marine aerosol measurement techniques, only few experiments have been carried out in the Baltic Sea. The Baltic Sea, a good example of a regional sea, surrounded by highly industrialized countries, is difficult as a measurement area mainly due to the highly developed transport infrastructure and a large number of highly urbanized areas surrounding the sea.

Studies of aerosol properties over the Baltic Sea have been conducted in the 1990s (Zielinski et al. 1998, 1999; Zielinski and Zielinski 2002). The experiments carried out at that time involved mostly LIDAR (range of 1 km) measurements and they were conducted only in selected areas of the Polish coastal zone where the mixing of anthropogenic and marine aerosols could be observed. Some other studies were also made by Smirnov et al. (1995), Kuśmierczyk-Michulec and Rozwadowska (1999); Kuśmierczyk-Michulec and Marks 2000, Kuśmierczyk-Michulec et al. (2002); Niemi et al. (2003, 2005). However, most of the data reported in these articles were from short measurement campaigns.

Those studies showed that the AOD in the Baltic region ranges between 0.10 and 0.40 (500 nm). Similar values were recorded in the Mediterranean and the Black Sea (Smirnov et al. 2011). The dependence of optical properties of aerosols

in the Baltic region on air mass trajectories have been studied. For example, in the case of the Arctic air masses the AOD value was around 0.09; however, when the analyzed air mass flow from Scandinavia aerosol optical depth value was around 0.45 (Smirnov 1995). According to the analysis carried out for the southern Baltic Sea it was found out that the measurements of pure sea spray are most probable in the spring, when the weather conditions are dominated by strong winds from over the sea (Zielinski and Zielinski 2002). For wind speeds less than 6 m/s, the increase in the concentration of aerosol particles due to the increasing wind speed is usually associated with chemical and biological processes in the sea (Zieliński 2006). High proportion of sea spray mixed with continental industrial type can be seen mostly in the summer (Zdun et al. 2011).

3 Methodology and Instrumentation

3.1 Aerosol Optical Depth

The aerosol optical depth (AOD) is a function of concentration of aerosol particles, their size distribution and chemical composition. It is a dimensionless value which refers to the weakening of direct sunlight passing through the atmosphere. The parameter value changes with the height above the sea level (Zielinski and Zielinski 2002). The AOD value is dependent on the wavelength.

Ray of sunlight passing through the atmosphere attenuates on aerosol particles as a result of processes such as absorption and scattering. Radiation reduction can be expressed by the following formula (Dera 1983):

$$\frac{dL_\lambda}{dl} = -\varepsilon L_\lambda$$

where L_λ is a radiation light source, and ε is the ratio of light attenuation. Let us consider light beam with a wavelength λ and an infinitely small cross-section, which moves at an angle ϑ relative to the Earth surface. Leaving aside the scattering function after passing the length l the spectral radiant flux $L_\lambda(l)$ changes in relation to the primary stream $L_\lambda(0)$ by the following formula:

$$L_\lambda(l) = L_\lambda(0) \exp \left(-\frac{1}{\cos \vartheta} \int_0^l \varepsilon(\lambda, h) dh \right).$$

In this equation, $h = l \cos \vartheta$ (for horizontal positioning of the atmosphere) and $\varepsilon(\lambda, h)$ is the extinction coefficient at the wavelength λ . Then

$$\tau = \int_0^1 \varepsilon(\lambda, h) dh$$

is a dimensionless quantity called the aerosol optical depth of the atmosphere.

In coastal areas, mixing of marine and continental aerosols occurs depending on wind direction. AOD decreases with increasing wavelength and usually increases with increasing wind speeds. This is especially evident over the sea surface and coastal areas. In case of winds coming from the land (high concentration of continental aerosol) higher values of aerosol optical depth are recorded. When winds are from the sea (high concentration of marine aerosol) AOD value is usually lower. This mixture is composed of particles which have different optical properties which are significantly different from pure marine aerosols. The aerosol optical depth is highly influenced by the air masses flowing over the research area and meteorological conditions.

3.2 Ångström Exponent

Ångström exponent (α) is used to estimate the size of aerosol particles. The least square method is used to calculate α , with use of all available wavelengths between 400 and 870 nm. If $\alpha > 1$ the AOD is a result of the presence of small particles, when $\alpha < 1$ the AOD is related to large particles. The Ångström law (Zielinski 2006):

$$\tau_a(\lambda) = \tau_{a0}\lambda^{-\alpha}$$

where $\tau_a(\lambda)$ is a value of AOD for a wavelength λ and τ_{a0} is a value of AOD for 1 nm wavelength. After selection of two wavelengths, λ_1 and λ_2 , and fit it linear to the ratio of the difference of logarithms τ_a and difference of logarithms λ , the following expression for the Ångström exponent is valid:

$$\alpha = \frac{\ln \frac{\tau_{\lambda_1}}{\tau_{\lambda_2}}}{\ln \frac{\lambda_1}{\lambda_2}}$$

3.3 Microtops

Microtops sun photometer (produced by Solar Light Company USA) is a handheld device capable of measuring aerosol optical depth of atmospheric aerosols, direct irradiance in each band and the water vapor column. The device is equipped with five channels and each of channels has different wavelength value (e.g., 380, 440, 500, 675, 870 nm). Measurements are performed manually. The instrument is characterized by high accuracy which is provided by high-quality filters embedded in a solid cast aluminum housing. Microtops is easy to use. To take a measurement it is needed to aim the meter at the solar disc and when all optical channels are aimed precisely at the sun, the measurements will start after pressing the SCAN button. That procedure results in quick, lasting only 10 s, scanning of vertical column of atmosphere. During a single measurement the radiation is sent to the collimator and then after passing through narrow-band interference filter goes to

the photodiode. Measurements of current flowing through the junction are measured in photodiode. Received signal is amplified and converted to digital form by analog-to-digital converter.

Immediately after the measurement, the result can be conveniently viewed on LCD. The raw data collected during the measurements, as well as calculated results are stored in non-volatile memory. The data saved in memory are annotated with the date, time, geographical coordinates, altitude, atmospheric pressure, air temperature and the solar angle. One of the biggest advantages of the device is its weight and small size. Microtops can be linked with hand-held GPS via serial cable. Measurements can be performed in any chosen place, even on board of research vessels. A serial interface allows for the transfer of data from the instrument to any computer.

3.3.1 Microtops Calibration

First Microtops sun photometers were calibrated by Langley method in the Mauna Loa Observatory (MLO) in Hawaii in June 1995 ([http://www.solarlight.com/products/sunphoto.html](http://www.solarlig ht.com/products/sunphoto.html), Morys et al. 2001; Zielinski et al. 2012). This experiment made it possible to create a calibration algorithm which can be used with any instrument. Knowledge of the correct calibration constants is extremely important and necessary for the proper calculation of the values of the aerosol optical depth and Ångström exponent. The Langley calibration is based on measurements of the signal that reaches the detector at different positions of the Sun over the horizon. It is very important that during calibration the weather conditions are constant, which guarantees homogeneity of the atmosphere, the immutability of the AOD and content of water vapor in the atmosphere. During the measurements, sky must be cloudless, the Sun must not be overshadowed by even thin clouds. The Sun's rays passing through the atmosphere at different angles affect the signal change (constant weather conditions, change of the geometry of radiation transmission). The best conditions for the calibration are usually in the mountains above the planetary boundary layer. The measurements should be performed after sunrise or before sunset, when there are significant changes in the optical mass. The calibration should be performed with the least possible zenith angles exceeding 30°, every 10–15 min. The results of a correct calibration have been shown in Fig. 1 as a comparison of the AOD obtained from two Microtops II instruments.

With proper and systematic instrument calibration, data obtained during the measurement have adequate quality. Devices used in the analyzed period were calibrated during various campaigns, such as the MACRON in 2007 (Zielinski et al. 2012) or POLAR-AOD (<http://polaroad.isti.cnr.it:8080/Polar/>) in 2008 and 2012 in Tenerife and in Zugspitze in 2011. For the purpose of calibration we used the best calibration of all analyzed data from the above campaigns. We used four instruments during the campaign. The wavelengths and the calibration values for these instruments are presented in Table 1.

Fig. 1 Comparison of the AOD at 500 nm obtained between the reference Microtops II instrument #10562 and instrument #08489

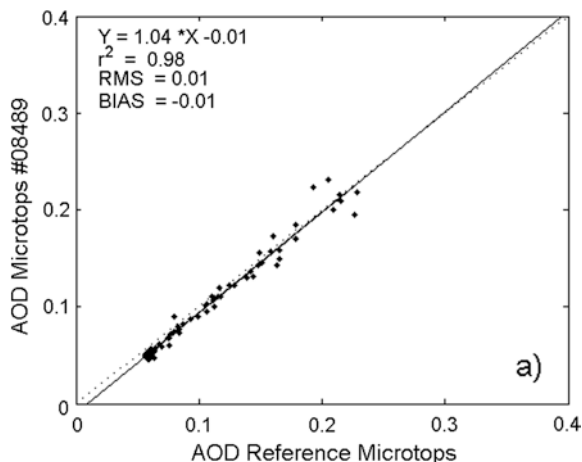


Table 1 Calibration values obtained for four Microtops II sun photometers

Microtops λ (nm)	340	380	440	500	675	870	1,020
SN 10562	–	7.6534	–	6.8347	7.0124	6.5218	7.0852
SN 08489	8.1937	7.5175	6.9518	6.8389	6.9496	–	–
SN 14475	–	7.8129	6.8425	6.7044	7.0236	6.6024	–
SN 15613	–	–	6.9014	6.7676	7.0388	6.5814	7.0667

4 Research Networks

4.1 Aeronet

AERONET (<http://aeronet.gsfc.nasa.gov>) is a global network established by NASA and PHOTONS (University of Lille, CNES and CNRS-INSU), which associates research stations performing remote, ground-based measurements of atmospheric aerosol properties. The network provides a long-term, easy and safe access to a public database of aerosol optical, microphysical and radiative properties for aerosol research and characterization and validation of satellite retrievals. The network imposes standardization of instruments, calibration, processing and distribution. The network processes the data according to an algorithm developed by NASA scientists. AERONET data are presented at three levels (1.0, 1.5, 2.0). Level 2.0 contains the data of the highest quality.

The measurement system at AERONET network is a solar-powered CIMEL 318 (Holben et al. 1998; Smirnov et al. 2003). Instrument measures Sun and sky radiances at a number of fixed wavelengths within the visible and near-infrared spectrum. CIMEL is equipped with two collimators (first collimator does not

have lens and the second has a built-in lens), electronics system and the robot. The measuring head has two built-in light detectors. These are silicon photodiode (measurements in the visible, near infrared and near ultraviolet) and InGaAs. The procedure involves measurement of solar radiation and sky radiation. The first one includes eight range of the spectrum. Sequential change in the interference filters made it possible to measure the intensity of radiation for several wavelengths. A single measurement lasts 10 s and consists of three sessions carried out in 30 s intervals. Measurements of sky radiation are performed after the direct measurement of solar radiation.

The measurement is performed in two sequences—azimuthally and zenithally. This allows to obtain high quality data for large range of angle of scattering of solar radiation. Aerosol optical thickness and size distribution of atmospheric aerosols are the result of this kind of action.

4.1.1 Maritime Aerosol Network

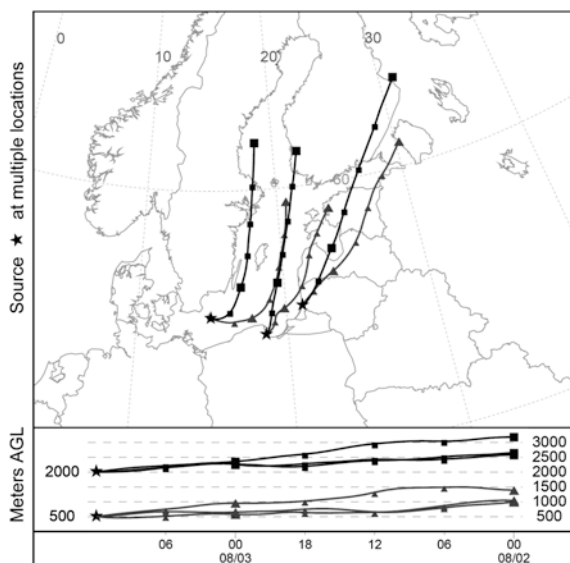
Since 2004 the Maritime Aerosol Network (MAN) (http://aeronet.gsfc.nasa.gov/new_web/maritime_aerosol_network.html) is a component of the AERONET network which provides ship-borne AOD measurements from the Microtops sun photometers. The network is focused on measurements of aerosol optical depth carried out during many research cruises.

The measurements are performed on the Atlantic Ocean, north and south Pacific, the southern Indian Ocean, the Arctic Ocean and inland seas such as the Baltic, the Black Sea and Mediterranean (Smirnov et al. 2011). These operations allow to monitor aerosol properties of atmospheric aerosols over the World Oceans. A copyright algorithm developed by the AERONET is used within the MAN for proper processing of the data. High quality data (free from measurement errors) can be downloaded from the MAN's internet page. Instruments are calibrated by the scientists from the NASA's Goddard Space Flight Center (GSFC) in Mauna Loa in Hawaii. Each Microtops sun photometer is calibrated by Langley method and then compared to the AOD values obtained with a CIMEL photometer. The estimated uncertainty of AOD measurements does not exceed value of ± 0.02 . Data obtained in this way are an alternative to the aerosol optical depth measurements carried out by Cimel sun photometers.

5 Comprehensive Approach to Aerosol Studies over the Baltic Sea

As an example of a modern approach to aerosol studies in the Baltic Sea, this article presents the results of analyses from a campaign which took place in the Baltic between 2 and 5 August 2011. During that time we performed simultaneous measurements at four stations (Sopot, Preila, Liepaja, and in Nexø, on the eastern coast of Bornholm) and the meteorological conditions were favorable

Fig. 2 HYSPLIT back-trajectories obtained for Borholm, Sopot, and Preila at 12:00 UTC on 3 August 2011. HYSPLIT model was run for 36 h with meteorological data from the GDAS



for such comprehensive study. The air mass trajectories have been calculated four times per day. The most representative altitudes for this study were 500 m a.s.l. (the potential impact of the sea surface) and 2,000 m a.s.l. (height above the boundary layer). We made simultaneous measurements with Microtops II sun photometers at all stations from morning till afternoon and we managed to collect different data sets at each station. This paper is focused on a case study of 3 August 2011.

On 3 August entire Poland was under a high pressure system. Lower parts of high pressure system over the northern part of the Baltic was stabilized because of advection of cold air masses from over Scandinavia. This situation enabled the continuous advection of cold air masses from the north. Stations Sopot, Liepaja and Nexo were influenced by the same streams of air masses. However, Sopot and Nexo differed slightly at 500 m a.s.l.. At 3,000 m a.s.l. Preila and Liepaja were influenced by clear air mass from North-East. Advection of air mass changes its direction to SE. Back trajectories at 2,000 m a.s.l. for 3 August show (Fig. 2) transport of Arctic air masses to southern part of the Baltic Sea.

Pollution transport model such as Navy Aerosol Analysis and Prediction System (NAAPS) can offer additional information on air pollution (Christensen et al. 1997; Witek et al. 2007). During the 3 August, air masses over the Baltic Sea were very clean. As it can be noticed in Fig. 3 no pollution with sulfates was predicted by the NAAPS over the studied area. Of course this is mainly a qualitative picture of the situation; however, it provides a general overview of the directions and the range of the sulfate distribution as well as robust concentration.

Microtops sun photometers with UV, visible, and IR wavelengths were used to retrieve AOD. In this study we used four Microtops instruments, one at every station. The instruments used during the study had the following technical characteristics (Table 2):

Fig. 3 Maps of sulfate mass mixing ratio ($\mu\text{g}/\text{m}^3$) at the surface from NAAPS model for 3 August 2011

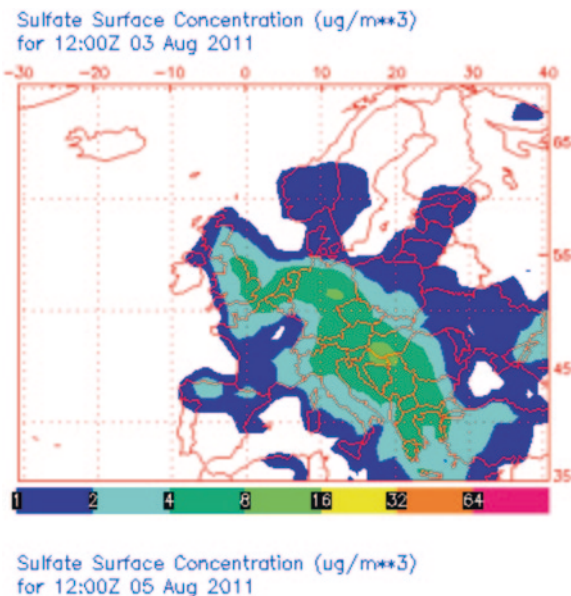


Table 2 Technical parameters of Microtops II sun photometers used during the studies

Optical channels	340 \pm 0.3 nm, 2 nm FWHM 380 \pm 0.4 nm, 4 nm FWHM 440 \pm 1.5 nm, 10 nm FWHM 500 \pm 1.5 nm, 10 nm FWHM 675 \pm 1.5 nm, 10 nm FWHM 870 \pm 1.5 nm, 10 nm FWHM 1020 \pm 1.5 nm, 10 nm FWHM
Resolution	0.1 Wm^{-2}
Dynamic range	>300,000
Viewing angle	2.5°
Precision	1–2 %
Non-linearity	Max. 0.002 %

Case study: 3 August 2011

On 3 August 2011 the measurements were performed at all stations. In Fig. 4 the AOD results at 500 nm are presented. The AOD values in Bornholm were slightly smaller than on 2 August and oscillated around 0.11. In Sopot and Liepaja a small decrease of the AOD was observed during the day. AOD values in Sopot ranged between 0.08 and 0.1 in Liepaja between 0.05 and 0.08. A similar trend was observed till 12:00 UTC on Preila—AOD between 0.08 and 0.09. Then the AOD significantly increased up to 0.13. These changes may be caused by some local effects or could indicate the advection from the land. HYSPLIT model did not show significant changes of the air mass transport in comparison to 2 August. Only the air mass (from the lowest troposphere) over Bornholm moved over the Baltic in the

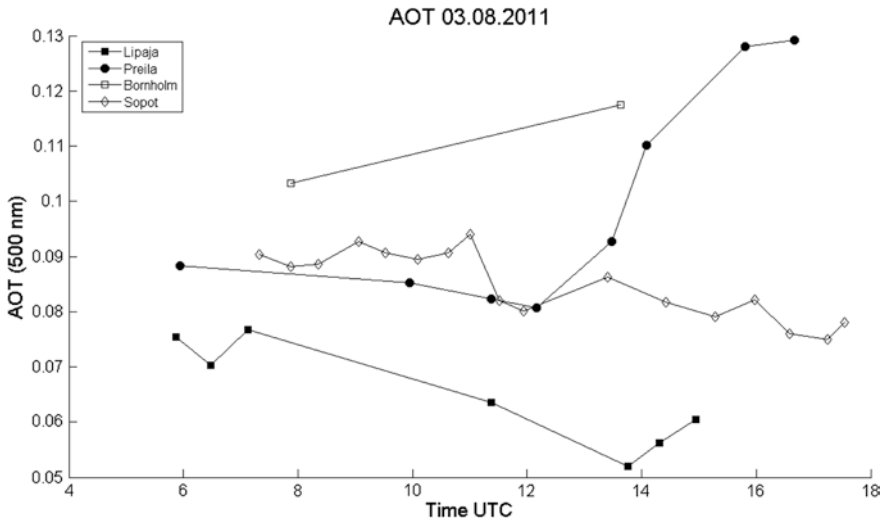


Fig. 4 Aerosol optical depth at 500 nm measured with Microtops II sun photometers on 3 August 2011 in Bornholm, Liepaja, Preila and Sopot

previous 36 h. In case of Sopot the flow over the planetary boundary layer (PBL) was over the Baltic Sea and the surface flow was over the Eastern Baltic Sea and over the coastal region of Latvia. Air masses over Preila and Liepaja were transported before mostly over the land. Unfortunately, for the correlation purposes between the four stations a relatively small number of data collected disqualifies such calculations since they would be very robust and based on a very weak bases.

The Ångström exponents are represented in Fig. 5 and show relatively high values for all stations. Its value varies significantly between the stations during the day. The lowest values were recorded in Sopot (between 1.4 and 1.6). In Preila, until around 2 p.m., relatively small particles were recorded, while later on during the day a significant drop in the exponent value can be observed indicating the presence of larger particles in the air.

5.1 Studies of Spatial Distribution of AOD on 3 August from the MODIS

Satellite data provided by the MODIS (Moderate Resolution Imaging Spectroradiometer) on board of Terra and Aqua satellite were also analyzed. Only data from Level 2 was used (Levy et al. 2010). The data obtained in the analysis were averaged for each day and gridded to 10×10 km spatial resolution. For the analyses it was assumed that the optical depth provided by the MODIS is only possible to estimate for cloudless pixels. The cloud mask was also checked for the chosen days. The overpasses for the Baltic Sea took place between 9:00 and 11:30

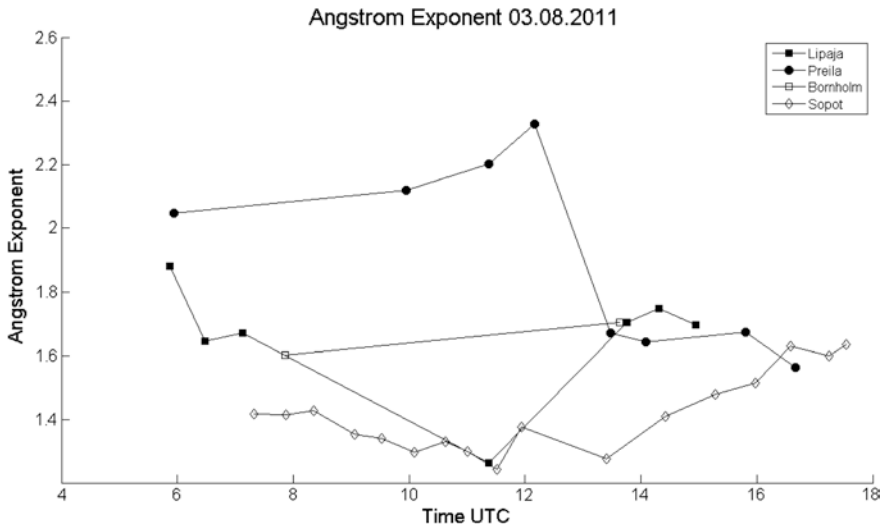
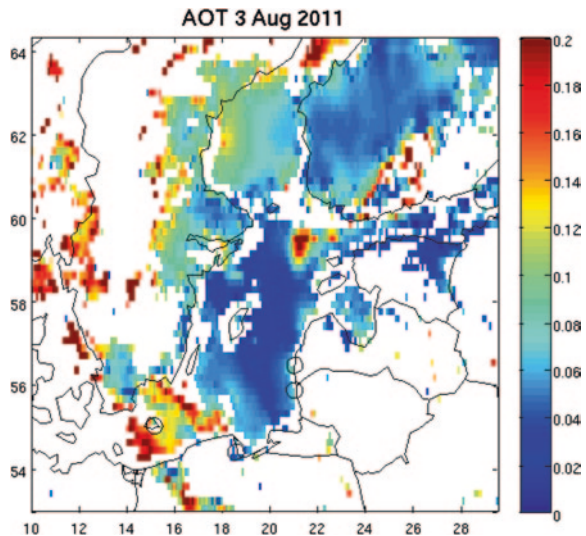


Fig. 5 Angstrom exponent obtained from Microtops II sun photometers on 3 August 2011 in Bornholm, Liepaja, Preila and Sopot

Fig. 6 Aerosol optical depth at 550 nm for the Baltic Sea area obtained from MODIS on 3 August 2011



UTC. On 3 August the AOD value was very low near the Gotland Island (about 0.05) and significantly higher around Bornholm (0.2–0.25) (Fig. 6).

On 3 August spatial variability of AOD over the Baltic Sea was significant despite stable air mass transport. It can be related to emission of sea salt and deposition processes (dry deposition only because of clear sky conditions). To verify this idea we made some analysis of wind speed using the 3D-CEMBS. Ecosystem

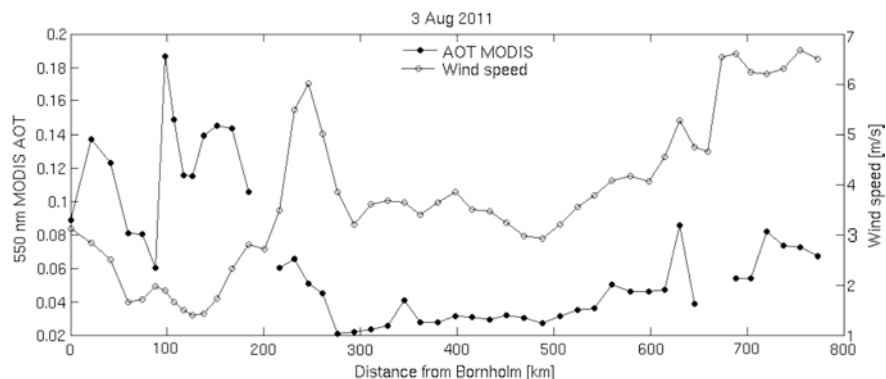


Fig. 7 Aerosol optical depth from MODIS (550 nm) on back trajectory ended at Bornholm on 3 August 2011 at 500 m a.s.l

Model of Baltic Sea. The model is forced by fields from the European Center for Medium Weather Forecast (ECMWF, ERA-40 reanalysis). Only data from lowest level (10 m) were used. Horizontal resolution of these data is 2 km. Figure 7 shows spatial variability of the AOD (solid line with open circles) and wind speed (solid line with dots). An average wind speed at a distance of 700–800 km from Bornholm was close to 7 m/s. At a distance of 500 km from Bornholm, the wind speed was 3 m/s. Along this back trajectory we can see good correlation with AOD, which decreased between 800 and 500 km from Bornholm. At a distance of 250 km from Bornholm wind speed was 6 m/s, and the value of AOD ranged from 0.02 to 0.06 (550 nm). Closer to the Island and the wind speed go down and AOD value increased to 0.19. In this area large temporal variability was recorded. This can be explained by the occurrence of unscrapped clouds, as well as to cloud microphysical processes involving hygroscopic aerosols.

6 Conclusions

The most representative measurement day during summer campaign in 2011 has been shown in the article. Measurements were performed at four stations around the Baltic Sea—Bornholm, Sopot, Preila and Liepaja. Simultaneous measurements at these stations with use of Microtops sun photometer can provide important information on the aerosol optical properties. On 3 August 2011, the AOD value near Bornholm was greater than that in other stations. This may be due to smaller number of collected data than in the other cases. This also can be related to the low wind speed which affects smaller local production of aerosols. The measurement results were complemented by satellite data (MODIS). Data obtained with Microtops have got good quality and complement well with those obtained from MODIS. The Microtops data quality has been further verified through the number

of calibration tests, also with an instrument from the NASA MAN program. Therefore, these instruments are ideal for measuring AOD in field campaign, especially when mobility is required. This one campaign provided a lot of experience and information on how to approach such measurements both scientifically and technically. Further campaigns on a similar or even larger scale, with use of a mobile platform such as a research vessel are planned in the near future.

Acknowledgments This research has been made within the framework of the NASA/AERONET Program and the support for this study was provided by the project Satellite Monitoring of the Baltic Sea Environment—SatBałtyk founded by European Union through European Regional Development Fund contract No. POIG 01.01.02-22-011/09. It has also been made within the framework of the NASA/AERONET Program.

References

- Blanchard DC, Woodcock AH (1957) Bubble formation and modification in the sea and its meteorological significance. *Tellus* 9:145–158
- Blanchard DC (1963) The electrification of the atmosphere by particle from bubbles in the sea. *Prog Oceanog* 1:171–202
- Christensen JH (1997) The Danish Eulerian hemispheric model: a three-dimensional air pollution model used for the Arctic. *Atmos Environ* 31:4169–4191
- Chylek P, Henderson B, Mishchenko M (2003) Aerosol radiative forcing and the accuracy of satellite aerosol optical depth retrieval. *J Geophys Res* 108(D24), 4764 pp
- d’Almeida G, Koepke P, Shettle EP (1991) Atmospheric aerosols: global climatology and radiative characteristics. A. Deepak Publication, Hampton, Va, 561 pp
- Dera J (1983) *Fizyka morza*, PWN (in Polish)
- Fitzgerald JW (1991) Marine aerosols: a review. *Atmos Environ ZSA* 25(3):533–546
- Gabric AJ, Gregg W, Najjar R, Erickson D, Matrai P (2001) Modelling the biogeochemical cycle of dimethylsulfide in the upper ocean: a review. *Chemosphere—global change. Science* 3:377–392
- Gabric AJ, Shepard JM., Knight JM, Jones G, Trevena AJ (2005) Correlations between the satellite-derived seasonal cycles of phytoplankton biomass and aerosol optical depth in the Southern Ocean: evidence for the influence of sea ice. *Global Biogeochemical Cycles* 19(GB4018). doi:10.1029/2005GB002546
- Gao B-C, Montes MJ, Ahmad Z, Davis CO (2000) Atmospheric correction algorithm for hyperspectral remote sensing of ocean color from space. *Appl Optics* 39(6):887–896
- Glantz P, Nilsson DE, von W Hoyningen-Huene (2006) Estimating a relationship between aerosol optical thickness and surface wind speed over the ocean. *Atmos Chem Phys Discuss* 6:11621–11651
- Hobbs PV (2000) *Introduction to atmospheric chemistry*. Cambridge University Press, USA, pp 82–100
- Holben BN, Eck TF, Slutsker I, Tanre D, Buis JP, Setzer A, Vermote E, Reagan JA, Kaufman YJ, Nakajima T, Lavenue F, Jankowiak I, Smirnov A (1998) AERONET—a federated instrument network and data archive for aerosol characterization. *Remote Sens Environ* 66(1):1–16
- Holben BN, Tanre D, Smirnov A, Eck TF, Slutsker I, Abuhassan N, Newcomb WW, Schafer J, Chatenet B, Lavenue F, Kaufman YJ, Vande Castle J, Setzer A, Markham B, Clark D, Frouin R, Halthore R, Karnieli A, O’Neill NT, Pietras C, Pinker RT, Voss K, Zibordi G (2001) An emerging ground-based aerosol climatology: aerosol optical depth from AERONET. *J Geophys Res* 106:12067–12097
- Holton JR, Curry JA, Pyle JA (2003) *Encyclopaedia of atmospheric science*, vol 1. Academic Press, Amsterdam, Boston, p 53

- Ichoku C, Kaufman YJ, Remer LA, Levy R (2004) Global aerosol remote sensing from MODIS. *Adv Space Res* 34:820–827
- IPCC Fourth Assessment Report (AR4), Climate Change (2007): Synthesis Report
- Jacob D.J., Andreas M.O., Bigg E.K., Duce R.A., Fung I., Hidy G.M., Legrand M., Prospero J.M., Raes F., Warren S.G., Wiedensohler A. (1995). Group Report: What Factors Influence Atmospheric Aerosols, How Have They Changed in the Past, and How Might They Change in the Future, in *Aerosol Forcing of Climate* Edited by R.J. Charlson and J. Heintzenburg. Wiley, pp. 183–195
- Kastendeuch PP, Najjar G (2003) Upper-air wind profiles investigation for tropospheric circulation study. *Theor Appl Climatol* 75:149–165
- Kauffman YJ, Smirnov A, Holben BN, Dubovik O (2001) Baseline maritime aerosol: methodology to derive the optical thickness and scattering properties. *Geophys Res Lett* 28(17):3251–3254
- Knobelspiesse KD, Pietras C, Fargion GS, Wang M, Frouin R, Miller MA, Subramaniam A, Balch WM (2004) Maritime aerosol optical thickness measured by handheld sun photometers. *Remote Sens Environ* 93:87–106
- Kratzer S, Vinterhav C (2010) Improvement of MERIS level 2 products in Baltic Sea coastal areas by applying the improved contrast between ocean and land processor (ICOL)—data analysis and validation. *Oceanologia* 52(2):211–236
- Kuśmierczyk-Michulec J, Rozwadowska A (1999) Seasonal changes of the aerosol optical thickness for the atmosphere over the Baltic Sea—preliminary results. *Oceanologia* 41(2):127–145
- Kuśmierczyk-Michulec J, Marks R (2000) The influence of sea-salt aerosols on the atmospheric extinction over the Baltic and North Seas. *J Aerosol Sci* 31(11):1299–1316
- Kuśmierczyk-Michulec J, de Leeuw G, Gonzalez CR (2002) Empirical relationships between mass concentration and Ångström parameter. *Geophys Res Lett* 29(7):1145. doi:[10.1029/2001GL014128](https://doi.org/10.1029/2001GL014128)
- Levy RC, Remer LA, Kleidman RG, Ichoku C, Kahn R, Eck TF (2010) Global evaluation of the collection 5 MODIS dark-target aerosol products over land. *Atmos Chem Phys* 10:10399–10420. doi:[10.5194/acp-10-10399-2010](https://doi.org/10.5194/acp-10-10399-2010)
- Morys M, Mims III FM, Hagerup S, Anderson SE, Baker A, Kia J, Walkup T (2001), Design, calibration, and performance of MICROTOPS II handheld ozone monitor and sun photometer. *J Geophys Res* 106(D13), 14573–14582. doi:[10.1029/2001JD900103](https://doi.org/10.1029/2001JD900103)
- Niemi JV, Tervahattu H, Koskentalo T, Sillanpää M, Hillamo R, Kumala M, Vehkamäki H (2003) Studies on the long-range transport episodes of particles in Finland in March and August 2002. Helsinki Metropolitan Area Council 10, 58 pp
- Niemi JV, Tervahattu H, Vehkamäki H, Martikainen J, Laakso L, Kumala M, Aarnio P, Koskentalo T, Sillanpää M, Makkonen U (2005) Characterization of aerosol particles episodes in Finland caused by wildfires in Eastern Europe. *Atmos Chem Phys* 5(8):2299–2310
- Porter JN, Miller M, Pietras C, Motell C (2000) Ship-based sun photometer measurements using sun photometers. *J Atmos Oceanic Technol* 18:765–774
- Ruddick KG, Ovidio F, Rijkeboer M (2000) Atmospheric correction of SeaWiFS imagery for turbid coastal and inland waters. *Appl Optics* 39(6):897–912
- Satheesh SK, Moorthy KK (2005) Radiative effects of natural aerosols: a review. *Atmos Environ* 39(11):2089–2110
- Schroeder T, Behnert I, Schaale M, Fischer J, Doerffer R (2007) Atmospheric correction algorithm for MERIS above case-2 waters. *Int J Remote Sens* 28(7):1469–1486
- Seinfeld JH, Pandis SN (1998) *Atmospheric chemistry and physics: from air pollution to climate change*. Wiley, New York, p 1326
- Smirnov A, Holben BN, Slutsker I, Giles DM, McClain CR, Eck TF, Sakerin SM, Macke A, Croot P, Zibordi G, Quinn PK, Sciare J, Kinne S, Harvey M, Smyth TJ, Piketh S, Zielinski T, Proshutinsky A, Goes JI, Nelson NB, Larouche P, Radionov VF, Goloub P, Krishna Moorthy K, Matarrese R, Robertson EJ, Jourdin F (2009) Maritime aerosol network as a component of aerosol robotic network. *J Geophys Res* 114:1–10. doi:[10.1029/2008JD011257](https://doi.org/10.1029/2008JD011257)
- Smirnov A, Holben BN, Dubovik O, O’Neill NT, Eck TF, Westphal DG, Goroch AK, Pietras C, Slutsker I (2002) Atmospheric aerosol optical properties in the Persian Gulf. *J Atmos Sci* 59:620–634

- Smirnov A, Holben BN, Eck TF, Dubovik O, Slutsker I (2003) Effect of wind speed on columnar aerosol optical properties at Midway Island. *J Geophys Res* 108(D24), 10 4802 pp. doi:[10.1029/2003JD003879](https://doi.org/10.1029/2003JD003879)
- Smirnov A A, Villevalde Y, O'Neill NT, Royer A, Tarussov A (1995) Aerosol optical depth over the ocean: analysis in term of synoptic air mass type. *J Geophys Res* 100(D8):16639–16650
- Smirnov, Holben BN, Giles DM, Slutsker I, O'Neill NT, Eck TF, Macke A, Croot P, Courcoux Y, Sakerin SM, Smyth TJ, Zielinski T, Zibordi G, Goes JI, Harvey MJ, Quinn PK, Nelson NB, Radionov VF, Duarte CM, Losno R, Sciare J, Voss KJ, Kinne S, Nalli NR, Joseph E, Krishna Moorthy K, Covert DS, Gulev SK, Milinevsky G, Larouche P, Belanger S, Horne E, Chin M, Remer LA, Kahn RA, Reid JS, Schulz M, Heald CL, Zhang J, Lapina K, Kleidman RG, Griesfeller J, Gaitley BJ, Tan Q, Diehl TL (2011) Maritime aerosol network as a component of AERONET—first results and comparison with global aerosol models and satellite retrievals. *Atmos Meas Tech* 4:583–597. doi:[10.5194/amt-4-583-2011](https://doi.org/10.5194/amt-4-583-2011)
- Stigebrandt A, Gustafsson BG (2003) Response of the Baltic Sea to climate change-theory and observations. *J Sea Res* 49(4):243–256
- Witek ML, Flatau PJ, Quinn PK, Westphal DL (2007) Global sea-salt modeling: results and validation against multicampaign shipboard measurements. *J Geophys Res* 112:D08215. doi:[10.1029/2006JD007779](https://doi.org/10.1029/2006JD007779)
- Zdun A, Rozwadowska A, Kratzer S (2011) Seasonal variability in the optical properties of Baltic aerosols. *Oceanologia* 53(1):7–34
- Zielinski T (1998) Changes in aerosol concentration with altitude in the marine boundary layer in coastal areas of the Southern Baltic Sea. *Bull Pol Acad Sci Earth Sci* 46(3–4):133–139
- Zielinski T, Petelski T, Makuch P, Strzalkowska A, Ponczkowska A, Markowicz K, Chourdakis G, Georgoussis G, Kratzer S (2012) Studies of aerosols advected to coastal areas with use of remote techniques. *Acta Geophys* 60(5):1359–1385. doi:[10.2478/s11600-011-0075-4](https://doi.org/10.2478/s11600-011-0075-4)
- Zielinski T, Zielinski A, Piskozub J, Drozdowska V, Irczuk M (1999) Aerosol optical thickness over the coastal area of the southern Baltic Sea. *Optica Applicata XXIX*(4):339–447
- Zielinski T, Zielinski A (2002) Aerosol extinction and optical thickness in the atmosphere over the Baltic Sea determined with lidar. *J Aerosol Sci* 33(6):47–61
- Zielinski T (2006) Physical properties of aerosol near-water layer in coastal areas. *Rozprawy i Monografie IOPAN* 18:164 (in Polish)

Water in the Deepest Crater of Mars

Natalia Zalewska

Abstract Hellas crater is a potential area where episodes of liquid water may appear. The depth of the structure (7,152 m below the standard topographic datum of Mars) explains the atmospheric pressure at the bottom: (11.55 mbar). This is higher than the pressure at the topographical datum (6.1 mbar) and above the triple point of water. That is why PFS and OMEGA, infrared spectrometers installed on Mars Express probe already determined the presence of minerals normally associated with the presence of liquid water on Hellas. Frequency of $1,160\text{ cm}^{-1}$ has been identified in the spectra of the PFS, that fits very well to the band of sulfates. The band responsible for the occurrence of clay minerals associated with the presence of water on Hellas has been also found in the spectra obtained with the OMEGA instrument.

Keywords Mars • Hellas • Infrared spectroscopy • Sulphates • Clay minerals

1 Introduction

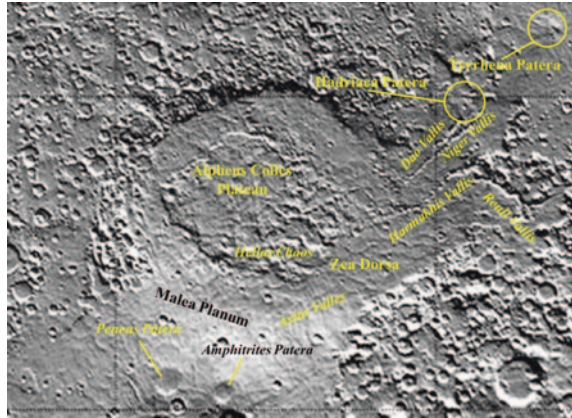
On the southern hemisphere of Mars, there is a gigantic oval area, measuring 3,000 km for 1,500 km, observed and described for the first time in the 19th century by English astronomer Richard Anthony Proctor, and then by Italian astronomer Giovanni Schiaparelli, who gave him the final name of Hellas. The center of the area lies on the 295° W and 40° S . The Hellas basin is an impact crater created about 3.9 billion years ago, in the early Noachian (see the Appendix). It is an impact site of the asteroid which was likely to hit from the south-east, forming a huge elliptical crater. Since the stroke occurred at an angle of less than 90° , the crater has an oval shape

N. Zalewska (✉)

Space Research Centre PAS, Bartycka 18 A, 00-716 Warsaw, Poland

e-mail: natalia@cbk.waw.pl

Fig. 1 Image from the Mars Orbiter Laser Altimeter (MOLA)—Mars Global Surveyor (MGS)



and its average depth is 6 km from the zero reference level (zero level is an equipotential surface whose average radius at the equator of Mars is 3394.2 km), while the innermost (-7.5 km) site is located in the northern part of the basin, which is the deepest location on the surface of Mars. The crater is surrounded by a 2 km high rock rim, formed by material thrown out and pushed out during the impact. Object that caused the collision probably had a diameter of about 300 km (Melosh and Beyer 2000; Collins and Melosh 2005). As a result, this collision created a large central uplift and several multiple concentric rings as isostatic response of the bedrock; this is typical for large crater forming events. Unfortunately, over billions of years, these morphological characteristics of the crater have completely eroded (Fig. 1).

If we look at the crater from top to bottom, we see that the basin is relatively smooth, dust-filled, with numerous small impact craters. In addition, based on the data from MOLA (Mars Orbiter Laser Altimeter) and MOC (Mars Orbiter Camera) installed on the probe Mars Global Surveyor (MGS), forms such as monadnocks, mesas yardangs and dune fields, polygonal forms associated with thermokarst and fluvio-glacial forms: moraines, drumlins and eskers as residue from the prevailing ice cap can be observed (Thomson and Head 1999). A vast number of branching channels lead to the bottom of the basin, the most visible from the east side being the Dao Vallis, Niger Vallis, Harmakhis Vallis, and Reull Vallis (Fig. 1). These channels are interpreted to be supplying water to the basin (Moore and Wilhelms 2001; Thomson and Head 2001), late volcanism lava channels on Tyrrhena Patera (Lahtela 2003), or earlier eroded tectonic cracks after impact, later filled by water. Coastline of the proglacial lake once filling Hellas basin is visible by MOLA (Thomson and Head 1999). The lake was filled by a system of canals supplying water released from the glacier or earlier by volcanic and geothermal processes (Moore and Wilhelms 2001; Thomson and Head 2001). The material filling the Hellas crater is layered, eroded, showing parallel layering, consolidated or loose, creating dune fields between mesas or specific ripplemarks in a smaller scale. Such features of the basins morphology are confirmed by the latest display of the High Resolution Camera

of HiRISE (High Resolution Imaging Science Experiment), installed on the Mars Reconnaissance Orbiter probe. Deposition of this material could have occurred during sedimentation of river, lake and during aeolian processes in the late Hesperian and Amazonian (see the Appendix). The thickness of the deposited material is determined to be 100–200 m (Tanaka and Leonard 1995; Leonard and Tanaka 2001; Crown and Pierce 2002; Crown et al. 2009) (Fig. 1).

2 General Geomorphology of Hellas

Based on images from MOLA, morphologically different parts of Hellas have been isolated (Moore and Wilhelms 2001). The basin is surrounded in its north-western part by the cratered area, one of the oldest areas of Mars. The rim around Hellas is covered by regolith, which is traversed by the east side sloping down to the previously mentioned basin's channels. The material that surrounds the channel is characterized as volcanic, or having the characteristics of basaltic lava. The interior of Hellas is rather flat, covered with dust of aeolian origin, except for a large pyroclastic plateau, located in the central part of the basin with highlighted areas of Alpheus Colles and Hellas Chaos, with predominant characteristics of wind erosion gullies and yardangs, the inselberg of a kind. A part of the plateau is also a very smooth terrain named Zea Dorsa, showing characteristics of aeolian activity. The plateau is probably an eroded central uplift after the collision with an asteroid which formed the crater. Moreover, irregular and “honeycomb” like material has been distinguished in the innermost north-west region of the reservoir, which presents the characteristics of the thermokarst after ice has melted. It is interpreted also as a remnant of the lake resulting from the melting of ice. “Honeycomb” material consists mainly of forms similar to kames and eskers and forms a kind of cirques, which indicate glacial and glaciﬂuvial activities. In addition, in the western part small rounded channels can be observed (Moore and Wilhelms 2001).

3 Volcanism of Hellas's Surroundings

The south-western rim of Hellas basin and adjacent eastern part of the area, along with canals that lead to the basin, exhibits properties of volcanic remnants (late Noachian). There have been such forms as: oval volcanic cones, solidified lava streams, undulating ridges, shield volcanoes and likely stratovolcanoes (Peterson 1978). South of Hellas is an area called Malea Planum, cut up in the north of the Hellas by narrow channels Axius Valles, where a complex of five calderas can be distinguished, the largest being Amphitrites Patera and Peneus Patera. To the east of Hellas, individual volcanoes Hadriaca Patera and Tyrrhena Patera are observed (Tanaka and Leonard 1995; Fig. 1). The former hypothesis is that they may have originally been impactor type craters, converted into the caldera volcanoes (Peterson

1978). It is believed that volcanism lasted quite a long time and repeated on a regular basis. Isolated volcanic cones such as Hadriaca Patera and Patera Tyrrhena stratovolcanoes were interpreted as alternately throwing lava and pyroclastic material, with a predominance of tephra in the final phase of their activity. However, Amphitrites Patera caldera complex and Peneus Patera could be the cause only of basalt lava flows. The most impressive cone is Hadriaca Patera, which seems to be the youngest of all volcanoes surrounding Hellas, and has the least erosion features. Tyrrhena Patera, a crater older than Hadriaca, has a collapsed cone through which channels extend radially. The caldera south of Hellas (Amphitrites Patera) represents the old type of volcanism on Mars (Murray et al. 1981; Tanaka and Leonard 1995). The crater is located on the second or third concentric ring of Hellas, which results in gravity anomalies here (Peterson 1978; Murray et al. 1981; Richardson 2002).

4 Geophysical Characteristics of Hellas

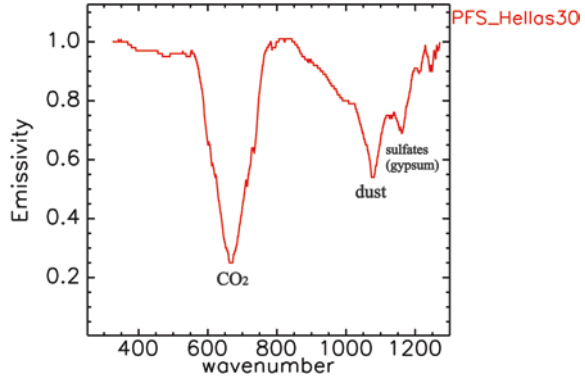
The interior of the basin manifests gravity anomalies (which are caused, among others, by differences in thickness of the Martian crust here), as measured by the gravimetric Radio Science (Gravity Field Experiment) device installed on the probe Mars Global Surveyor (MGS). The Martian mantle beneath Hellas is raised very high, and compressed by the impact. The Martian crust at this point is from 5 to 6.2 km thick, and around the crater of the shell the thickness reaches 67 km (Richardson, 2002). The basin remains in isostatic equilibrium. The most powerful gravitational anomalies are observed in the northern part of the basin, where the bottom lies at a depth of 7.5 km. Anomalies within the Hellas are referred to as free-air anomalies, with the maximum of 200.4 mGal and the minimum of -261.6 mGal.

Based on measurements of Radio Science (Gravity Field Experiment), the average density of the crust is $2,900 \text{ kg/m}^3$ and the density of the shell was estimated to be $3,500 \text{ kg/m}^3$ (Richardson 2002), while the Earth's continental crust density is of $2,700 \text{ kg/m}^3$, oceanic being $3,000 \text{ kg/m}^3$. In the case of Mars it is very difficult to say whether we are dealing with the continental or oceanic crust.

5 Study of the Surface

In view of the conditions prevailing at the bottom of Hellas, the pressure of about 11 mb (millibars), higher compared to the average pressure on Mars (6 mb), there exists a possibility of liquid water, because it exceeded the triple point of H_2O . Therefore, the occurrence of minerals associated with liquid water is highly probable in this area, such as sulfates, carbonates, clays and oxides. The presence of such minerals is confirmed by examining the surface of Mars by infrared spectroscopy. The probes Mars Express and Mars Reconnaissance Orbiter have detectors for scanning the surface of Mars. Scanning of the surface in the case of Mars Express is being performed from different levels of elevation, as the probe moves along an elliptical orbit, which results in different spatial resolution.

Fig. 2 PFS spectrum (red) of Hellas Planitia with $1,160\text{ cm}^{-1}$ band which is interpreted as sulfates. A minimum of $1,160\text{ cm}^{-1}$ of gypsum fits the spectrum with a minimum of Hellas from 30th orbit. Other minima: CO_2 667 cm^{-1} , dust $1,075\text{ cm}^{-1}$, CO_2 $1,250\text{ cm}^{-1}$



Infrared spectroscopy is used, among others, as a method of structural analysis to the study of minerals and rocks. IR absorption is caused by vibration of functional groups and chemical bonds in the molecule of the test compound. Going through a sample of the test substance, radiation induces vibrations of chemical bonds of a length corresponding to the absorbed wavelength. The fact that each compound has its own characteristic vibration makes it possible to determine the binding present in the sample (Alpert et al. 1974; Farmer 1974).

I will describe how to interpret the infrared spectra of the two spectrometers installed on the probes Mars Express PFS (Planetary Fourier Spectrometer) and OMEGA (Observatoire pour la Mineralogy, l'Eau et l'Activité les Glaces). The first PFS scans the surface of Mars in the infrared range $1.2\text{--}45\text{ }\mu\text{m}$ ($8,333\text{--}222\text{ cm}^{-1}$) in two channels: shortwave (SW) $1.2\text{--}5\text{ }\mu\text{m}$ ($8,333\text{--}2,000\text{ cm}^{-1}$) and longwave (LW) $5\text{--}45\text{ }\mu\text{m}$ ($2,000\text{--}222\text{ cm}^{-1}$). Spectral resolution is 2 cm^{-1} and the field of view of about 2° in shortwave (SW), and about 4° in longwave (LW) channels. From an altitude of 300 km , spatial resolution is within the range of $10\text{--}20\text{ km}$. It is best to use longwave channel for surface measurements in case of this spectrometer, as there is a smallest atmospheric influence observed, which can affect the spectrum of the surface substantially (PFS for Mars Express Planetary Fourier Spectrometer 1998).

Analysis of the spectra from PFS relies on finding characteristic bands of emission/absorption, which are not known band components of the Martian atmosphere, or CO_2 , H_2O , ice crystals and dust (Smith et al. 2000). The spectra are analyzed without separation of atmospheric influences, which is a problem in interpretation, as due to the reservoir depth (7.5 km) the atmosphere around Mars is the thickest (Grassi et al. 2007; Fig. 2).

1. The spectra are averaged over a dozen or so individual PFS radiance measurements in order to eliminate random noise.
2. For a clear interpretation of spectra, radiance is being converted to emissivity by dividing the spectrum by the spectrum of a black body at the right temperature, selected in the optical window.
3. The averaged spectra are smoothed to eliminate noise, using the least squares method.

4. The emissivity without minimums should reach the number 1, so the best choice is an optical window range of $320\text{--}370\text{ cm}^{-1}$ (the other window is the range of $1250\text{--}1350\text{ cm}^{-1}$).
5. The band reveals distinctive characteristic minimums. High noise often makes the image more blurry in emissivity. This is due to the choice of the temperature in the optical window of the atmosphere; as a result of dividing the spectrum by the Planck's spectrum, radiance at a specified temperature range of the spectrum above $1,200\text{ cm}^{-1}$ in the emissivity becomes unreadable. Resulting emission spectra of Mars have been carefully observed for finding interesting minima (bands), and then compared with the known infrared spectra of minerals. Emissivity spectra of minerals were taken from the online library (ASU Thermal Emission Spectral Library 2000 [<http://speclib.asu.edu/>]).

The most apparent band (sharp minimum), in addition to dust $1,075\text{ cm}^{-1}$ band, is around $1,160\text{ cm}^{-1}$ (Fig. 2; Zalewska 2013). Spectral band range varies around the wave number $1,160\text{ cm}^{-1}$. This wave number corresponds to sulfates in particular and casts a sharp minimum at this point. Plagioclase belonging to the silicates, in particular albite, is in this respect a lot weaker than the sulfates but it is at least possible to have an impact on the shape of the spectrum (Characteristic albite minimum, the so-called doublet band, interferes with dust band here). Volcanic glass with a high content of SiO_2 also has a minimum in this part of the spectrum. Asteroid fell down forming Hellas, and under high temperature and pressure the amorphous glass smelted from the bedrock (Wright et al. 2006; Wright and Newsom 2006; Zalewska 2009).

The OMEGA imaging spectrometer, onboard the Mars Express probe, is used to study the surface, water, ice and atmosphere of Mars. Mineralogical composition is determined on the basis of multispectral infrared image formed by the radiation reflected from the surface. Spectral range consists of three channels: VNIR $0.38\text{--}1.05\text{ }\mu\text{m}$ ($26,315\text{--}9,523\text{ cm}^{-1}$), SWIR-C $0.93\text{--}2.73\text{ }\mu\text{m}$ ($10,752\text{--}3,663\text{ cm}^{-1}$), SWIR-L $2.55\text{--}5.2\text{ }\mu\text{m}$ ($3,921\text{--}1,923\text{ cm}^{-1}$). Spatial resolution is: $300\text{ m--}4.8\text{ km/pixel}$, and the spectral resolution is, respectively, 7.5 nm , 14 nm , 20 nm ; their interpretation is based on multispectral images of the surface reflectance and emission spectra, unlike in the case of PFS (Bibring et al. 2006; Gendrin et al. 2005).

In interpreting the infrared spectra of the OMEGA spectrometer from the Hellas impact crater, water ice and dust are most abundant. Besides, it can be concluded that the dominant rock is pure basalt with minerals such as pyroxenes, feldspars (silicates), hematite (iron oxide), olivines (silicates) included in the basalt and the accompanying sulfates and carbonates. The second major band is weathered basalt with the dominant clay minerals.

The interpretation was made only for data from the channel SWIR-C, the least noisy. The spectra were interpreted after the separation of the atmosphere, but most of the spectra have noticeable atmospheric influences due to its thick layer over the surface of Hellas. The influence of CO_2 is visible in the range of about $2\text{ }\mu\text{m}$ of the spectrum with very sharp peaks and minimums. Then the spectra from Hellas were compared to laboratory spectra, pure basalt and weathered basalt derived from USGS Digital Spectral Library (2007) (Fig. 3).

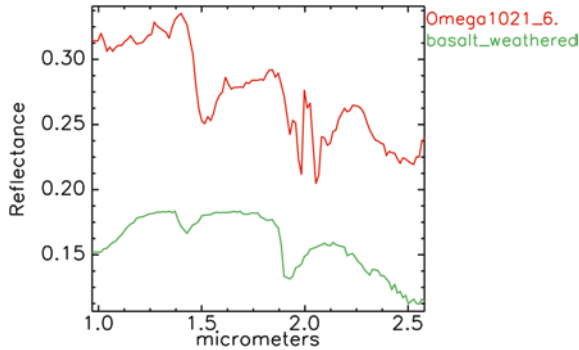


Fig. 3 Comparison of OMEGA orbits 1021_6 (red) with weathered basalt (green) from the USGS Digital Spectral Library [USGS Digital Spectral Library (2007) (<http://speclab.cr.usgs.gov/spectral.lib06/ds231/datatable.html>)]. Spectrum from OMEGA is interpreted as a weathered basalt. The spectrum shows contribution of clay minerals and water ice. Characteristic bands of water are 1.4 and 1.9 μm . The region around 2 μm is disturbed by the influence of CO_2 (Zalewska 2009, 2013)

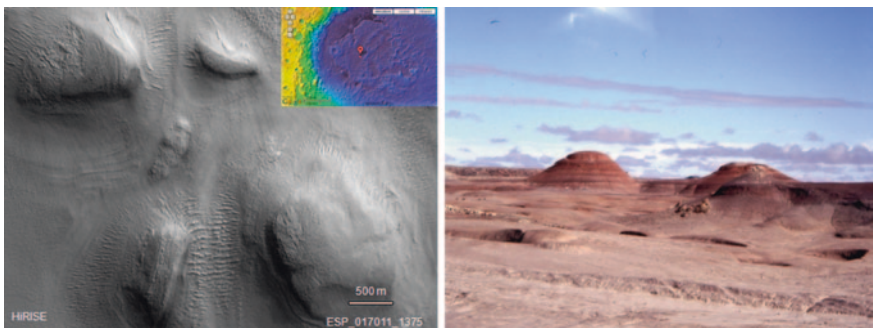


Fig. 4 Comparison of images from HiRISE (left) and pictures of the Utah desert (right). The two pictures show a similar type of surface weathering, which indicates the high content of clay minerals, which is confirmed by the results from the OMEGA. As a result of weathering, forms are hilly with rounded shapes. Weathering is caused by the water fraction. Clay minerals are the result of chemical weathering of silicate contained in the rocks. Then a layer of clay minerals undergoes liquefaction by water and flowing forms monadnocks of rounded shapes. (The height of the Utah hills is approximately 3–4 m)

To separate the atmospheric influences, the spectral optical thickness of the atmosphere over the volcano Olympus Mons was used. Namely, we divided the measured spectral reflectance above the top of the volcano by reflectance from the base of a volcano, assuming that the volcano itself is made of a single rock. This resulted in an approximate spectrum of the same atmosphere. Assuming that this effect is the same all over Mars, a spectrum of other areas of Mars was divided by the spectrum of the atmosphere, which resulted in a spectral reflectance of the land surface over which the measurement was performed.

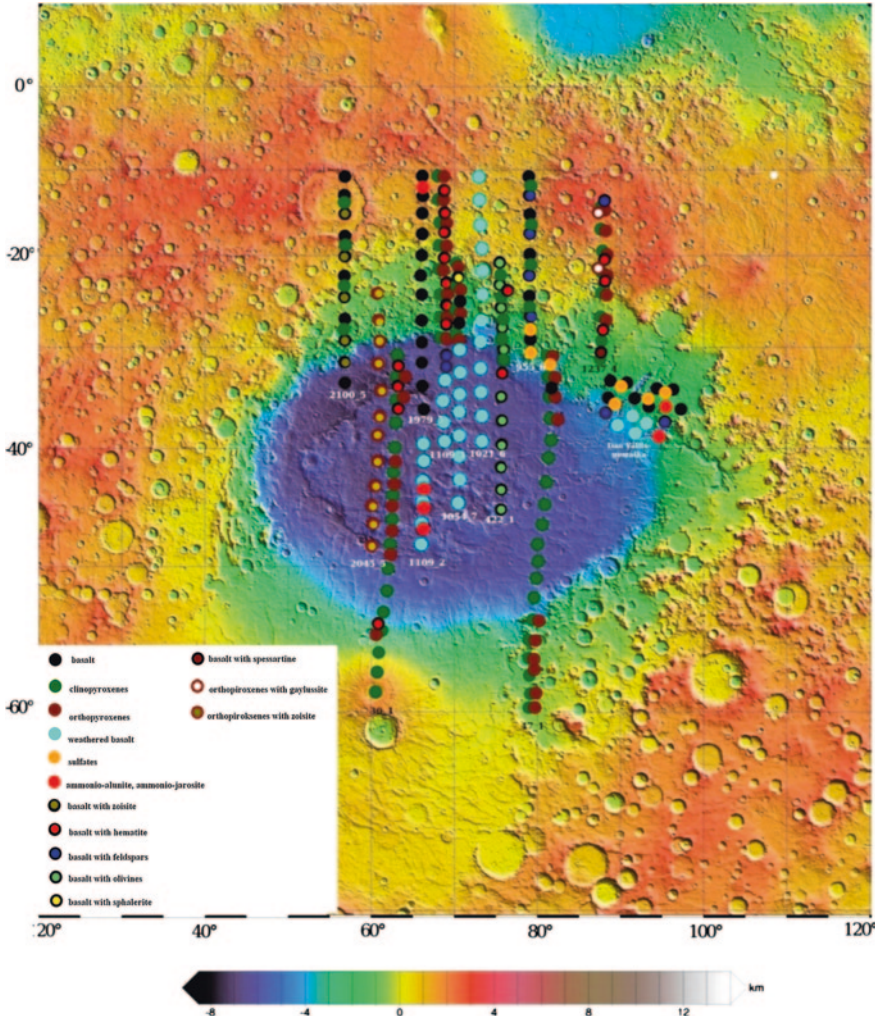


Fig. 5 Distribution map of specific groups of minerals based on data from OMEGA, and on MOLA hypsometric map. Key to the map (Zalewska 2009)

As mentioned in the detailed interpretation of the spectra from OMEGA, the basic building block of Hellas, and the surrounding area is basalt found in not weathered and weathered forms. Regolith is mainly composed of clay minerals and iron oxides - hematite. Weathered basalt was detected mainly in the interior of the basin where the surface is dominated by younger Hesperian and Amazonian rocks (Fig. 4). On the outskirts of Hellas, in the border of the rim, there is more pure basalt, the dominance of pyroxene and hematite, where is an older, Noachian bedrock. On the eastern rim, olivines appear at the height of the volcano Hadriaca Patera, carbonate influences (gaylussite) and dominating clinopyroxenes are in the spectrum (Fig. 5; Zalewska 2009).

Based on the interpretation of the spectra from OMEGA and PFS, instead of using two infrared spectral ranges: short and thermal, it can be concluded that the highest concentration of clay minerals in the weathered basalt and, additionally, water ice is in the centre of Hellas. It is possible that the central area is seasonally ice-covered (Lahtela 2003; Holt et al. 2008). In addition, the entire northern part and the areas north of Hellas, and extending south of the crater reveal rocks made of pure basalt, the ingredients comprising the basalt-silicates: orthopyroxenes, clinopyroxenes and plagioclase and accompanying minerals: zoisite (silicate), hematite (iron oxide), olivine (silicate), sphalerite (zinc sulfide) spessartine (silicate from garnet group) (Zalewska and Wolkenberg 2008). Sulfates occur in northeast Hellas, especially in large quantities within the channels of Dao Vallis, where they can be the origin of volcanic exhalations of the caldera located near Hadriaca Patera. Lake evaporation in the area is also not precluded. In addition, sulfates such as ammoniojarosite or ammonioalunite, whose existence is only probable, appear in the central part of Hellas, and the Dao Vallis channel (Fig. 5; Zalewska 2009). Recent data from the CRISM (Compact Reconnaissance Imaging Spectrometer) for Mars instrument of Mars Reconnaissance Orbiter confirmed the presence of clay minerals—iron-magnesium smectites on the northern outskirts of Hellas (Carter et al. 2011).

6 Summary

Was there ever the sea? This far, no one knows but the Hellas crater is a potential area where episodes of liquid water can appear. Pressure of up to 11 mb in the deepest places of Hellas, which exceeds the pressure in the triple point and consequently allows the water to come in liquid form, is the evidence of this. Some images from HiRISE equipment (Mars Reconnaissance Orbiter) for the Hellas region reveal weathered surface on which water erosion dominates, which is confirmed by the infrared spectrum of the apparatus of PFS and OMEGA (Mars Express). Clay minerals, acting as a component of weathered basalt, discovered by the OMEGA spectrometer, are an obvious testimony to the existence of water. Spectra measured in the laboratory spectrometer fit well into the shape of the spectrum measured by the spectrometer OMEGA. Another band of $1,160\text{ cm}^{-1}$ is disclosed in the spectra of the PFS apparatus, which is interpreted as originating from a range of sulfate minerals also produced in an aqueous circumambience. The demonstration of the existence of these minerals in the Martian crater Hellas brings us to the conclusion that life on Mars in some form could have existed and may even exist.

Acknowledgments Thanks for the use of data for: PI: J.P. Bibring (Institut d'Astrophysique Spatiale, France)-OMEGA; PI: V. Formisano (Istituto di Fisica dello Spazio Interplanetario-INAf, Rome, Italy)-PFS; PI: A. McEwen- (University of Arizona)-HiRISE; Stéphane Le Mouélic (CNRS/Université de Nantes Laboratoire de Planetologie et Geodynamique, France) for using ENVI Spectral Hourglass Wizard to OMEGA data. This paper was supported by grants: No. 2P04D053 30, Financed by Ministry of Science and Higher Education; No. UMO-2011/01/B/ST9/05442, Financed by National Science Centre.

Appendix: Martian Rock Age

The geological history of Mars has been divided into three periods, and in fact the three eras. From oldest to youngest, these are the Noachian, Hesperian, and Amazonian. These names come from Martian places: Noachian from Noachis Terra, Hesperian from Hesperia Planum and Amazonian from Amazonis Planitia. The duration of these eras is defined by the number of meteorite craters on the surface of Mars. The oldest Martian surface has more craters. The younger surface will have less impact craters. Real-time of eras cannot be determined using this method. In depth studies of isotopes of elements are needed that are used when testing the age of rocks on Earth.

Noachian era dates back to the origins of the planet, about 4.5 billion years ago, and its end is estimated somewhere between 3.8 and 3.5 billion years ago (depending on the adopted model). The surfaces of this age are heavily wounded by many large craters.

During Noachian, Martian atmosphere was thicker than it is now, and the climate is likely to be warm enough to allow large amounts of rainfall. Huge lakes and rivers were present in the southern hemisphere, and the ocean could cover the northern lowland plains. Extensive volcanism took place in the Tharsis region, building a huge mass of volcanic material (Tharsis dome) and released large amounts of gases into the atmosphere. Weathering of rocks on the surface and producing minerals associated with the aquatic environment (clay minerals, carbonates, sulfates, etc.) occurred on a large scale.

In the next, Hesperian era, that lasted somewhere between 3.55 and 1.8 billion years ago, volcanism has become the basic geological processes on Mars, producing massive basalt plains in the form of broad pillow lava structures (highland paterae). During this time, all large volcanoes on Mars, including Olympus Mons, were being formed. Volcanic eruptions produced large amounts of sulfur dioxide (SO_2) and hydrogen sulfide (H_2S) to the atmosphere, causing a change in the chemistry of weathering more acid, thereby forming a sulfuric acid.

At the beginning of the late Hesperian, the atmospheric density started to decrease, resulting in a gradual cooling of the planet. Water contained in the upper part of the crust began to freeze to form a cryosphere covering the deeper strata containing liquid water. Expiring volcanic and tectonic activity sometimes caused cryosphere melt, releasing large amounts of water deep underground to the surface and sculpting large drainage channels. Most of this water flowed into the northern hemisphere, where large lakes, partially covered with ice, were probably formed in the estuaries. Basically, Hesperian is treated as a transition period between the end of heavy bombardment and the onset of cold and dry period of Mars.

Finally, the era of the Amazonian covers a period from about 1.8 billion years ago to today. The surfaces of the era of the Amazonian have few meteorite craters, but are quite varied. After this, the “martiancreation” processes were slowly dying, and glacial aeolian processes have been taking their place, forming landslides in Valles Marineris (such as in Gangis Chasma) on the broad plains of sand

dunes near the poles of Mars. Large parts of Mars started to be covered by ice caps. Climate changed to dry and cold, and that state continues to the present day (Nimmo and Tanaka 2005; Hartmann 2005).

References

- Alpert NL et al (1974) Spektroskopia w podczerwieni. Teoria i praktyka Państwowe Wydawnictwa Naukowe, Warszawa
- ASU Thermal Emission Spectral Library (2000). (<http://speclib.asu.edu/>)
- Bibring J-P et al (2006) Global mineralogical and aqueous mars history derived from OMEGA/Mars express data. *Science* 312:400–404
- Carter J et al. (2011) Mineralogical evidence for major aqueous activity in the northern Hellas province, Mars EPSC Abstracts, vol 6, EPSC-DPS2011-1044, EPSC-DPS Joint Meeting
- Crown DA et al (2009) Geologic mapping of the NW rim of Hellas Basin, Mars. 40th lunar and planetary science conference, Houston, Abstr. 1705
- Collins GS, Melosh HJ (2005) Earth impact effects program: a web-based computer program for calculating the regional environmental consequences of a meteoroid impact on Earth. *Meteorit Planet Sci* 40(6):817–840. (<http://www.lpl.arizona.edu/impaceteffects/>)
- Crown DA, Pierce TL (2002) Debris aprons in the eastern Hellas region of Mars: Implications for styles and rates of highland degradation. *Lunar and planetary science XXXIII*, Houston, Abstr. 1642
- Farmer VC (1974) The infrared spectra of minerals. Mineralogical Society, London
- Gendrin A et al (2005) Sulfates in martian layered terrains: the OMEGA/Mars express view. *Science* 307:1587–1591
- Grassi D et al (2007) The Martian atmosphere in the region of Hellas basin as observed by the planetary Fourier spectrometer (PFS-MEX). *Planet Space Sci* 55(10):1346–1357
- Hartmann WK (2005) Martian cratering 8: isochron refinement and the chronology of mars. *Icarus* 174:294–320
- Holt JW et al (2008) Radar sounding evidence for ice within lobate debris aprons near Hellas Basin, mid-southern latitudes of Mars. *Lunar and planetary science XXXIX* Houston, Abstr. 2441
- Lahtela H (2003) The lacustrine reservoir in Hellas impact basin region. *Large Meteorite Impacts*, Abstr. 4073
- Leonard GJ, Tanaka KL (2001) Geologic map of the Hellas region of Mars. Geologic Investigation Series I-2694. U.S. Geological Survey
- Melosh HJ, Beyer RA (2000) Crater, (<http://www.lpl.arizona.edu/tekton/crater.html>)
- Moore JM, Wilhelms DE (2001) Hellas as a possible site of ancient ice-covered lakes. *Lunar and Planetary Science XXXII*, Houston, Abstr. 1446
- Murray SS et al (1981) (by members of), Basaltic Volcanism on the Terrestrial Planets, in the Basaltic Volcanism Study Project. Lunar and Planetary Institute, Houston, p 77058
- Nimmo F, Tanaka K (2005) Early crustal evolution of mars. *Annu Rev Earth Planet Sci* 33:133–161
- Peterson JE (1978) Volcanism in the Noachis-Hellas region of Mars. 9th Lunar and planetary science conference, Proceedings, vol 3., Houston, March 13–17, (A79-39253 16-91) New York, pp 3411–3432
- PFS for Mars Express, Planetary Fourier Spectrometer, 1998 IFSI-98-2
- Richardson J (2002) Isostasy in the Hellas Basin on Mars. Department of Planetary Sciences, University of Arizona, GEOS 540 term paper
- Smith MD et al (2000) Separation of atmospheric and surface spectral features in Mars Global Surveyor (Thermal Emission Spectrometer) spectra. *J Geophys Res* 105(E4):9584–9607

- Tanaka KL, Leonard GJ (1995) Geology and landscape evolution of Hellas region of Mars. *J Geophys Res* 100(E3):5407–5432
- Thomson BJ, Head JW III (2001) An investigation of proposed glacial landforms in the Hellas Basin, Mars. *Lunar and Planetary Science XXXII*, Houston Abstr. 1374
- Thomson BJ, Head III JW (1999) The role of water/ice in the resurfacing history of Hellas Basin. 5th international mars conference, LPI, Houston, Abstr. 6200
- USGS Digital Spectral Library (2007) <http://speclab.cr.usgs.gov/spectral.lib06/ds231/datatable.html>
- Wright SP, Newsom HE (2006) Thermal infrared spectroscopy of basalt from Lonar Crater, India: implications for the remote sensing of impact craters on Mars. <http://www.marscraterconsortium.nau.edu/WrightMCC7>
- Wright SP et al (2006) Thermal emission spectroscopy of shocked basalt from the Earth and Mars: A review plus new insights. *Lunar and Planetary Science XXXVII*, Houston Abstr. 1786
- Zalewska NE (2009) Geology and mineral composition of Martian Hellas Basin surface, and hypothetical role of liquid water on the planet Mars—based on infrared spectroscopic data, Doctor thesis wrote in Space Research Center PAS Warsaw 2009
- Zalewska (Andrzejewska) NE (2013) Hellas Planitia as a potential site of sedimentary minerals. *Planet Space Sci.* doi: [10.1016/j.pss.2012.12.006](https://doi.org/10.1016/j.pss.2012.12.006)
- Zalewska NE, Wolkenberg P (2008) Mineralogical composition of the Martian surface on the basis of infrared spectroscopy. *Martian phyllosilicates: recorders of aqueous processes*, 7010

Application of an Object Classification Method for Determining the Spatial Distribution of Sea Bottom Structures and Their Cover Using Images from a Side Scan Sonar

Paulina Pakszys

Abstract Side Scan Sonars combined to positioning systems constitute an exceptionally valuable tool for collecting information about seabed characteristics. The main objective of this study is to apply the new methods of object classification, based on Side Scan Sonar images for determining the bottom structure and coverage. The aim is to adapt land image analysis for acoustic data and to produce a reliable model that can be applied in further analysis. Software development tailored for this type of data enables wide-range analysis and visualization of spatial data. The main tool used in postprocessing of sonar images was the Trimble eCognition™ Developer. The classification process is a categorization of objects and phenomena in the analyzed area. Classification uses information contained in a single pixel creating more general scheme. An automated mode of the classification method is used in this study OBIA (*Object-Based Image Analysis*). Classification is based on the segmentation process, in which pixels are divided into homogeneous regions with respect to neighboring pixels, which determines the final shape of each class object. Objects and parameters, controlling the processing of supervised classification, are selected by user. Representative functions of every object are defined by the user to depict each class, helping to assign them to specific classes. The adopted approach for mixed type of classification processes, is based on the reference objects and training samples and subsequently classifies them by class discriminants. As a result a sonar mosaic map of the seabed image classes is provided in relationship to the bottom sediments and the bottom surface roughness. The presented results could help to transform a protected area HELCOM BSPA into the undersea sanctuary in the Gulf of Gdansk (Baltic Sea) and support this

P. Pakszys (✉)

Physical Oceanography Department, Institute of Oceanology of Polish Academy of Sciences,
Powstańców Warszawy 55, 81-712 Sopot, Poland
e-mail: pakszys@iopan.gda.pl

very important interdisciplinary environmental study. In this paper, I have demonstrated that a multistage image segmentation methodology can be more efficiently used for geomorphometry and terrain classification for underwater areas obtained from a side scan sonar mosaic. The methodology introduced in this paper can be applied for many other applications where relationships between topographic features and other components are to be assessed (samples etc.). In this way, we hope to address a time-consuming task to produce underwater maps with bigger scales but still with an appropriate resolution.

Keywords Side scan sonar • Object classification • GIS • eCognition developer • Definiens • Interpolation • Sea bottom structure • Acoustic methods

1 Introduction

Methods for analysing seafloor properties can be divided into two classes: (1) methods which directly interfere with bottom (cores, sediment sampling), thus require a contact with environment and (2) remote methods which do not influence the environment. The second group contains satellite and airborne methods like lidars, satellite images and undersea videos as well as echosounders and side scan sonars (SSS). The latter one is the main objective data-collection method to determine seabed structure and its cover—during data post-processing.

Acoustic seabed classification is a standard tool in seafloor surveying and underwater remote sensing (Wienberg and Bartholoma 2005). Mapping seabed characteristics by means of remote sensing, side scan sonars or echosounders is becoming of an increasing importance. This efficient and fast method provides higher spatial and temporal resolution than in situ sampling or video-recording (Blondel 2003; Kenny et al. 2003). Ground truthing analysis helps to identify the real bottom sediment types as a complementary information to the underwater sensors. Methodology used in this study presents a new approach to image analysis. It shows that automatic sonar image analysis is a reliable tool for habitat mapping. Human operators who analyse images can cause mistakes, while a computer with a proper software is more repeatable tool for these kind of analysis.

Each of these techniques involves collection of data that after analysis can generate the bathymetric, geomorphologic or biological models of seabed (Kostylev et al. 2001; Lucieer and Lamarche 2011; Ryan et al. 2007).

Evolution of software makes a comprehensive analysis and visualization of the spatial data easier. Visualization of the seafloor for upcoming sanctuary in Gdynia-Orłowo (Gulf of Gdańsk, Gdynia, Poland) was based on the mosaic. Sonar images (mosaic) provide information of intensity of backscattered signal that is related to the geomorphological bottom properties. From this information we can obtain sediment type and bottom morphology. The ArcGIS and eCognition™ Developer (Definiens) software were the main tools applied for pre- and post-processing, analysis and visualization of acoustic data. Developer eCognition is a powerful development environment for an

object-based image analysis. It is used in earth sciences to develop set of rules for the automatic analysis of remote sensing data.¹ The Esri's ArcGIS is a geographic information system (GIS) for working with maps and obtaining spatial information. It is used for: creating and using maps; compiling geographic data; analyzing mapped information; sharing and classifying geographic information; using obtained features in a range of applications and spatial data management in databases.² A grain-size analysis of sediments was carried out in the laboratory and underwater videos and photos were collected in situ.

The SSS data were processed using the CodaOctopus software. The process of data combining includes the line by line compilation of an image from registered SSS data in accordance with geographical system. In other words, it is a transformation of several small sonar images into a regular bitmap which can be saved as, e.g. GeoTiff format. The mosaic is corrected for slant-range and signal loss and presented in a proper geodetic system and with spatial resolution. Software development, tailored for this type of images enables wide-range analysis and visualization of spatial data. The main tool used in postprocessing of the sonar images were the eCognition™ Developer (developed by Trimble). This software is dedicated to spatial data processing, mostly land images. However it was adapted to acoustic imaging purpose. It adapts a relatively new method of image analysis, in which the interpretation of an image is similar to human reception. Information contained in a single pixel creates into more general scheme, which are homogeneous objects separated from pixels of an image and then analyzed them. An automated version of the OBIA (*Object Based Image Analysis*) method was used in this study. A user selects objects and parameters, which control the process of supervised classification. A precise description of this method can be found in the [Sect. 3 \(Methodology\)](#).

Modeling in the Definiens software requires from the user the basic information about the sea bottom. It was provided by the manual classification of mosaic (through digitization) with the ArcGIS software. This way, a choice of training samples were found and used in further classification. The granulation composition and multimedia specification were attributed to hand-mapped separated zones of various structures. The map was also used to check the agreement between classification stages.

The GIS software was also used to visualize the results of classification analysis, combining continuous map of different bottom sediments and discrete sampling data.

2 Study Area

The planned underwater sanctuary is situated in the southwestern part of the Gulf of Gdansk (Southern Baltic Sea) (Fig. 1) as an extension of the land reserve "Kepa Redłowska". It is about 1 km offshore up to the depth of 10 m, which was formerly the border of the underwater meadows.

¹ <http://www.ecognition.com/products/ecognition-developer>.

² <http://www.esri.com/software/arcgis/arcinfo>, Esri- Product Page.

Fig. 1 Location of study area, Gulf of Gdansk, Poland

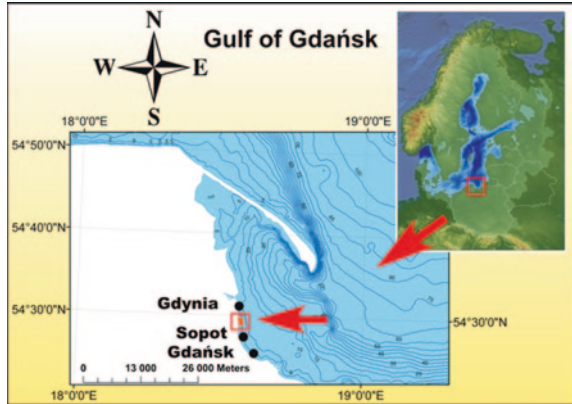
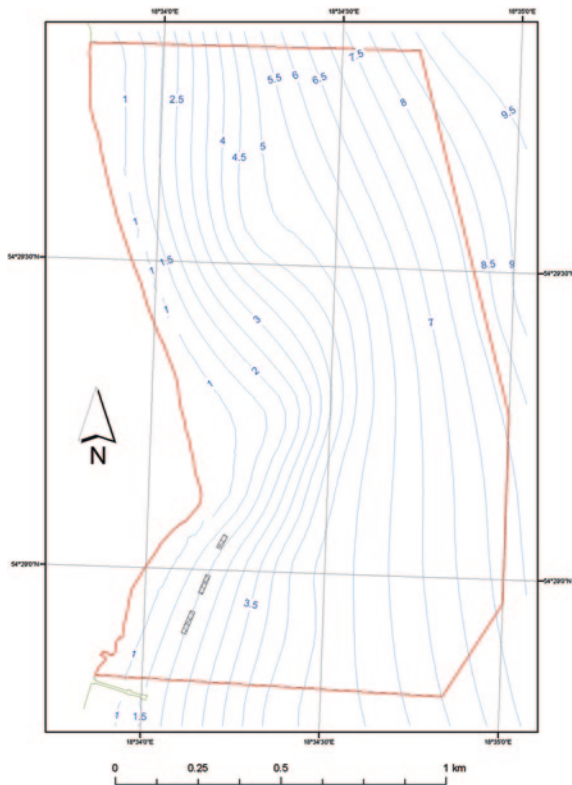


Fig. 2 Borders of planned underwater sanctuary “Orlowo Cliff”



The borders of the planned sanctuary were proposed by the Baltic System Protected Area HELCOM (HELCOM BSPA) in 1991. Eastern border is determined by the isobath of 10 m. The distance from the border to the coast is about 1,000 m. The western boundary is located at the coastal line. The northern border

is designated by the parallel that begins in the central part of a concrete band of the armed cape. From the south, the sanctuary is limited by a parallel beginning at the Orlowo Pier (Fig. 2). The area of the “Orlowo Cliff” stretches to about 185 ha (Osowiecki A and Zmudziński L 2000).

The water depth increases continuously linearly away from the shore. It can be assumed that the shape of isobaths reflects the shape of a shoreline. The sediment layer is relatively thin and filled with diverse material. Near the coasts and over shallows a mixture of sands and origin stones can be often found (Majewski 1992). In extreme shallows (to isobaths of 6 m) large rocks and stones, pebbles and different granulation sands can be observed (Wicher 2003).

3 Instrumentation and Measurements

3.1 Side Scan Sonar

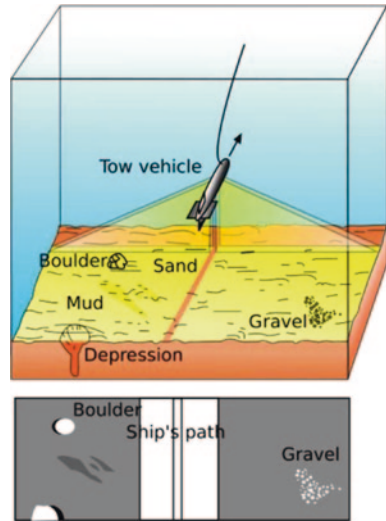
Side scan sonar (SSS) is a hydroacoustical device which is commonly used for imaging morphological features of the seafloor as well as detection and positioning of various objects at the sea bottom. Registering bottom topography by SSS enables creation of the sea bottom model and the shape from the backscattered signal. Several studies have shown a direct relationship between the backscattered signal and seabed characteristics such as grain size, bedforms and biotic parameters (Anderson et al. 2002; Collier and Brown 2005; Collins et al. 1996; Freitas et al. 2003; Preston 2001).

The sonar performance is based on generating fan-shaped acoustic pulses which are backscattered by the sea bottom or by objects. Intensity of backscattered signal reflects such parameters of the sea bottom as its roughness or hardness. A set of cross-track slices forms image of the sea bottom, often with an almost photo realistic quality (Penrose et al. 2005).

Sonar measurements are based on emission of an acoustic single beam (“ping”) and the receiving of the backscattered signal (an intensity reflects the “roughness” and “hardness” of the seabed), which is an incoming echo of a transmitted wave, reflected from the sea bottom or bottom objects (Fig. 3) (Salamon 2006). A SSS has two transducers and each has a highly asymmetrical beam pattern which is narrow in the along-track direction and wide across-track, typically 1° by 40° (in EdgeTech 1,000 case it is 0.5 × 50 deg) (Simmonds and MacLennan 2005). Side scan sonars provide only backscatter data and little information about depth. Grey-scale images reflect signal amplitudes but can vary between swaths, usually due to backscattered signal angle and distortions related to orientation of the sonar (Blondel 2003). It causes problems during images classification. With the use of complementary ground-truth samples (grabs and videos) one can reveal the differences in sediments type which is not always easily identifiable in the SSS image.

Data were collected in May 2010 by the Marine Acoustic group of the Institute of Oceanology PAS, Sopot. During the measurements sonar was towed behind the

Fig. 3 A side scan sonar towfish, showing the two sonar beams (*top*) and the resulting image (*bottom*) from the sonar echoes (http://en.wikipedia.org/wiki/Side-scan_sonar)



rubber boat on a cable-line. This cable connects the towfish with the registering computer, equipped with the Linux system and Octopus Coda DA-100 acquisition software. The sonar works at two standard frequencies: 100 ± 10 kHz and 400 ± 20 kHz.³ Due to the need of collecting high resolution data, the high frequency (390 kHz) was used. Due to the larger absorption of high frequency sound in a water, the sonar range decreased. For the chosen frequency, (and also power and transducer design), the measurement was carried out with each transducer covering 25 m that results in an average 50 m wide band of seabed covered per ping (Kruss 2008).

Taking into account a relatively flat bottom in the studied area and a parallel relation to the shore, the spatial distribution of the sonar transects, did not influence the data quality. The larger changes of depth, e.g. slopes, can result in the lower quality of recorded data. Transects were distributed every 30–40 m to provide proper data overlap between lines. After pre-processing with CodaOctopus software we obtained a mosaic with a resolution of 0.1 m (Fig. 4) in UTM 34 N (Universal Transverse Mercator) with geoid WGS84 (World Geodetic System 1984) (CODA 2001).^{4, 5}

Like any other acoustic devices, SSS is susceptible for interference with many sources. There are many variables which affect sonar data, such as waves, currents, temperature and salinity gradients. These errors were recognized in the data and cut off as well as areas with the nadir effect, before classification procedure.

³ EdgeTech.560-D Digital Side Scan Sonar Sytem, Key Specifications—technical specification.

⁴ CodaOctopus, <http://www.gserentals.co.uk/pdf/Geokit%20Mosaic%20Replay1.pdf>.

⁵ <http://www.codaoctopus.com/>.

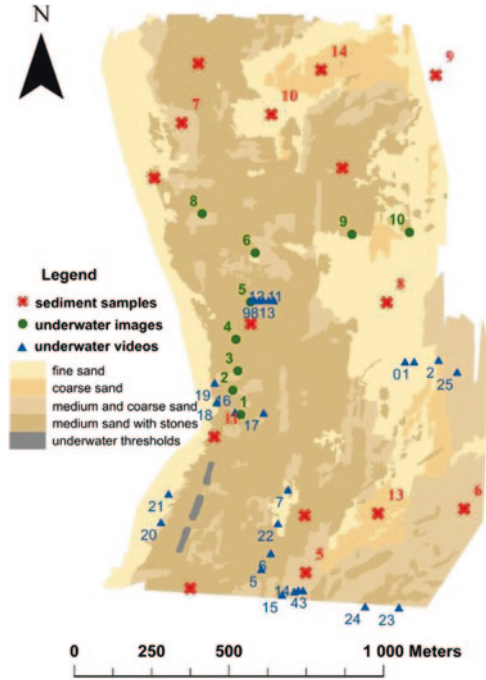


Fig. 4 Mosaic from SSS data with the spatial resolution of 0.1 m obtained by Coda Octopus software

3.2 Manual Classification, Images, Videos, Sea Bottom Samples

If a sea bottom is characterized by significant variability, both lithological and textural, it is possible to distinguish these variations from a mosaic picture. It is based on analysis of sound reflected from the seafloor (Blondel 2003; Wienberg and Bartholoma 2005). Differences in the received signal (and thus already on a the mosaic image) allow to distinguish zones that are similar and different from the other zones. It is easy to notice ripplemarks, stones and rocks or different sediments which results in differences in image texture. Pre-processing of mosaic depends on delimitation of zones, which differ from each other in texture, structure, reflection intensity, characteristic shape etc. Sonar imaging reproduces particularly well the physical properties of bottom substrata: thickness, compaction, size of individual components, bottom shape. However, the backscatter is much more complex and includes other bottom and signal features influencing Seafloor characteristic can be interpreted from an intensity of reflex tone, its uniformity distribution, occurrence of acoustic shadows and strips (Wicher 2001). The ArcGIS software was employed for the pre-processing data purpose (Fig. 5). Acoustic measurements are validated using sampling techniques such as video, photography

Fig. 5 Manual classification with localization of bottom samples and localization of the bottom photos and videos



or direct geophysical and biological sampling (by grab). They are often used in conjunction with multibeam or single beam sonars and subbottom profilers (Penrose et al. 2005). The bottom samples were analyzed to minimize the mistakes in recognition of the seafloor types. The bottom samples were collected on 28–29 May 2011, with the special attention paid to the collection of every type of surface sediment (Fig. 5). Grain-size analysis was used to qualify their granulose. Photos and videos were useful to validate the preliminary assumptions (Fig. 5). The accurate geographical position of each multimedia sample was also determined. This eliminated uncertainty resulting from perturbations visible in the image and confirmed a varying character of the studied area.

4 Methods

4.1 Classification

The complexity and high resolution of sonar images required a new method for understanding their characteristic and for proper interpretation. Better understanding of the whole complexity of an image can be helpful to resolve the details. This is the main goal of a classification process which is based on the recognition

(categorization) of the objects and various phenomena within an analyzed area (Lang 2008). One can recognize the state, range and dynamics of a processes and predict their changes. Classification should be understood as a simplification of the real images through grouping an image content into classes. The classes can be optionally defined by the user, in this case as a classes of bottom coverage. The result of a classification can be presented as a vector layer which is the base for map creation in further analysis (Adamczyk and Będkowski 2005).

4.2 Object Classification

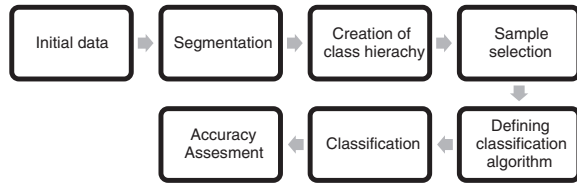
Image analysis of remotely sensed data is the science behind extracting information from the pixels within a scene or an image. Remote sensing tools like the SSS are designed to capture the reflected energy from various objects on the ground and to convert this information into digital numbers (DNs) that comprise an image. Traditional techniques are pixel-based. They explore the spectral differences of various features to extract the thematic information of interest (Navulur 2007).

It is easy to understand that finer spatial resolutions result in more detailed imagery. It is also worth noting that the land cover classification accuracy may decrease due to the increased intra-class variability, inherent from more detailed and higher spatial resolution data (Su et al. 2004; Ouyang et al. 2011). These methods are often not suitable for processing complex images due to the lack of spatial concept (Blaschke et al. 2000; Blaschke and Strobl 2001; Ouyang et al. 2011). As the spatial resolution of remote sensing data increases, the so-called “salt-and-pepper” problem of pixel-based classification (PBC) becomes more serious (Ouyang et al. 2011). In contrast, an object-based image analysis technique overcomes these difficulties by first segmenting the image into meaningful seabed zones of various sizes (Blaschke 2010; Lucieer and Lamarche 2011).

One of the methods to automatize classification process is based on a principle of object-oriented classifications OBIA (Object Based Image Analysis). Information contained in a single pixel, creates into more general scheme, containing the homogeneous objects separated from pixels of an image (Adamczyk and Będkowski 2005). Thus, applying the object paradigm to image analysis refers to analyzing the image in object space rather than in pixel space. Object can be used as the primitives for image classification rather than pixels. Compared to pixels, objects have numerous attributes, including shape, texture, morphology, relationships between categories and other properties (Navulur 2007). An automated version of this method was used in this study. User selects objects and parameters which control the processing of a supervised classification.

During a classification process a program “is taught” by the user to recognize objects through defining parameters and choosing object samples, which define a general class of objects. The supervised classification requires from the user certain knowledge about the character of the chosen objects. The user chooses training samples (it is a sample of each class that will be compared with image content)

Fig. 6 A schematic of classification process



and analysis, which will be executed for every class (Adamczyk and Będkowski 2005). Pixel concentration contains information about an object as well as class characteristics that the object belongs to. This information is necessary to elaborate suitable functions discriminating classes apart—class discriminant (decision rules). Every algorithm requires defined under-objects and then algorithm is added to them and applied during the classification process (Baatz et al. 2008). An OBIA method with the Trimble—eCognition Developer™ (Definiens) software was used to classify single-channel sonar mosaic.

A simple scheme of a classification process is presented in Fig. 6. At the beginning image data (sonar mosaic) and thematic data (supplementation for digital data in the raster format) are initialized. In this case we use the processed mosaic data, prepared in an ArcGIS: the median, standard deviation, the average, slope inclination and data standardization. The last two were also used in the second cycle of classification. Thematic data were used for map smoothing (the median layer) or to eliminate the values deviating from an average (the mean layer). The segmentation is the next step of processing, which creates a preliminary object based on the pixel content. Classification is based on the segmentation⁶ process, in which pixels are divided into homogeneous regions with respect to neighboring pixels (Castilla and Hay 2008). Multiresolution segmentation algorithm minimizes the heterogeneity of the image objects and can be applied at the existing object level or pixel level, to create new objects at the new level. It sequentially merges pixels or objects minimizing heterogeneity on average and maximizing their homogeneity. In multiresolution segmentation, homogeneity criterion is defined as a combination of spectral and shape homogeneity. The calculation can be influenced by a change of the scale parameter (higher values result in larger objects, smaller values in smaller objects). The Scale Parameter is an abstract term that determines the maximum allowed heterogeneity for the resulting image objects. It is the most important step of classification process, because it determines the final shape of each class object. However, it is often not possible to determine the correct scale of analysis in advance because different kinds of images require different scales of analysis. In many cases significant objects appear at different scales of analysis of the same image (Arbiol et al. 2006; Blaschke 2010). The next step is a creation of class hierarchy, where objects from segmentation level will be assigned to different classes. As a result we need one-level class hierarchy defining the character of a seafloor. We can distinguish variety of grain-size in the seabed

⁶ ‘Window of perception’ (Penrose et al. 2005).

(grain-size analysis shows only sand with different granulose), underwater breakwaters, rocks and stones concentration and ripplemarks. After creating the class hierarchy training samples were assigned to them. There are image areas chosen from each class, which “teach” the program how to distinguish objects during the segmentation. The training set is the user interpretation of representative subsets for each class. Defining classifiers (class description), characteristic functions for defined classes (thresholds) determine the next step. Every rule must be fulfilled to classify an exemplary object. Rules can be made from a combination of different algorithms. We identify a distribution of classes and confirm (from the previous stage) whether the objects are well-defined (Marpu PR Niemeyer et al. 2008). This step can be executed automatically by finding the best sets of rules from chosen features describing the differences between classes or with subjective method—Feature Space Optimization through the NN method. Their ranges are automatically optimized by the program. The classification algorithm uses class descriptions to divide image objects. It evaluates the class description and determines whether an image object can be a member of a class. Character of this classification is one-level, what results in the image representing the range of all objects belonging to the defined class of a sea bottom covered and with information about authenticity of the assigned objects (Trimble eCognition® Developer 2010a, b). Accuracy assessment methods can produce statistical outputs to check the quality of the classification results.

5 Results

The classification process was divided into two steps. First of all a continuous map was created. It represents a type of a seafloor cover (variety of grain-size sands). The second step was to create a non-continuous map of sea bottom structures (sandy strips, sandy bands, ripplemarks) and mark the stone concentration or huge rocks and underwater breakwaters.

The input data sets are the SSS mosaic with 0.1 m resolution as a basic layer, and thematic layers prepared in an ArcGIS: mean, median and standard deviation each in a 9×9 pixel window. The attributed weights are presented in Table 2. Despite the correction, the SSS image still contains many distortions as a consequence of the nadir effect⁷ and motion disturbances, therefore it was cut off. Mentioned areas, characterized by chaotic intensity values, alter the structure of the adjacent layers, what is particularly visible in data statistics. Multiresolution Segmentation was used with the scale parameter of 50. We obtained 88,264 objects. From that number, was used 12,903 objects were used and assigned to the classes (Table 1). It is 15 % of all objects that is statistically a represent subset for

⁷ Pattern of survey tracks under the towfish; specific line spacing is less than the swath width that depends on a beam width and under-sea bottom position (distance between towfish and the bottom).

Table 1 Number of training samples in each class

Class	Fine sand	Medium sand	Coarse sand	Nadir effect
Number of training samples	317	487	533	1,156
Percentage of objects in the class	7.6	8.3	9	16

Table 2 Weight for each layer for bottom covering classification

Layer	Weight
Mosaic	2
Median	1
Mean	1
Standard deviation	1

further analysis. Fourteen parameters were chosen with the use of a Feature Space Optimization. The best results were found for 8 of these 14 parameters: Border Index, Compactness, Skewness, STD, Border Contrast, Contrast to neighbor pixel for mosaic layer, Contrast to neighbor pixel for mean layer, Shape index.

An overview of the used features is given in the eCognition Reference Book (Trimble eCognition® Developer 2010a).

As a result we obtained 88,264 objects that were attributed to the classes:

- Fine sand—4177 objects, 4.73 % of all objects;
- Medium sand—5857 objects, 6.63 % of all objects;
- Coarse sand—5944 objects, 6.73 % of all objects;
- Nadir effect—72286 objects, 81.90 % of all objects.

The best class-fit, as an effect of 8 features controlling the classification is approximately 96.79 % \pm 0.06 (similar to each class). It is a part of accuracy assessment calculated for each class in percentage. Therefore, the average probability for the correct fitting (probability that the object can be also assigned to the other class calculated for every class) is approx. 5.12 % \pm 0.08. Coarse sand was distinguished most easily with a probability of 3.6 %, while the worst probability was obtained for fine sand—7 %. However, a number of errors in the classification are very low compared to the number of objects. Therefore, the errors are negligible and erroneously classified areas (pixels) can be omitted.

The resulting map still has non-continuous features due to the missing parts where the nadir effects areas are (vector datasets as polygon features). Areas were eliminated by using an interpolation method. The purpose of interpolation is to calculate the most realistic value in each model calculation cell and thus to create a continuous area from points. Among many methods the NN was used. When the data points are non-uniformly distributed, definition of neighboring points can be a critical issue. This method does not result in any smoothing, and can lead to unrealistic changes of a slope. The interpolation routine has been run twice and exclusively within the area with distorted data (regions with nadir effect were

Fig. 7 Spatial distribution of sea bottom structure and its overlay after interpolation with the number of 10,000 created data points and distance criteria of 0.3 m

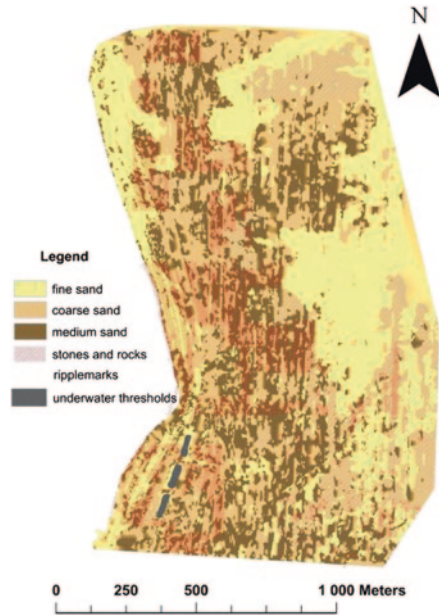
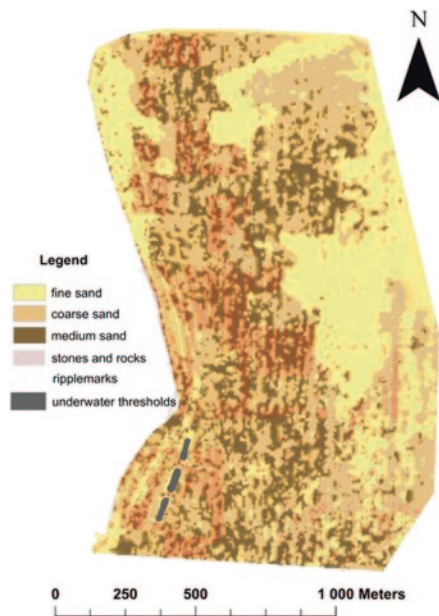


Fig. 8 Spatial distribution of sea bottom structure and its cover after interpolation with the number of 1,000 created data points 3 m



excluded). It was also compared how number of created points and distance criteria influenced the results of an interpolation:

1. For a 10,000 of created points and distance criteria of 0.3 m, we obtained 2,406,548 points (Fig. 7 right)
2. For a 1,000 of created points and distance criteria of 3 m, we obtained 28,020 points (Fig. 8 left)

Table 3 Numerical data about objects used in classification process

Layer	Number of created object	Number of objects obtained after classification	Object obtained after classification (%)	Covered area of underwater sanctuary (%)	Covered area (m ²)
Stones and rocks layer	2,906,253	17,554	0.6	15.32	302,593,17
Ripplemarks layer	274,282	41,203	15	23.40	462,268,84

Two continuous maps were obtained with spatial resolution of 0.1 m using Natural Neighbor method.

Secondly, a map was created with a sea bottom structure. A principal layer is the SSS mosaic and the standardization⁸ layer (prepared in an ArcGIS). Segmentation is a key. For smaller objects a smaller scale was applied, for larger a bigger one (Benz et al. 2004). We performed segmentation on scale 20 by 50 with weights for mosaic and standardization layer of 2 and 3, respectively. Smaller scale results in a larger number of smaller objects, as presented in the analysis of the stone concentration and rocks (but not smaller than image resolution which is 0.1 m). The bigger scale is suitable for ripplemarks and sand bands. From the Feature View we have chosen 16 parameters, and an optimization use algorithm adequately:

- Segmentation with scale of 20: Length of main line, Length/width (only main line), Shape index, Number of darker objects
- Segmentation with scale of 50: Length/width (only main line), Shape index, Number of darker objects, Length of main line, Number of brighter objects

As previously, an overview of the used features is given in the eCognition Reference Book (Trimble eCognition® Developer 2010a).

From the segmentation with the scale of 20, classification provided a non-continuous rocks and stone layers, which we overlaid on the distribution of the bottom cover. Segmentation was performed on 2,906,253 objects. Due to computation costs, classification was conducted not for the whole area but only for the selected fragments. In particular the coastal zones were classified due to highly variable concentration of stones and rocks. Around 70 % of studied area was used and after classification we obtained area of 302,593.17 m² (that is 15.32 % of underwater sanctuary area) which reflects the stones and rocks (Table 3). Segmentation on level 50 created a ripplemark layer, which was added to the above-mentioned map. 274,282 objects were obtained as a result (it is 23.40 % of underwater sanctuary area). More than 60 % of created objects in the segmentation were used in

⁸ Standardization is a quotient from subtraction pixel average and its average by standard deviation. Result from standardization is variable with an average value and variance equals 1.

classification processes but only 15 % was assigned to stone's and rock's class (Table 3). Classification was conducted in deeper parts, where ripplemark forms occurred (in the southwestern and north-eastern parts of the map).

The presented analysis provided the spatial distribution of a bottom cover and its structure as a final product (Figs. 7 and 8). The main difference between these two maps is number of points and distance criteria given through interpolation. With the less number of points used and the less distance criteria used, smaller resolution of final map was obtained. An advantage is to avoid influence of cut parts with nadir effects.

6 Conclusions

Stone concentrations and rocks cover considerable areas of the seafloor. The space between those structures is filled with sand. Therefore, in a majority of cases, boulders and gravel sediments prevail. Sandy areas are covered by ripplemarks, mostly on coarse sands.

The obtained maps differ in terms of their accuracy. The first one (Fig. 7, left) is more accurate in better resolution, but also reflects the zones under the sonar (vertical bands joining individual polygons). It is possible to avoid this effect by applying smaller number of data introduced by interpolation or by reducing the resolution. The latter case is illustrated at the second map (Fig. 8, right).

The data obtained from the SSS mosaic and then classification routines can be employed to create maps of the sea bottom cover. Presented method can be used to obtain an image of morphological and deposition structures, especially for underwater areas. Parameters applied to control the map creation process (segmentation, classification, etc.) depend on the data introduced to the models. The rules depend directly on existing knowledge about the sea bottom structure and indirectly on the user's decisions. The object-oriented classification is a suitable method for acoustic, high resolution image analysis and its classification. The segmentation process effectively creates required objects with the help of an appropriate scale. Generated objects were qualified to proper classes which shows a capability of the method to quantify the character of the environment. The method addresses the issues of environment qualification both on local and global scales. The ArcGIS software provides an integral tool for visualization of the obtained results.

The analysis confirms that the results of the half-automatic procedure with use of the Definiens environment are not identical to manual classification results. The object-oriented classification provides more repeatable results. A simple way of changing the segmentation and classification rules or parameters is an advantage of the Definiens software. It means that the same initial data can be easily reclassified into a new map. The superiority of this method also lays in the fact that the application model can be re-used for other images, being adopted and changed during each classification step.

The methodology introduced in this paper can be used for almost any application where relationships between topographic features and other components are to be assessed (samples etc.). In this way, we hope to address a time-consuming task to produce underwater maps with bigger scales but still with an appropriate resolution. In earlier applications, the process of map creation was limited by hardware, software and interpretation theories. A pixel-based analysis has provided reasonably satisfying results and remained the industry standard for a long time. Advanced pixel-based processes such as texture measurements, linear mixture modeling, fuzzy sets and neural network classifiers were invented to enhance per-pixel image analysis (Blaschke and Strobl 2001). In this paper, I have demonstrated that a multistage image segmentation methodology can be more efficiently used for geomorphometry and terrain classification for underwater areas obtained from a side scan sonar mosaic.

Acknowledgments This research paper is made possible through the help and support from my Master's Degree Tutor—Associate Professor Jacek Urbański.

References

- Adamczyk J, Będkowski K (2005) *Metody cyfrowe w teledetekcji*. SGGW, Warszawa, 227s, ISBN 83-7244-671-7
- Anderson JT, Gregory RS, Collins WT (2002) Acoustic classification of marine habitats in coastal Newfoundland. *ICES J Mar Sci* 59:156–167
- Arboli R, Zhang Y, Palá V (2006) Advanced classification techniques: a review. ISPRS commission 4th mid-term symposium “From Pixel to Processes”, Enschede, 8–11 May 2006
- Baatz M, Hoffmann C, Willhauck G (2008) Progressing from object-based to object-oriented image analysis. In: Blaschke T, Lang S, Hay GJ (eds) *Object based image analysis*. Springer, Heidelberg, pp 29–42
- Benz UC, Hofmann P, Willhauck G, Lingenfelder I, Heynen M (2004) Multiresolution object-oriented fuzzy analysis of remote sensing data for GIS-ready information. *ISPRS J Photogrammetry Remote Sens* 58(3–4):239–258 ISSN 0924-2716
- Blaschke T (2010) Object based image analysis for remote sensing. *ISPRS J Photogrammetry Remote Sens* 65(1):2–16 ISSN 0924-2716
- Blaschke T, Lang S, Lorup E, Strobl S, Zeil P (2000) Object-oriented image processing in an integrated GIS/remote sensing environment and perspectives for environmental application. *Environ Inf Plann Polit Pub* 2:555–570
- Blaschke T, Strobl J (2001) What's wrong with pixels? Some recent developments interfacing remote sensing and GIS. *GeoBIT/GIS* 6:12–17
- Blondel P (2003) Seabed classification of ocean margins. In: Wefer G, Billet D, Hebbeln D, Jorgensen BB, Schlüter M, van Weering TCE (eds) *Ocean margin systems*. Springer, Berlin, pp 125–141
- Castilla G, Hay GJ (2008) Image objects and geographic objects. In: Blaschke T, Lang S, Hay GJ (eds) *Object based image analysis*. Springer, Berlin, p 75–89
- CODA (2001) *Trackplot/Mosaic User Manual*, Coda Technologies Ltd
- CodaOctopus. <http://www.gserentals.co.uk/pdf/Geokit%20Mosaic%20Replay1.pdf>
- Collier JS, Brown CJ (2005) Correlation of side scan backscatter with grain size distribution of surficial seabed sediments. *Mar Geol* 214(4):431–449

- Collins WT, Gregory R, Anderson J (1996) A digital approach to seabed classification. *Sea Technol* 37(8):83–87
- Edge Tech. 560-D Digital Side Scan Sonar System, Key Specifications—technical specification. http://www.terrasond.com/files/Datasheet_DF1000.pdf
- Freitas R, Silva S, Quintino V, Rodrigues AM, Rhynas KP, Collins WT (2003) Acoustic seabed classification of marine habitats: studies in the western coastal-shelf area of Portugal. *ICES J Mar Sci* 60(3):599–608
- Kenny AJ, Cato I, Desprez M, Fader G, Schüttenhelm RTE, Side J (2003) An overview of seabed-mapping technologies in the context of marine habitat classification. *ICES J Mar Sci* 60(2):411–418
- Kostylev VE, Todd BJ, Fader GBJ, Courtney RC, Cameron GDM, Pickrill RA (2001) Benthic habitat mapping on the Scotian Shelf based on multibeam bathymetry, surficial geology and sea floor photographs. *Mar Ecol Prog Ser* 219:121–137
- Kruss A (2008) Akustyczna identyfikacja habitatów bentosowych Arctyki. Ph.D. thesis, Library of Institute of Oceanology PAS in Sopot, Poland
- Lang S (2008) Object-based image analysis for remote sensing applications: modeling reality—dealing with complexity. In: Blaschke T, Lang S, Hay GJ (eds) *Object based image analysis*. Springer, Berlin, p 1–25
- Lucieer V, Lamarche G (2011) Unsupervised fuzzy classification and object-based image analysis of multibeam data to map deep water substrates, Cook Strait. *Continental Shelf Research* 31(11):1236–1247
- Majewski A (1992) *Oceany i morza*. Wydawnictwo Naukowe PWN, Warszawa
- Marpu PR, Niemeyer I, Nussbaum S, Gloaguen R (2008) A procedure for automatic object-based classification. In: Blaschke T, Lang S, Hay GJ (eds) *Object based image analysis*. Springer, Berlin, p 169–184
- Navulur K (2007) *Multispectral image analysis using the object-oriented paradigm*. CRC Press Taylor & Francis Group, Boca Raton, p 153
- Osowiecki A, Żmudzński L (eds) (2000) *Przyrodnicza waloryzacja morskich części obszarów chronionych HELCOM BSPA woj. pomorskiego, vol 2. Rezerwat Przyrody Kępa Redłowska*. CRANGON 6, Gdynia, p 76
- Penrose JD, SiwaBessy PJW, Gavrilov A, Parnum I, Hamilton LJ, Bickers A, Brooke B, Ryan DA, Kennedy P (2005) *Acoustic techniques for seabed classification*. Cooperative Research Centre for Coastal Zone Estuary and Waterway Management. Technical Report 32
- Preston J (2001) Shallow-water bottom classification. High speed echo-sampling captures detail for precise sediment. *Hydro Int* 5:30–33
- Ryan DA, Brooke BP, Collins LB, Kendrick GA, Baxter KJ, Bickers AN, Siwabessy JW, Pattiaratchi CB (2007) The influence of geomorphology and sedimentary processes on shallow-water benthic habitat distribution: Esperance Bay, Western Australia. *Estuar Coast Shelf Sci* 72:379–386
- Salamon R (2006) *Systemy hydrolokacyjne*. Gdańskie Towarzystwo Naukowe, Gdańsk, p 807
- Simmonds J, MacLennan D, (2005) *Fisheries acoustics. Theory and practice*, 2nd edn. Blackwell Science Ltd, Oxford. ISBN-10: 0-632-05994-X; ISBN-13: 978-0-632-05994-2
- Su Y, Huang PS, Lin CF, Tu TM (2004) Target-cluster fusion approach for classifying high resolution IKONOS imagery. *IEEE Proc Vis Image Signal Proc* 151:241–249
- Trimble eCognition® Developer 8.64.0 (2010a) Reference book. Trimble Documentation, München
- Trimble eCognition® Developer 8.64.0 (2010b) User guide. Trimble Documentation, München. In: Kumar N (2007) *Multispectral image analysis using the object-oriented paradigm*. CRC Press Taylor & Francis Group, 153s, Boca Raton
- Wicher W (2001) *Klasyfikacja dna przybrzeża Kępy Redłowskiej na podstawie zdjęcia sonarowego*. Geologia i geomorfologia przybrzeża i dna południowego Bałtyku 4:83–89
- Wicher W (2003) *Określenie struktury geologicznej i tendencji zmian dna przybrzeża Gdynia Orłowo na podstawie rejestracji sejsmoakustycznych*. Ph.D. thesis, Archive of Institute of Oceanography in University of Gdańsk, Gdańsk

- Wienberg C, Bartholoma A (2005) Acoustic seabed classification in a coastal environment (outer Weser Estuary, German Bight)—a new approach to monitor dredging and dredge spoil disposal. *Cont Shelf Res* 25:1143–1156
- Ouyang Zu-Tao, Zhang Mo-Qian, Xie Xiao, Shen Qi, Guo Hai-Qiang, Zhao Bin (2011) A comparison of pixel-based and object-oriented approaches to VHR imagery for mapping salt-marsh plants. *Ecol Inform* 6:136–146

The Role of Extreme Events in the Development of the Coastline in the Darlowko Area

Małgorzata Merchel

Abstract Storm surges that are generated by storms have a very strong impact on the seashore. Section of the seashore in Darlowko surrounding is particularly vulnerable to the effects of storm surges. High impact on the seashore in this area is also exerted by the port breakwaters, which is a persistent obstacle to movement of alongshore stream of sediments. Storms form the beach and are the largest cause of damage on the coast. The largest losses on the Polish coast definitely concern damage of bank sand. The study shows that the most intense coastal destruction occurs during heavy storms, when large wave is applied to the high level of the sea. There was a significant dependence between the shoreline changes in analyzed 15- and 45-year periods and losses of bank sand as a result of storm surges. The research shows that storm surges play a particular role in both seasonal and long-term changes in the coastline.

Keywords Storm • Darlowko • Storm sure • Shoreline changes • Storm damage • Port breakwaters

1 Introduction

The importance of research in coastal processes is constantly increasing, along with economic development and recreational functions of the coastline. The research is carried out by different methods, and concerns the correct development of the coastline, especially its behavior in a larger time scale. This forms the basis of well-balanced management of coastal areas (Dobrzyński 1998).

M. Merchel (✉)

Institute of Oceanology Polish Academy of Sciences, Sopot, Poland
e-mail: merchel@iopan.gda.pl

I decided to investigate the role of storms in the seashore formation of the analyzed coast section around Darlowko, because few people in Poland have been engaged in research on storm surges and their impact on this part of the coast. I chose into the test the area around Darlowko, because it is very exposed to storm surges due to its location.

Development of the coast is variable in time and space and depends on many factors. Storms with storm surges that are their consequences have a special role in the development of the coast (Castelle et al. 2007; Lowe et al. 2001; Unnikrishnan et al. 2004).

According to Tonnison et al. (2008) strong storm waves combined with high sea level have caused substantial changes in the coastal geomorphology of depositional shores on Saaremaa Island, Estonia. The most spectacular changes occurred in the areas that were well exposed to the storm winds and wave activity.

Oriviku et al. (2009) show in their paper that almost all of erosion occurring within the sandy beaches is caused by a rare storms. They concluded that the four extreme storms in 10 years resulted in 95 % of the erosion of the sandy slope at Cape Kiipsaare (Estonia).

According to Weisse and Plüß (2006) storm surges represent a particular threat for low-lying coastal areas like those along the North Sea coast. Much of the hinterland (especially in the Netherlands, Denmark, and Germany) is below or only slightly above mean sea level and has to be protected from the effects of storm surges.

Among the many low-lying areas, also the United States' densely populated Atlantic and Gulf Coast lie less than 3 m above mean sea level and are vulnerable to coastal storm surge and associated surge damages (Bromirski and Kossin 2008; Irish et al. 2011; <http://www.noaa.gov>).

The present study area is particularly vulnerable to the effects of storm surges due to the SW–NE course of its coastline, causing its exposure to prevailing winds in Poland from the western sector and the northern sector. In the case of Darlowko surrounding, important role in the development of the coast is also played by hydrotechnical constructions, geological structure, bottom carving and sediments thickness of southern Baltic foreshore.

Between all the factors influencing the development of the coast there are strong relationships. Disruption of even one of them may have a negative impact on a substantial length of the coast (Zawadzka-Kahlau 1999).

This paper highlights the special role of storms and storm surges that are their consequences in the development of the seashore.

2 Methods

The study is based on data obtained from different units of the Maritime Office in Slupsk.

The headquarters of the Maritime Office in Slupsk provided data on the history of the analyzed section of coastline in 1960, 1970, 1980, 1990 and 2005, materials on methods of protecting the coast study area and the current storm damage pricing.

From the Coast Guard District in Darlowo we obtained Storm Reports for the years 2000–2007, including information on the type and size of the damage caused by storm surges.

Harbour Master's Office in Darlowek made available for us the Captain's Logs from the years 2000 to 2007, with information on the storms that occurred during this period, in the form of: dates of storms, wind force and direction, sea state and the level of water in the channel.

3 Study Area

Location of the study area in the physical and geographical division of the country by Kondracki (2001) is as follows:

- province: Niż Środkowoeuropejski (31.0)
- subprovince: Pobrzeże Południowobałtyckie (313.0)
- macroregion: Pobrzeże Koszalińskie (313.4).
- mesoregion: Wybrzeże Słowińskie (313.41)

Wybrzeże Słowińskie is a narrow strip of land along the shore of the Baltic Sea, 200 km in length and about 1,120 km² in area, which stretches from the Parsęta river mouth after Kepa Swarzewska (Kondracki 2001).

The test section of the coast is located in the western part of Wybrzeże Słowińskie and stretches for about 20 km between the fistula lake Bukowo and fistula lake Kopań (Fig. 1). Its landscape consists of: beach, coastal dunes and coastal

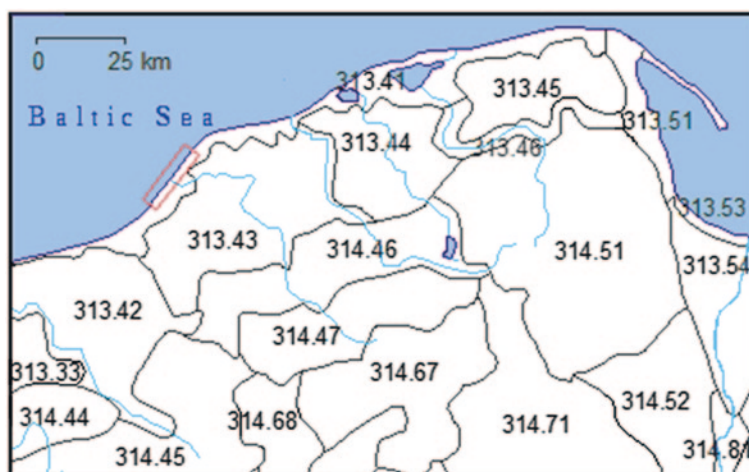


Fig. 1 Location of the study area against the division of the northern Polish mesoregions (Source Kondracki 2001)

lakes. Spits separate the sea from shallow lakes Bukowo and Kopań. Bukowo Lake is fed by the Grabowa River. Within the study area, directly into the Baltic Sea discharges Wieprza River. At its mouth there is a small fishing port Darlowko (Kondracki 2001).

4 Extreme Events

According to the International Panel on Climate Change (IPCC), extreme weather phenomenon is a phenomenon that is referred to as rare under appropriate for the probability distribution of occurrence. The statement “rare” can be interpreted differently in different regions. It is usually assumed that rare phenomenon is one that is more frequent than those specified by the value of quantile 10 and 90 % of that probability distribution (Miętus 2005).

The most dangerous extreme events occurring on the southern Baltic Sea are storms with storm surges which are their consequence.

A storm is a strong, long-lasting wind, blowing at a rate of 6° (39–49 km/h) on the Baltic Sea, and 8° (62–74 km/h) on the oceans, according to the Beaufort scale (Pietrkiewicz and Żmuda 1973).

A storm surge (by Hydrological Aspects of Combined Effects of Storm Surges and Heavy Rainfall on River Flow, WMO—No. 704, Geneva 1988) means the rapid rise in sea level above the level that would be observed in the same place and time, if there was no strong wind from the mainland (Sztobryn and Stigge 2005).

In Poland, Majewski et al. (1983) classifies as a storm surge any hydrological situation in which the sea level reaches or exceeds 570 cm (Sztobryn and Stigge 2005).

The occurrence of strong and storm winds cause passing troughs with frontal systems (or without). Strong shoreward wind causes surge and offshore wind reducing the level of the sea. In case of storm winds it will result for some coasts in the reduction of the water level, while in the others' in a surge. A large part of low pressure systems, moving over the Baltic Sea region, is causing the storm surges on the south coast (Sztobryn and Stigge 2005).

5 Characteristics of Storms in the Years 2000–2007

In 2000–2007, in the study area there occurred 20 storm events. The largest number occurred in 2001 and 2004 (Table 1). In 2005 there were no storm events, and in 2000 there was only one storm. The reported storms occurred most frequently in November (8 storms), and least frequently in March and April (1 storm) (Table 1).

The greatest strength of the wind was recorded during the storm of 17–18.11.2004. It achieved the value of 10–11, gusting to 12 on the Beaufort scale (Table 1). The wind was blowing from the smallest force 6–7, gusting to 8 on the

Table 1 Tabulation of storms in the years 2000–2007

Ordinal	Date	Beaufort force	Wind direction	State of the sea (Douglas scale)	Water level (cm)
1	2000	6–8	N	5	580
2	2001	9–10	NW–W	5–6	580
3		9–10	W–NW	6	570
4		8–9	NW	5–6	550
5		8–10	W–NW	5–6	600
6		6–7 (8)	NW–N	4–5	585
7	2002	9–10	NW	6	570
8		10	NE–N	5–7	580
9	2003	9–10	NE–N	6	560
10		10–11	NW–N	6	580
11	2004	7–9	W–SW	5	495
12		7–8	NW–W	5	510
13		8–9	W–NW	5	535
14		10–11 (12)	W–NW	5–6	550
15		8–9 (10)	NW–N	6	620
16	2006	8–9	N–NE	6	650
17	06/07	9–10 (11)	W–NW	6	540
18	2007	8–9 (10)	W–NW	6	610
19		8–9 (10)	W–NW	5	640
20		8–9 (10)	NW–N	5	560

Source Dzienniki kapitańskie

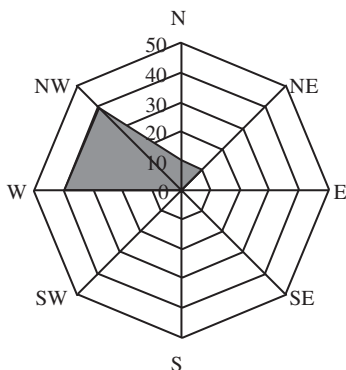


Fig. 2 Wind rose for storms (see Table 1)

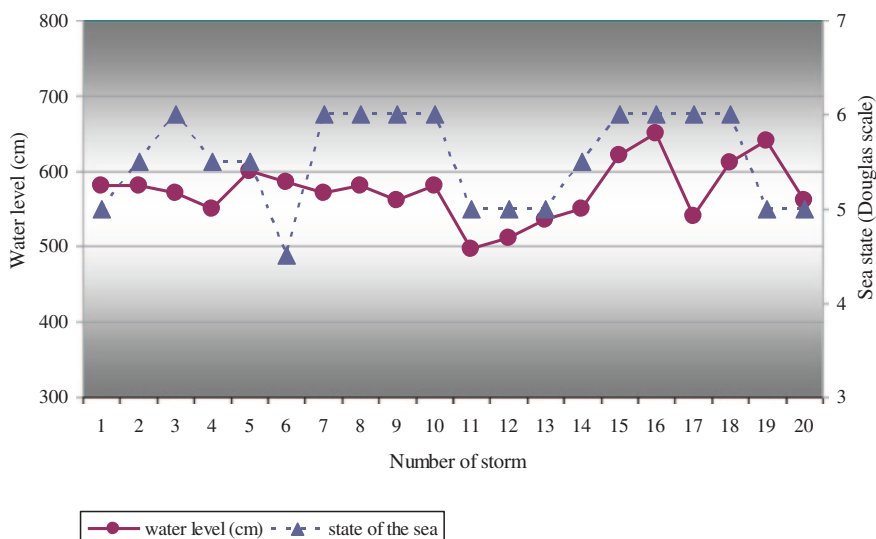


Fig. 3 State of the sea and the water level during storms (see Table 1)

Beaufort scale in the storm of 23.11.2001. The weakest wind blew from the north, and the strongest from the west and north-west. Average wind speed during the storm was 9 on the Beaufort scale.

During the analyzed storm events, in the case of eight (40 % of the twenty) the storm wind blew from the west, in further eight (40 %) from the north-west, in two (10 %) from the north and two (10 %) from the north-east (Fig. 2).

The highest state of the sea occurred on 01–02.01.2002, and was 5–7, and the lowest was recorded on 23.11.2001 and reached a value of 4–5 (Fig. 3). Average state of the sea during the storm was 5.5.

The water level in the channel reached the highest value of 650 cm in a storm of 01–02.11.2000, and 640 cm on 19–21.01.2007, the lowest water level in the channel was recorded during the storm of 19–21.03.2004 (495 cm) and 15–16.09.2004 (510 cm) (Fig. 3). The average water level during the storm was 573 cm.

6 The Role of Extreme Events in the Development of the Coast

Extreme events play a very important role in the development of the coastal zone. Among them, the biggest influence on Polish coast is exerted by storms, and a much smaller influence comes from low sea states.

Linked with the wind from the land, low sea states pose a threat to shipping: on routes running near the sea coast, on the fairways to the ports and waters of shallow and port waters (Bogdanowicz et al. 2005).

Storms, occurring mainly in the autumn and winter, are associated with the occurrence of strong winds from the sea and have character of storm surges (Boniecka and Zawadzka 1999).

If the beach is wide and high enough, it completely quenches the energy of an upcoming wave, which is not able to come to the base of the dunes and does not cause its erosion. However, if the profile of the beach is narrowed or reduced, or if the storm is extremely strong, the wave crossing the beach erodes the basis of the dunes, causing its slide and shifting its upper edge toward the land (Basiński 1995).

On Polish transit dune shores, which are not built-up hydrotechnically, the beach is generally relatively wide. Such a beach, even if it is blurred in the storm, is rebuilt in the periods between storms and the dry material collected on it, carried by the wind, is expanding or rebuilding the existing dune sequences (Basiński 1995).

The largest erosion occurs in the first part of the storm, and then gradually decreases, although the hydrodynamic conditions do not change. This is related to the transformation of the output profile to the physical profile of equilibrium, but it is never reached because of the relative shortness of the hydrodynamic conditions (Basiński 1995).

The main factor causing phenomena of dune erosions is the level of storm surge. Height and period of storm wave have smaller input during maximum storm, but if the wave lessen, erosion phenomena decrease rapidly (Basiński 1995).

According to the existing measurements from nature, at some points of the Polish coast displacement of the dune base by a few meters may happen during an average storm, a dozen meters—in the strong storm (the probability of occurrence once every few years) and 20 or more meters during a catastrophic storm, when the water surge level significantly exceeds ordinate 600 cm for many hours (Basiński 1995).

Variability of storm surges at the time, including the undulation, causing the most damage on the coast, and its reconstruction depends on the speed of sea level fall (Musielak 1978, 1980, 1990) after (Dobrzyński 1998).



Picture 1 Mini-cliff created around the beach by storm surges (272 km); 07.12.2007 r. (photograph M. Merchel)

First of all, we owe the storm phenomena the existence of beaches at the foot of the shore and their main external features such as height, width, angle of inclination and orientation of sandy-gravel material of beach cover. Pomeranian beaches are in fact formed only in storm time. Strong storms shape them on entire width, making a total replacement of the beach cover material as well as destroying sediments on its ground. Weaker, but frequent storms often convert the lower parts of the beach (Rosa 1984).

7 Storm Damage

Storm damage was analyzed on the basis of eight sample storms. The damage was provided for the bank sand, fascine cover, fascine hurdle and grass cover. The greatest damages definitely involve loss of the bank sand (Pictures 1 and 2). They ranged from 84.7 to 99.2 % of the total storm damage. Much lower losses concern fascine cover (from 0.4 to 12.3 %) and fascine hurdle (from 1.3 to 3.5 %), and the smallest grass cover (from 0.2 to 0.8 %).

The greatest damage was caused by the storm of 01–02.01.2002, with a total value of losses amounting to about 1.1 million zlotys, and the storm of 12–15.01.2007 with the total value of losses of about 945 thousand zł (Table 2). It follows from this that



Picture 2 Mini-cliff created around the beach by storm surges (277 km); 07.12.2007 r. (photograph M. Merchel)

Table 2 Tabulation of storm damage in the years 2000–2007 (in zloty)

Date of storm phenomena	Valuation of the damages (thous. zl)				
	Bank sand	Fascine cover	Grass cover	Fascine hurdle	Total
16–19.01.2000	252.000	11.175	2.140	3.526	268.841
01–02.01.2002	1,122.000	4.250	9.370	–	1,135.620
06–07.04.2003	232.500	11.250	–	–	243.750
05–07.12.2003	77.500	10.750	0.700	–	88.950
17–18.11.2004	110.000	6.000	–	2.150	118.150
31.12.2006–01.01.2007	82.500	–	–	3.010	85.510
12–15.01.2007	937.500	5.500	1.700	–	944.700
09–10.11.2007	134.375	19.600	0.875	3.870	158.720
Price per unit	25.00 zl/m ³	2.50 zl/m ²	0.50 zl/m ²	4.30 zl/mb	3,044.241

Source Meldunki posztormowe

the most intense coastal destruction occurs during heavy storms, when large undulation is applied to the high level of the sea.

The smallest damage was caused the storm of 31.12.2006–01.01.2007, with the value of losses approximately 85.5 thousand zl, and the storm of 05–07.12.2003 causing losses of about 89 thousand zl (Table 2).

Storms that occurred during the period 2000–2007 caused losses amounting to more than 3 million zl. This implies that the average value of the damage caused during one storm is approximately 380.5 thousand zl.



Picture 3 The effects of the front dune erosion due to storm surges in the form of fallen trees (265 km); 19.11.2006 r. (photograph M. Merchel)

During most of these storms, in addition to bank sand, grass cover, fascine cover and fascine hurdle, there were destroyed trees and hydrotechnical constructions (Pictures 3 and 4). In total, 1,713 trees have fallen during storm surges, with the result that 95 trees were destroyed during one storm.

8 Impact of Storms on Coastline Change

In the years 1960–2005, the coastline along a distance of 19 km (264.0–283.0 km) has moved, on the average, by -2.13 m, and in 1990–2005 by -3.75 m (Fig. 4), which indicates the intensity of erosion in the last 15 years of the analyzed section.

In the years 1960–2005, erosion occurred in the sections from 264.0 to 270.0 km, from 278.5 to 281.5 km, and from 282.0 to 282.5 km, and accumulation in the sections from 270.0 to 278.5 km, from 281.5 to 282.0, and 282.5 to 283.0 km. It follows that the study area experienced three sections of erosion, with a total length of 9.5 km, and the three sections of the accumulation, of a total length 9.5 km, but the average losses in eroded sections were -39.63 m/km, while the average increase on accumulated sections was 35.37 m. This is a proof that the seashore erosion exceeded quantitatively its growth.

The main sections of erosion, which is located between 264.0 and 270.0 km and accumulation, between 270.0 and 278.5 km, are largely associated with the port



Picture 4 The effects of the front dune erosion due to storm surges in the form of fallen trees (267 km); 19.11.2006 r. (photograph M. Merchel)

breakwaters (located at 270 km), which are a persistent obstacle to movement of alongshore stream of sediments. Consequently, the sediment is retained on the western side of the port breakwater, which is the cause of the deficiency to the east.

The erosion section (264.0–270.0 km) is constantly destroyed, despite the fact that the entire length is protected by hydrotechnical buildings, and in some of its parts is also protected by biotechnical buildings and artificial recharge of seashore. Storms contribute to these phenomena, which are a major factor in the destruction of the bank sand.

There is no beach that would be wide and high enough to completely quench the upcoming wave, preventing it from reaching the base of the dune and causing erosion. Also the lack of abundant sandbanks is a cause of direct impact waves on the beach- and dune-zone, which resulted in almost total disappearance of the dunes (Merschel 2008).

The lower rank valley forms, occurring in the Darlowko area and abrasive platform at the height of the Kopan lake, contribute to the erosion of these sections (Zawadzka 2001).

The advantageous increasing of the seashore over its losing, at the section between 270.0 and 278.5 km, is affected by many factors. Aside from the impact of the port breakwaters, a great influence is exerted by morphology and surface sediments of the coastal zone of the section.

Accumulative plains at an altitude of Jamno lake can be periodically a source of sediment for shores of Bukowo lake spit located in the east, and the erosive inliers on upland marginal zone of the Koszalin Bay weaken the erosion processes

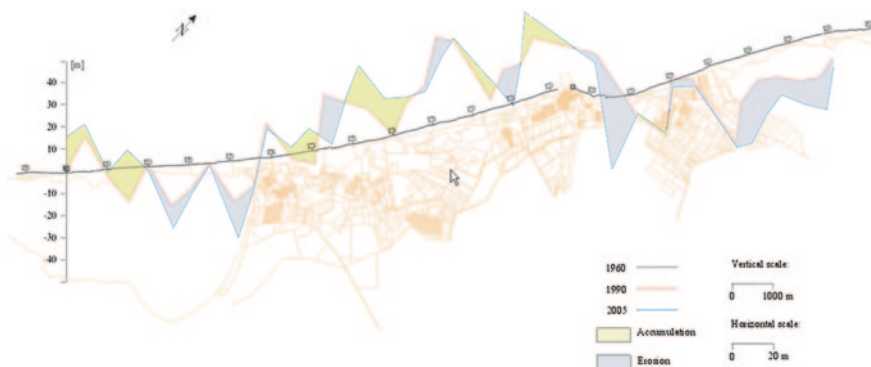


Fig. 4 Shoreline change in the years 1990–2005 (m) (prepared by M. Merchel)

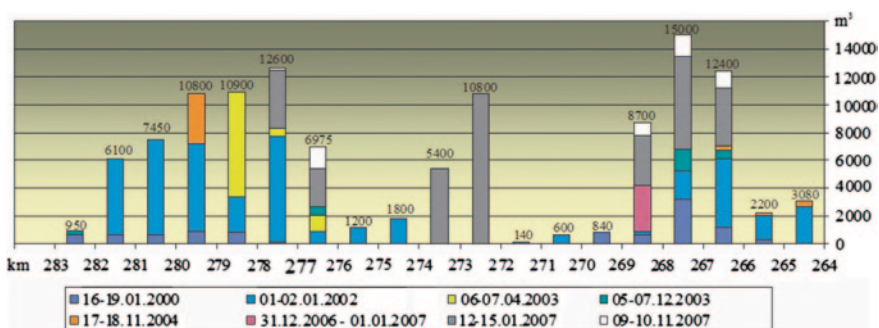


Fig. 5 Total losses of the bank sand after storms in the years 2000–2007 (m³) (prepared by M. Merchel)

in the section of Bukowo lake—Darlowek. The wide beach and dune zone, as well as sediment-rich sandbanks, largely contribute to the quench energy of the onrushing wave during the storm surge (Zawadzka 2001).

East of the port breakwaters, shoreline displacement in the analyzed 45-year period was -40.8 m, and in the 15-year period it was -19.12 m. West of the breakwaters, these values are $+17.98$ and $+4.24$ m, respectively.

In the years 1990–2005, the main sections of erosion had a length of 3.5 and 3.0 km. The first section is between 278.0 and 281.5 km, and the second between 264.0 and 267.0 km. More important sections of accumulation are, respectively, 2.0 and 1.5 km and are located between 274.5 and 276.5 km, and between 281.5 and 283.0 km. Other sections, both eroded and accumulated, are from 0,5 to 1 km in length.

In the analyzed 15 years, the average losses on eroded sections were -20.83 m, while the average increase on accumulated sections was $+17.35$ m. There were at that time seven erosive sections with a total length of 10.5 km, and seven accumulated section with a total length of 8.5 km. Thus, erosion processes covered 55.3 % of the length of the analyzed shore and accumulation processes 44.7 % of its length. It follows that, in the last decade the amount of both the increment and wastage of the shore has decreased, but erosive section was extended.

There was a significant dependence between the coastline changes in the analyzed 15- and 45-year period and losses of bank sand as a result of storm surges (Figs. 4 and 5).

At the test section of the coast, in large losses of bank sand, generally there was a significant shift of the coastline towards the mainland. The opposite situation occurred in places where storm losses were small. There coastline generally shifted towards the sea (Figs. 4 and 5).

It follows that storm surges play a particular role in both seasonal and long-term changes in the coastline.

9 Conclusions

Storms with storm surges which are their consequences, play a very important role in the development of the coast of the test section. It is particularly vulnerable to the effects of storm surges due to the SW–NE course of its coastline, causing its exposure to winds from the western sector and the northern sector that prevail in Poland.

In the case of Darlowko surrounding, important role in the development of the coast is also played hydrotechnical constructions (especially the port breakwaters), geological structure, bottom carving and sediments thickness of southern Baltic foreshore.

In 2000–2007 in the study area there occurred 20 storm events, that caused huge losses, mainly in bank sand, but also in fascine cover, fascine hurdle, grass cover, hydrotechnical constructions and trees.

The study shows that the most intense coastal destruction occurs during heavy storms, when large waving is applied to the high level of the sea.

In the paper, changes of the coastline in the years 1960, 1990, 2005 were compared with losses of bank sand over the years 2000–2007. There was a significant dependence between the coastline changes in the analyzed 15 and 45 year period and losses of bank sand as a result of storm surges.

At the test section of the coast, in large losses of bank sand, there was, generally speaking, a significant shift of the coastline towards the mainland. The opposite situation occurred in places where storm losses were small. There, coastline has generally shifted towards the sea.

It follows that storm surges play a particular role in both seasonal and long-term changes in the coastline.

References

- Basiński, T (1995) Przebieg i wielkość sztormowej erozji wydmy. In: Florek W (ed.) *Geologia i geomorfologia pobraża i południowego Bałtyku*, 2. Słupsk, 187–199
- Bogdanowicz E, Kossakowska-Cezak U, Szkutnicki J (2005) *Ekstremalne zjawiska hydrologiczne i meteorologiczne*. IMGW, Warszawa
- Boniecka H, Zawadzka E (1999) *Uwarunkowania naturalne rozwoju brzegu morskiego wód wewnętrznych*. Wydawnictwo Wewnętrzne Instytutu Morskiego, Gdańsk

- Bromirski PD, Kossin JP (2008) Increasing hurricane wave power along the U.S. Atlantic and Gulf coasts. *J Geophys Res* 113:C07012
- Castelle B, Turner IL, Ruessik BG, Tomlinson RB (2007) Impact of storms on beach erosion: broadbeach (Gold Coast, Australia). *J Coast Res* SI 50:534–539
- Dobrzyński S (1998) Współczesny rozwój brzegu morskiego w świetle badań litologicznych (na odcinku Jarosławiec-Czołpino). Wyższa Szkoła Pedagogiczna w Słupsku, Słupsk
- Dzienniki kapitańskie (Captain's Logs) z lat (2000–2007) Kapitanat w Darłównu
- Irish JL, Resio DT, Divoky D (2011) Statistical properties of hurricane surge along a coast. *J Geophys Res* 116:C10007
- Kondracki J (2001) Geografia regionalna Polski. Wydawnictwo Naukowe PWN, Warszawa
- Lowe JA, Gregory JM, Flatter RA (2001) Changes in the occurrence of storm surges around the United Kingdom under a future climate scenario using a dynamic storm model driven by the Hadley Centre climate models. *Clim Dyn* 18:179–188
- Majewski A, Dziadziuszko Z, Wiśniewska A (1983) Monografia powodzi sztormowych 1951–1975. Ogólna charakterystyka powodzi sztormowych u polskiego wybrzeża Bałtyku, Wydawnictwa Komunikacji i Łączności Warszawa
- Merchel M (2008) Praca magisterska—Rola zjawisk ekstremalnych w rozwoju brzegu morskiego w rejonie Darłowa (na odcinku od przetoki jeziora Bukowo do przetoki jeziora Kopań). Master's Thesis, Akademia Pomorska w Słupsku, Słupsk
- Miętus M (2005) Ekstremalne zjawiska klimatyczne z perspektywy IPCC. In: Bogdanowicz E i in (ed.) Ekstremalne zjawiska hydrologiczne i meteorologiczne, IMGW, Warszawa, 19–31
- Meldunki posztormowe (Storm Reports) z lat (2000–2007) Urząd Morski w Słupsku
- Musieliak S (1978) Procesy litodynamiczne w strefie przyboju, *Oceanologia* 8
- Musieliak S (1980) Współczesne procesy brzegowe w rejonie Zatoki Gdańskiej. *Peribalticum GTN*, Gdańsk
- Musieliak S (1990) Morfolitodynamika morskich plaż piaszczystych, *Studia i Materiały Oceanologiczne* 55, Brzeg Morski 1, Ossolineum, Gdańsk, 67–78
- National Oceanic and Atmospheric Administration. <http://www.noaa.gov>
- Orviku K, Suursaar Ü, Tõnisson H, Kullas T, Rivis R, Kontv A (2009) Coastal changes in Saaremaa Island, Estonia, caused by winter storm in 1999, 2001, 2005 and 2007. *J Coast Res* SI 56:1651–1655
- Pietrkiewicz S, Żmuda S (1973) Słownik pojęć geograficznych. Wiedza Powszechna, Warszawa
- Rosa B (1984) Rozwój brzegu i jego odcinki akumulacyjne. In: Augustowski B (ed.) *Pobrzeże Pomorskie*. Ossolineum, Gdańsk, 67–120
- Sztobryn M, Stigge HJ (eds) (2005) *Wezbrania sztormowe wzdłuż południowego Bałtyku (zachodnia i środkowa część)*. Instytut Meteorologii i Gospodarki Wodnej, Warszawa
- Tõnisson H, Orviku K, Jaagus J, Suursaar Ü, Kontv A, Rivis R (2008) Coastal damages on Saaremaa Island, Estonia, caused by extreme storm and flooding on January 9, 2005. *J Coast Res* 24(3):602–614
- Unnikrishnan AS, Sundar D, Blackman D (2004) Analysis of extreme sea level along the east coast of India. *J Geophys Res* 109:C06023
- Weisse R, Plüß A (2006) Storm-related sea level variations along the North Sea as simulated by a high-resolution model 1958–2002 coast. *Ocean Dyn* 56:16–25
- Zawadzka-Kahlau E (1999) Tendencje rozwojowe polskich brzegów Bałtyku Południowego, Gdańsk
- Zawadzka E (2001) Wpływ rzeźby dna oraz miąższości osadów litoralnych przybrzeża Bałtyku południowego na dynamikę brzegów. In: Florek W (ed.) *Geologia i geomorfologia pobraża i południowego Bałtyku* 4, Słupsk

Attenuation of Groundwater Flow Due to Irregular Waves in Permeable Sea Bottom

Anna Przyborska

Abstract The disappearance of wave energy in porous medium, expressed by the decreasing pore pressure, depends on the properties of the soil matrix and compressibility of water in the matrix pores. On the other hand, the compressibility of pore water depends to a large extent on the content of air/gas in water. Thus, it seems that the problem of water circulation resulting from surface waves is in fact a problem from the theory of multiphase media. Transmittance functions between surface waves and pore pressure at different depths as a result of the linear wave theory well reproduce the experimental data at frequencies close to the spectrum of peak energy.

Keywords Pore pressure • Permeable beach • Circulation of groundwater
Filtering • Modeling • Irregular waves

1 Introduction

For tideless seas the groundwater flow is governed entirely by the surface wave dynamics and current on the beach, the crucial role is played by the surface wave dynamics. As waves propagate towards the shore, they become steeper owing to the decreasing water depth and at some depth the waves lose their stability and start to break. When waves break, wave energy is dissipated and the spatial changes of the radiation stress give rise to changes in the mean sea level. After the wave reaches the shore, it will run up and run down the beach face. This phenomena drives a complex groundwater circulation in a porous medium. Water infiltrates into the coastal aquifer on the upper part of the beach near the

A. Przyborska (✉)

Institute of Oceanology, Polish Academy of Sciences, Warsaw, Poland

e-mail: aniast@iopan.gda.pl

maximum run-up, and exfiltration occurs on the lower part of the beach face near the breaking point (Longuet-Higgins 1983).

The research on the propagation above a permeable bottom, but over constant depth, began about 35 years ago (Moshagen and Torum 1975; Massel 1976). It turned out that the loss of wave energy in a porous medium, expressed by the loss of pore pressure depends on the properties of the soil matrix and the compressibility of water moving within the pores of the matrix.

The compressibility of pore water depends to a large extent on air/gas content in water. The relation shows that circulation of water induced by surface waves is essentially a problem of the multiphase media dynamics (Biot 1956; Mei and Foda 1981). Water in a porous medium, which transports oxygen, plays an important role in maintaining the biological life in the beach sand (McLachlan 1989; Shum 1993; Weslawski et al. 2006). It was observed that natural sea-water filtration in bottom sand consists of two types of processes: physical and biological. Advective physical processes have a significant impact on sedimentary processes. Sandy sediments may thus be a unique environment that differs significantly from cohesive sediments (Huettel and Rush 2000; Huettel et al. 2003).

Some interesting results were obtained in a three-year international research program COSA. The COSA (Coastal sands as biocatalytic filters) demonstrated the important role of sand in the functioning of marine coastal ecosystems. One of the most striking features of beach sand is the fact that these deposits can effectively catch particles in the water column near the bottom, allowing thereby to provide effectively non-organic matter to the sediment (Huettel and Rush 2000).

Numerous references show that the potential solution well reproduces the movement of water in a porous bottom of high permeability, i.e. fine stones, coarse and medium sand. For very low permeability potential solution differs from experimental data (e.g. Massel et al. 2004), since such soil requires taking into account the consolidation of the bottom material and water compressibility. Previous studies showed that pore water is not a single phase medium. Initial work on the development of two phase liquid-matrix theory, was started by Terzaghi (1943). Biot (1956) improved and generalized his theory. The basic idea is the adoption of Biot's theory of elastic soil matrix and laminar flow of pore fluid, according to Darcy's law. Massel et al. (2004, 2005) formulated a solution based on the theory of multiphase media with an assumption of constant sea depth. This article is an extension of these studies and presents the results for irregular waves. The paper is organized as follows. At the beginning it discusses the governing equations for groundwater pressure and its circulation. In particular, it describes transmittance functions between surface waves and pore pressure at different depths as a result of the linear wave theory. The next part compares the theoretical results with the experimental data obtained during laboratory measurement on Grofier Wellenkanal (GWK) in Hannover (Germany) and the experimental data collected in natural conditions. Finally, the last section gives the summary and main conclusions.

2 Theoretical Basis

In natural conditions and sometimes in the laboratory—generated waves have random nature. Consider, therefore, the stochastic relationships between the sea surface and the pore pressures based on linear systems theory.

According to the theory of linear systems, the relationship between the output signal $y(t)$ and the input signal $x(t)$ is described using the convolution integral:

$$y(t) = h(t) \star x(t) = \int_0^{\infty} h(\tau)x(t - \tau)d\tau \quad (1)$$

where the symbol \star is a convolution operation and $h(\tau)$ is the impulse response function.

For transmittance function $H(\omega)$ we have the (Otnes and Enochson 1972) relation:

$$H(\omega) = \int_0^{\infty} h(\tau)e^{-i\omega\tau} d\tau \quad (2)$$

Knowing $h(t)$ for the input $x(t)$, the $y(t)$ system response may be determined. Equation (1) is not always practical, the relationship between the respective input signal spectrum densities and the system responses is more useful:

$$Y(i\omega) = |H(i\omega)|^2 X(i\omega) \quad (3)$$

where

$$H(i\omega) = \mathcal{F}(h(t)) = \frac{1}{2\pi} \int_{-\infty}^{+\infty} h(t) \exp(-i\omega t) dt \quad (4)$$

is the Fourier transform of the response $h(t)$, and:

$$X(i\omega) = \mathcal{F}(x(t)) = \frac{1}{2\pi} \int_{-\infty}^{+\infty} x(t) \exp(-i\omega t) dt \quad (5)$$

and

$$Y(i\omega) = \mathcal{F}(y(t)) = \frac{1}{2\pi} \int_{-\infty}^{+\infty} y(t) \exp(-i\omega t) dt \quad (6)$$

are respective Fourier transforms of signals $x(t)$ and $y(t)$.

If we assume that the spectral wave density $S_{\zeta}(\omega)$ is the system input function and the output function is pressure spectral density at a set depth, $S_p(\omega, z)$ in (3), we obtain:

$$S_p(\omega, z) = |H(\omega, z)|^2 S_{\zeta}(\omega) \quad (7)$$

and

$$S_{\zeta p}(\omega) = H(\omega)S_{\zeta}(\omega) \tag{8}$$

In practical applications the so-called coherence function between the signals at the input and output is often used. Thus, we have:

$$\gamma_{\zeta p}^2(\omega) = \frac{|S_{\zeta p}(\omega)|^2}{S_x(\omega)S_y(\omega)} \tag{9}$$

First let us consider planar motion in the plane $O(x, z)$ (Fig. 1).

Let the surface wave of height H , frequency ω and the wave number k move towards the positive sense of axis x . The water depth is constant and is h , and under the bottom there is a porous layer of thickness $(h_n - h)$.

The proposed solution is based on the theoretical concepts of multiphase flows in porous media of the beach. The basic value determined experimentally or calculated in the model is pore pressure in the beach sand.

In the general case, the loss of pore pressure in the soils is complex and depends strongly on the mechanical and hydraulic properties of the medium and the surface wave properties forcing water movement. Theoretical model, based on Biot's theory, takes into account soil deformations, the content of the air/gas dissolved in pore water and the change of pore water volume and flow direction (Biot 1956), resulting in vertical gradients and vertical pore pressure gradient. It is assumed that the deformation of the soil matrix satisfied the linear elasticity law and the relationship between the pressure gradient and the pore water velocity is expressed by the Darcy's law. This means that we examine the case of low

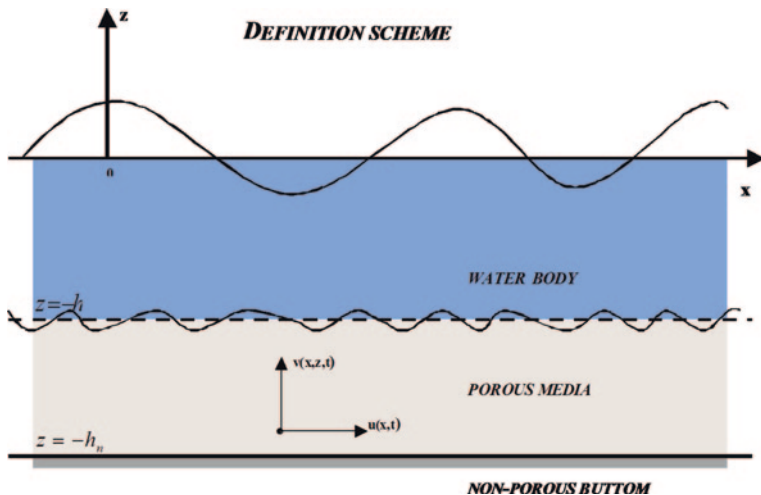


Fig. 1 Reference system

permeability. The case of high permeability. When the Darcy's law cannot be used, requires a different approach.

It is important for the studied issue that when waves break, they inject air and gases into the porous medium. In addition, gases are produced by organisms living in the sand. As a result, we deal with a three-phase medium which consists of a soil skeleton, pore water and gas/air. As a result, the elastic modulus of pore water E'_w depends on the degree of water saturation with air (Verruijt 1969):

$$\frac{1}{E'_w} = \frac{S}{E_w} + \frac{1-S}{p_0} \quad 1 - S \ll 1, \quad (10)$$

where:

- E_w true bulk modulus of pore water without air ($E_w = 2.3 \cdot 10^9 \text{N/m}^2$),
- S the degree of saturation of the soil matrix pores with water,
- p_0 absolute pressure at a given point (the sum of pressure hydrostatic pressure and pressure induced by sea surface),
- E'_w apparent bulk modulus of water.

E'_w is different for different levels and decrease with depth of the pore layer, which suggests that E'_w ratio depends not only on the air content but also on the absolute pressure. Even at low air content, ca. 0.1 %, modulus E'_w is about 10 times lower than the modulus of E_w , (Verruijt 1969).

The value of E'_w is very difficult to estimate in experimental conditions due to the lack of a good device for measuring gas content in the porous seabed. de Rouck and Troch (2002) conducted field research on the basis of $(1-S)$ in pore water was estimated at about 3 %. The measurements were carried out in connection with the planned expansion of the Zeebrugge Port in Belgium. Pore pressures were measured at a depth of 18 m under the sea bed in areas where water depth ranged between 5 and 10 m. Under laboratory conditions (Tørum 2007), assessed the value of the parameter S at 3–10 %.

In the paper by Massel et al. (2005) they proved that an important parameter that determines the accuracy of the solution is the ratio of the soil matrix modulus G and the modulus of elasticity of pore water E'_w . The shear modulus of the soil G takes the following form:

$$G = \frac{E_s}{2(1 + \nu)} \quad (11)$$

where:

- E_s Young's modulus of soil,
- ν Poisson's ratio.

The following general equation for disappearance of pressure in the porous layer, resulting from the Biot theory, was obtained:

$$\nabla^2 p - \frac{\gamma n}{K_f E'_w} \left[\frac{\partial p}{\partial t} + \frac{E'_w}{n} \left(\frac{\partial v_x}{\partial x} + \frac{\partial v_z}{\partial z} \right) \right] = 0 \quad (12)$$

where:

- K_f coefficient of permeability,
- $\gamma = \rho g$ specific gravity of water,
- k wave number,
- n porosity of the porous medium,
- ω frequency wave,
- L wavelength,
- E'_w the bulk modulus of pore water,
- G modulus of the soil matrix,
- $(nu_x \ nu_z)$ components of the velocity vector of the soil matrix deformation,
- p pore pressure.

Equation (12) expresses the effect of saturation of soil matrix with air/gas and the influence of the dynamic pressure on the do formation of the matrix. When soil is completely saturated with water and pore water does not contain air $\left(\frac{G}{E'_w} \rightarrow 0\right)$, the solution of Eq. (12) for the steady state is identical to that received by Putman (1949), who assumed that soil is stiff and water is incompressible.

Therefore, for fully saturated soil, e.g. rough gravel when K_f is high, the expression (12) reduces to Laplace's equation:

$$\nabla^2 p = 0 \quad (13)$$

and the solution of boundary value problem has the following form:

$$p(x, z, t) = \rho_w g \frac{H \cosh(kh) \cosh[k(z + h_n)]}{2 \cosh[k(h_n - h)]} \cos(kx - \omega t) \quad (14)$$

or:

$$p(x, z, t) = \rho_w g \frac{\cosh[k(z + h_n)]}{\cosh[k(h_n - h)]} \zeta(x, t), \quad (15)$$

where $\zeta(x, t)$ is the see surface elevation.

On the basis of the above, there is no phase delay between the ordinates of the sea surface elevation and pore ~ pressure, and the change of the sea surface elevation causes an immediate change in pore pressure. Massel et al. (2005), analyzed the results of laboratory experiments and showed that Eq. (13) cannot be used for fine sand. In another extreme case where fine sand is saturated with air or gas, soil stiffness becomes significantly greater than the stiffness of pore water. When $\left(\frac{G}{E'_w} \rightarrow \infty\right)$, part of the equation $\frac{E'_w}{nG} \left(\frac{\partial v_x}{\partial x} + \frac{\partial v_z}{\partial z}\right) \rightarrow 0$ and the equation for pore water pressure (12) can be written in a simpler form:

$$\nabla^2 p - \frac{\gamma n}{K_f E'_w} \frac{\partial p}{\partial t} = 0 \quad (16)$$

For example, when $S = 95\%$ (air content is therefore 5%), the modulus of water elasticity is about three orders of magnitude lower than the modulus for water without air and is $E'_w = 2 \cdot 10^6 \text{N/m}^2$ (Tørum 2007). For example, for fine sand, where $G \approx 10^8 \text{N/m}^2$, $\frac{G}{E'_w} \approx 100$.

The solution of Eq. (16) is a function of:

$$p(x, z, t) = \Re \left\{ \rho_w g \frac{H}{2} \frac{\cosh[\psi(z + h_n)]}{\cosh(kh) \cosh[\psi(h_n - h)]} \exp[i(kx - \omega t)] \right\} \quad (17)$$

where

$$\psi^2 = k^2 \left(1 - i \frac{n\gamma\omega}{k^2 K_f E'_w} \right), \quad (18)$$

where n is a measure of porosity (volume ratio of free to total volume of pores), \Re is the real part of complex value. Solution (17) can be rewritten in the following form:

$$p(x, z, t) = \Re \left\{ \frac{\rho_w g}{\cosh(kh)} \left| \frac{\cosh[\psi(z + h_n)]}{\cosh[\psi(h_n - h)]} \right| \exp[i\varphi] \right\} \zeta(x, t) \quad (19)$$

The solution (19) shows that air in the porous medium causes a phase delay φ between the deflection of the sea surface elevation and pore pressure. The experiment in Hannover showed that the ratio $\frac{G}{E'_w} \in (50, 400)$.

For $\frac{G}{E'_w} > 50$, vertical pressure distribution in soil pores was very close to the distribution from Eq. (16), identical to the solution obtained in the work of (Moshagen and Torum 1975), where the soil matrix is stiff and the fluid is compressible which indicates that the compressibility of soil matrix in the case of fine sand does not affect the distribution of pore water pressure.

The solutions of Eqs. (12) and (16) coincide well with the experimental data (Massel et al. 2004). Due to a simpler form of Eq. (16), it will be used in further analysis.

Spectral properties of the relation between surface waves and pressures in the soil layer are described based on the selected test data.

Let us assume the following labels:

ζ elevation of the free surface registered by the wave probe,

p_{ij} pore pressure measured by sensor j in system i .

Thus, we determine the transmittance functions resulting from the linear theory and compare them with the corresponding experimental values.

For linear system, the following spectral relation is true, (Bendat and Piersol 1976):

$$S_p(\omega, z) = |H(\omega, z)|^2 S_\zeta(\omega) \quad (20)$$

$$H(\omega, z) = \sqrt{\frac{S_p}{S_\zeta}} \quad (21)$$

As a result of the calculation, the theoretical transmittance function has the following form:

- surface—pressure in soil at a depth of z_m

$$|H(\omega, z)| = \frac{\cosh(\psi(z + h_n))}{\cosh(kh) \cosh(\psi(hn - h))} \quad (22)$$

- pore pressure at a depth of z_1m —pore pressure at a depth of z_2m

$$|H(\omega)| = \frac{\frac{\cosh(\psi(z_2 + h_n))}{\cosh(kh) \cosh(\psi(hn - h))}}{\frac{\cosh(\psi(z_1 + h_n))}{\cosh(kh) \cosh(\psi(hn - h))}} \quad (23)$$

3 Experimental Data

To enhance the knowledge of marine hydrodynamics of coastal zone for permeable sandy bottom, experiments were performed in a laboratory and in natural conditions and data on the dynamics of pore pressure in the permeable seabed layer immediately adjacent to the aqueous layer were collected.

Given the many constraints and technical difficulties of such an examination in natural conditions, the main material is the data from the experiment in the Grosse Walencannal in Hannover. The methodology of this study was extensively described in Massel et al. (2004). On one hand, the huge wave channel allowed to create conditions of movement of water in almost natural scale 011 the other hand. It allowed to repeat the tests and provided strict control of input and output parameters.

During the study, natural sand was heaped to form an artificial beach with a uniform slope 1:20. The bottom material was well sorted out fine sand of which more than 95 % grains fell within the range of 0.125–0.5 mm.

Four sensor systems were installed to measure pore water pressure in the beach sand. This paper will present the results of the system located where still water level was 2 m. The place was chosen so that the system was located before the breaking zone and the sensors recorded only the *phase-resolving* component, the *phase-average* component was not observed in that location.

Each system consisted of four piezoelectric pressure sensors attached to the metal rod arranged in the form of a cross (Fig. 2). This approach made it possible to estimate not only the pore pressure but also the horizontal and vertical velocity of water in the beach sand.

The systems were buried so that the upper pressure sensor was 10 cm below the bottom. Additionally waring was measured using wave probes. In the experiment with irregular waves wave sequences corresponding to the JONSWAP spectrum ($\gamma = 3.3$) were generated. 13 tests were carried out for irregular waves (Table 1) which aimed at simulating wind waves in almost natural conditions.

Wave surface in the wave channel, just like the surface of the sea in the real world, had irregular and complex shape. Analysed data consisted of 20–25 min recordings of surface waves and pore pressures at various depths. The data were recorded with a frequency of 120 Hz.



Fig. 2 System with pressure sensors

Table 1 Tests with irregular waves

Number test	File (number)	H_{sm}	T_p (s)	Water depth (m)	H_{max} (m)	$\{x_{br}\}_{min}$	x_{max}
43	28110303	0.2	6.0	4.10	0.330	221.0	235.0
44	01120301	0.1	6.0	4.10	0.660	214.0	–
45	02120301	0.6	6.0	4.10	0.781	212.0	244.0
46	02120302	0.8	6.0	4.10	1.016	206.0	248.0
47	02120303	0.2	7.0	4.10	0.261	224.0	236.0
48	02120301	0.1	7.0	4.10	0.523	216.0	240.0
49	02120305	0.6	7.0	4.10	0.781	214.0	242.0
50	02120306	0.8	7.0	4.10	1.016	204.0	248.0
51	02120307	1.0	7.0	4.10	1.731	196.0	251.0
52	03120301	1.0	6.0	4.10	1.731	192.0	250.0
53	03120302	0.2	8.0	4.10	0.261	223.0	238.0
54	03120303	0.1	8.0	4.08	0692	212.0	241.0
55	03120301	0.6	8.0	4.08	0784	212.0	244.0

The study provided valuable material for comparison of experimental data with theoretical solutions.

The method of distribution of energy supplied between individual frequencies of surface waves is illustrated by the features the spectral energy density $S(\omega)$. The energy distribution is approximated by the spectrum estimation based on the Wieier-Kliinchine’a theory called the Blackmail-Tukey method. The basis of the Blackmail-Tukey method is determining the estimator of the power spectral density function as the Fourier transform of the product of the autocorrelation function and the smoothing function, such as e.g. Hanning function.

The Blackmail-Tukey method improves the resulting spectrum vector, emphasizing proper components, while suppressing the noise effect. Figures 3 and 4 show the autocorrelation function for the selected tests 44 and 45, and the corresponding spectral function waveforms $S(\omega)$.

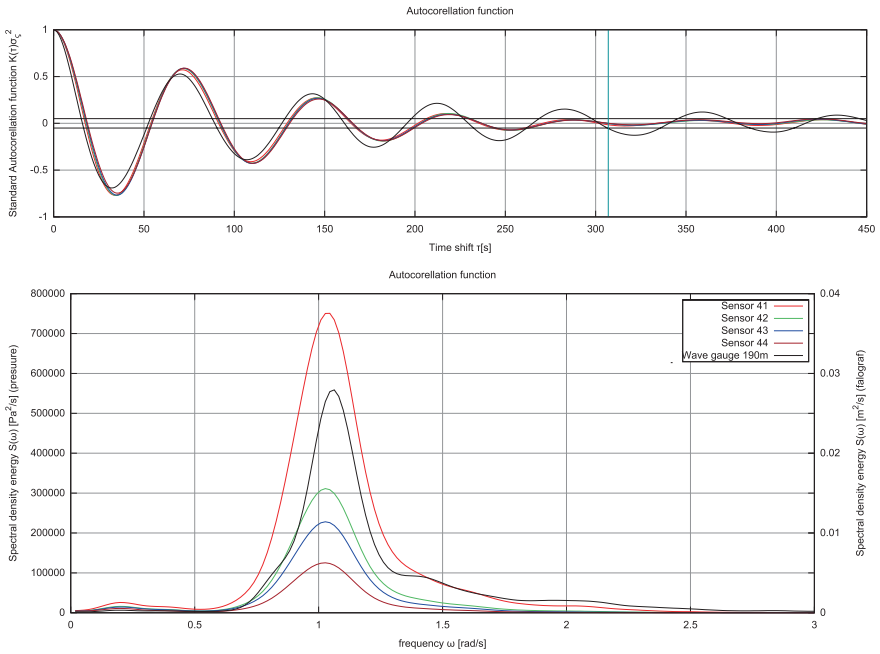


Fig. 3 Autocorrelation functions and frequency spectra of pore pressure—test 44

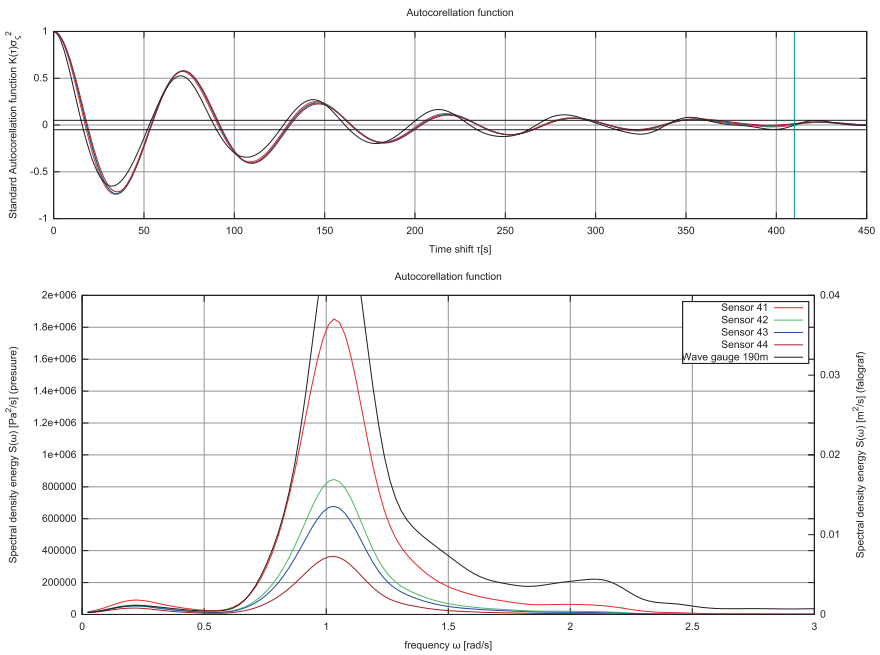


Fig. 4 Spectrum of the wave function and the spectrum of pore pressure—test 45

These figures shows that individual waves that make up the final shape of wave surface are supplied with energy in a non uniform way. Most energy is transferred to wave of frequency ω_p and adjacent frequencies. Vertical lines in figures indicate the maximum number of shifts m , which corresponds to the normalized autocorrelation function $K = 0.05$

Slight shift of the peaks of surface wave spectra and pore pressures indicates the presence of non-linear mechanisms. This is confirmed by the spectral wave function. Additional peaks, both in the band of high and low frequencies, in relation to the primary peak frequency, are visible for both the wave function spectra. These additional peaks disappear as the depth increases. This means that the movement of pore water becomes more linear as the depth of the porous bottom increases.

Figures 5 and 6 show comparison between experimental and theoretical transmittance function for test 45 and 46. $H_{p_i\zeta}$ are transmittance functions between surface waves ζ and pore pressure register by gauges p_i (p_i was located at the depth $z = 0.1\text{ m}$, $p_{2z} = 0.2\text{ m}$, $p_{4z} = 0.3\text{ m}$.) Function $H_{p_{4p1}}$ is a transmittance function between pore pressure at various depths, for gauge 1 (depth $z = 0.1\text{ m}$) and pore pressure registered by sensor 4 (depth 0.3 m).

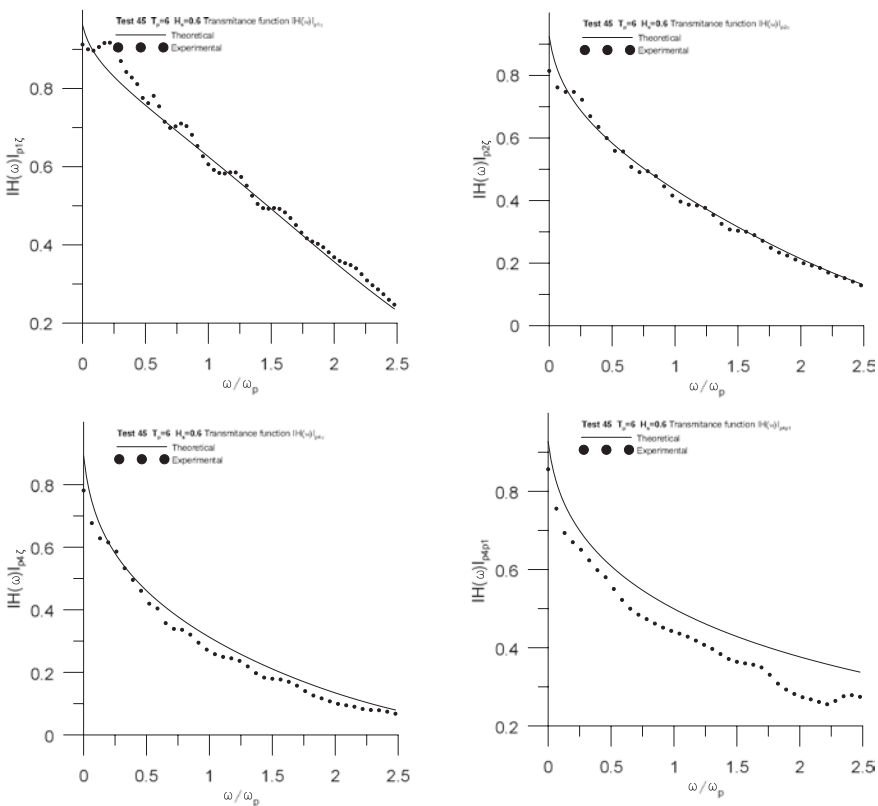


Fig. 5 Theoretical and experimental transmittance function for the test no. 45

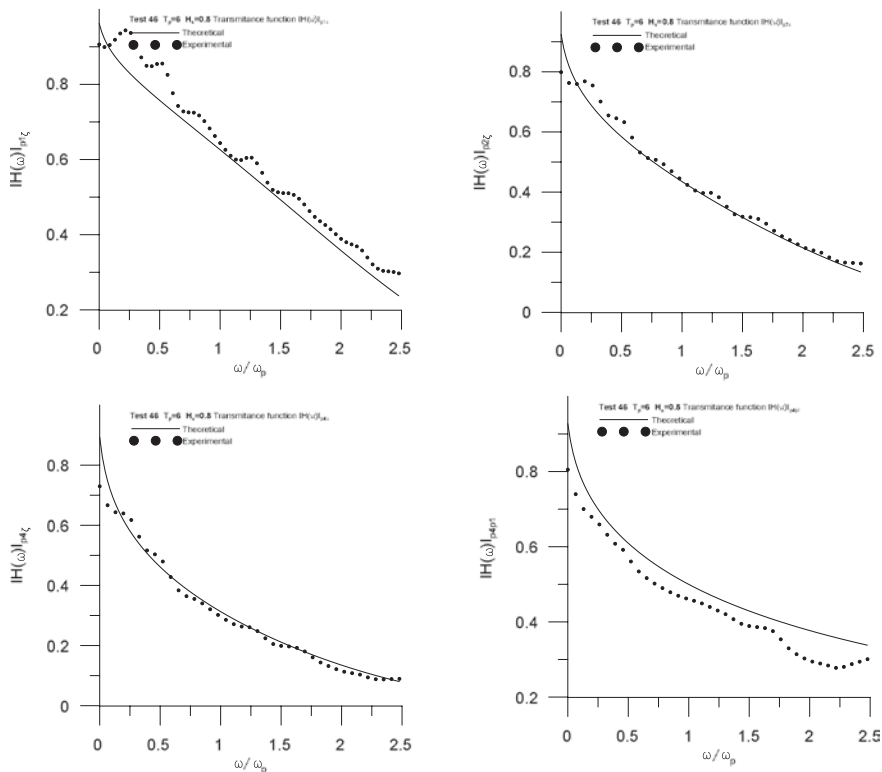


Fig. 6 Theoretical and experiential transmittance function for the test no. 46

Results show that in frequency range $0 < \frac{\omega}{\omega_p} < 2.5$ experimental transmittance function does not deviate too much from the theoretical functions.

This suggests that in laboratory conditions pore pressure in the soil surface layer disappears according to the presented theory. Less compliance for transfer function H_{p4p1} is probably due to a condition of errors in estimating both pressure p_1 and pressure p_4 .

Similar results were obtained from the analysis of the data collected in natural conditions on the Jurata beach. The soil in the area of research was fine, homogeneous and relatively clean sand. The porosity of n size was not measured during the test; its value was estimated at 0.3–0.4 based on the reference data.

The measurement of pore pressure at various depths in the seabed permeable layer immediately adjacent to the aqueous layer was performed with a set of pressure sensors (Fig. 7) designed and built by the Institute of Oceanology.

This instrument consists of six membrane pore pressure sensors, sensitivity of 0.019 mbar, contained in a metal tube at 0.1 m intervals. During the study on the Jurata beach the pore pressure sensors took measurements for 20 min at the frequency of 5 Hz with 15 min breaks. The structure with the sensors was placed in the porous bottom in such a way that the sensors were at the following depths: 0.18,

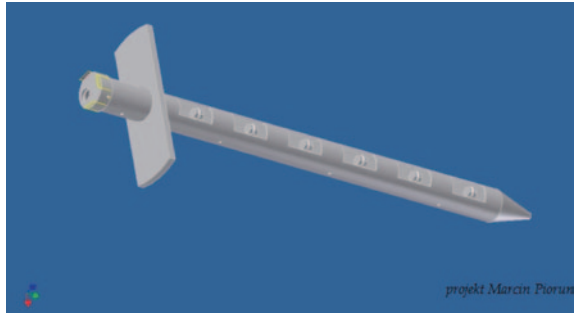


Fig. 7 Housing of pore pressure sensors

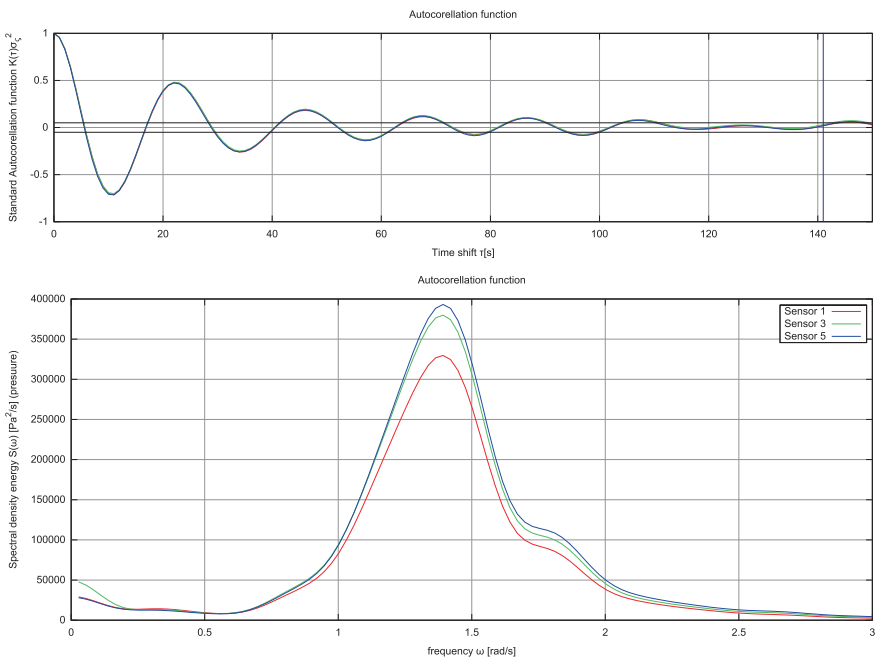


Fig. 8 Autocorrelation functions and spectra of pore pressure for the data from Jurata (record 2)

0.28, 0.38, 0.48, 0.58 and 0.68 m. The device with pressure sensors was placed in a location where water depth was ca. 0.6 m, which was ca. 30 m from the shore.

Next, a test was performed on the Data Logger in front of the breaking zone, ca. 70 m from the shore where water depth was ca. 1.4 m, and the pressure sensor on wave recorder was at the level of 0.6 m above the bottom. Although the experiment in Jurata was part of the tests of the newly built instrument, and its purpose was to check the quality of the data collected by the newly constructed Data Logger, and still requires testing in different conditions, the outcome confirms the results obtained in laboratory. Figures 8 and 9 show the autocorrelation functions and the corresponding spectral functions $S(\omega_k)$ for selected logs.

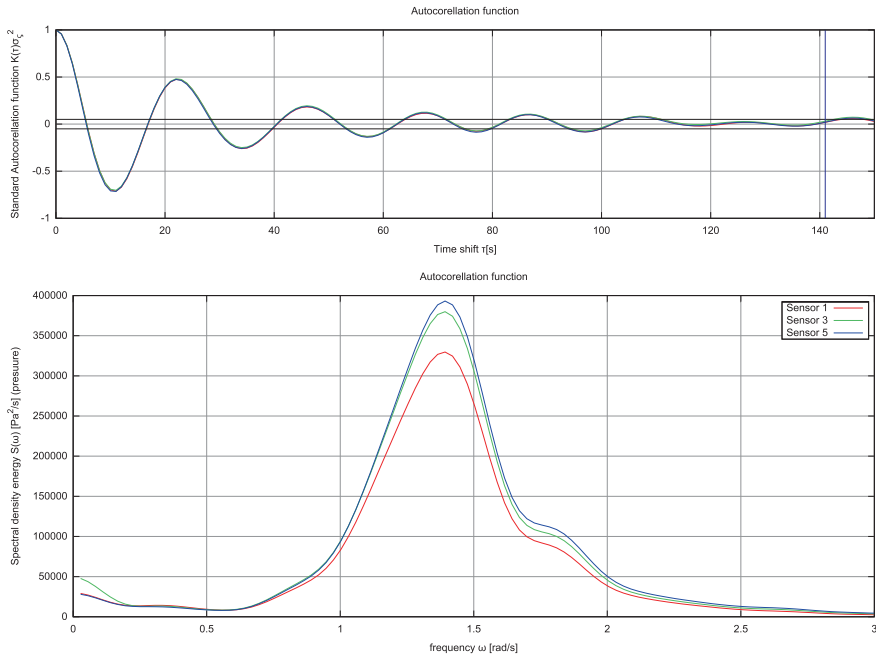


Fig. 9 Autocorrelation functions and spectra of pore pressure for the data from Jurata (record 4)

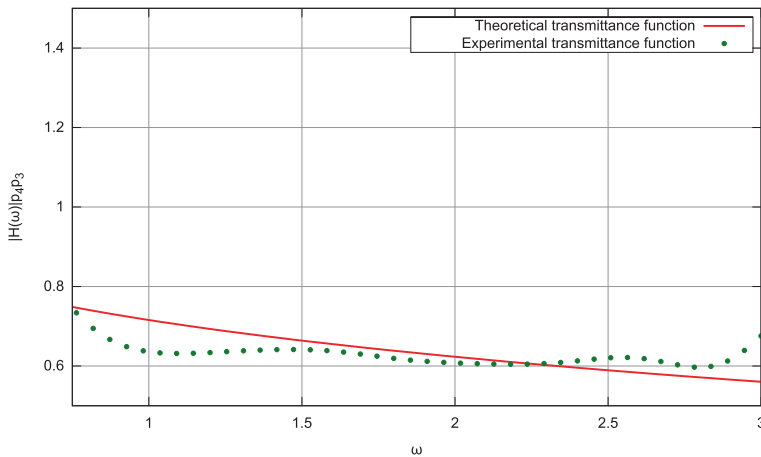


Fig. 10 The transmittance between the pore pressure at different depths

Equation (7) was used to determine theoretically the transmittance functions between the pore pressures at two different depths, 0.36 and 0.46 m, and to compare the data recorded by the sensor p_3 and sens or p_4 . An example of transmittance functions for the data from Jurata is shown in Fig. 10. In the frequency range

of ($0.8 < \omega < 2.5$) the transmittance function between the pore pressures at two different depths fairly well coincides with the transmittance function determined from the linear theory (23), except for the band of low frequencies. This is likely due to the fact that exact depth of pressure sensors is not known. The values are estimated only on the basis of what was recorded when the equipment was being installed. A similar result was obtained by Massel (1982) during the coastline experiment in Lubiatowo.

4 Summary

Natural seawater filtration mechanism in the sand is a very complex system, it includes knowledge from many fields. Research has shown that the sands are very active. High rate of the process is due to high level of water permeability. Water easily soaks into the sand and actually in the spaces between the grains, transporting dissolved oxygen which, combined with the activity of seabed organisms and porous sand sediments, form a high efficiency filtration system, which is necessary for transformation of organic matter into simple inorganic compounds, combined with the activity of the organisms present on the seabed sediments form a porous sand filtering system with high efficiency.

This paper proposes a theoretical model of determining pore water pressure for typical sandy beaches when the slope of the bottom of the area before the breaking zone is very small, which takes into account the deformation of the soil matrix and the content of air dissolved in the pore water, as well as the change matrix of pore water flow volume and direction with an assumption that soil matrix deformation satisfies the linear elasticity of law and the relationship between the pressure gradient and the pore water velocity is expressed by Darcy's law. Research is performed on a three-phases medium consisting of soil matrix, pore water and air.

The present model, as an approximation to a very slowly varying medium, provides useful information; we know that in natural condition, it is possible that in homogeneous environments characterised by more complex and steep variations can be more consistently treated by coupled-mode models, as the one presented in Belibassakis (2012).

Biot's theory of multi-phase media is a good basis for building models of the decay of pore water pressures induced by varying sea surface. The analysis shows that transmittance functions between surface waves and pore pressure and between the pore pressures at various depths for fine uniform well-graded sand correspond quite well with the experimental data and the in situ data. The transmittance functions between the surface waves and the pore pressure, and between pore pressures at various depths resulting from the linear wave theory, well reproduce the experimental data in the frequency band close to the peak wave energy. This method may be used in static calculations for structures erected on seabed and for evaluating the impact of waves on the movement of bed material.

As the estimation of infiltration into beach sand is very difficult to carry out under real sea conditions, a controlled large-scale laboratory experiment was

carried out in the Groser Wellenkanal (GWK) in Hannover (Germany) as part of the project “Run-up of waves on beaches and induced infiltration in the beach body” supported by the European Community (contract HPRI-CT-2001-00157).

The experimental data were collected in natural conditions under the supervisor’s research from the Ministry of Science and Higher Education- Circulation of groundwater induced by surface wave dynamic on the beach N N306 003536.

The theoretical results of the paper have been compared with the experimental data collected during the laboratory work and in natural conditions experiment and showed very good agreement.

References

- Belibassakis K (2012) Water-wave induced groundwater pressure and flow in variable bathymetry regions and sandy beaches by an enhanced coupled-mode model. *Ocean Eng* 47:104–118
- Bendat JS, Piersol AG (1976) *Metody analizy i pomiaru sygnalów losowych*. PWN, Warszawa
- Biot MA (1956) Theory of propagation of elastic waves in a fluid-saturated porous solid. Part 1: low frequency range, Part 2: higher frequency range. *J Acoust Soc Am* 28:168–191
- Huettel M, Roy H, Precht E, Ehrenhauss S (2003) Hydrodynamical impact on biogeochemical processes in aquatic sediments. *Hydrobiologia* 494:231–236
- Huettel M, Rush A (2000) Transport and degradation of phytoplankton in permeable sediment. *Limnol Oceanogr* 45(3):534–549
- Longuet-Higgins MS (1983) Wave set-up, percolation and undertow in the surf zone. *Proc Roy Soc London A* 390:283–291
- Massel SR, Przyborska A, Przyborski M (2005) Attenuation of wave-induced groundwater pressure in shallow water. Part 2. Theory. *Oceanologia* 47(3):291–323
- Massel SR, Przyborska A, Przyborski M (2004) Attenuation of wave-induced groundwater pressure in shallow water. Part 1. *Oceanologia* 46(3):383–404
- Massel SR (1982) Rozkład ciśnień porowych wywołanych falowaniem wiatrowym w piaszczystej warstwie dna morskiego. *Rozprawy Hydrotechniczne - Zeszyt 44*
- Massel SR (1976) Gravity waves propagated over a permeable bottom. *J Waterway Div* 102:111–121
- McLachlan A (1989) Water filtration by dissipative beaches. *Limnol Oceanogr* 34:774–780
- Mei CC, Foda MA (1981) Wave-induced responses in a fluid-filled poro-elastic solid with a free surface—a boundary layer theory. *Geophys J Roy Astron Soc* 66:597–631
- Moshagen H, Torum A (1975) Wave-induced pressures in permeable sea-beds. *J Waterway Div* 101:49–57
- Otnes EK, Enochson L (1972) *Analiza numeryczna szeregów czasowych*. Tytuł oryginalny: Time-series analysis—data processing. Wiley, New York, 467 stron
- Putman JA (1949) Loss of wave energy due to percolation in a permeable sea bottom. *Trans Am Geophys Union* 30:349–356
- de Rouck J, Troch P (2002) Pore water pressure response due to tides and waves based on prototype measurements. *PIANC Bull* 110:9–31
- Shum KT (1993) The effects of wave-induced pore water circulation on the transport of reactive solutes below a rippled sediment bed. *J Geoph Res* 98:10289–10301
- Terzaghi K (1943) *Theoretical soil mechanics*. Wiley, New York
- Tørum A (2007) Wave induced pore pressure—air/gas content. *J Waterway, Port, Coastal, Ocean Eng* 133:83–86
- Węśławski JM, Andrulewicz E, Kotwicki L, Kuzebski E, Lewandowski A, Linkowski T, Massel SR, Musielak S, Olenczuk-Neyman K, Pempkowiak J, Piekarek-Jankowska H, Radziejewska

- T, Różynski G, Sagan I, Skóra KE, Szeffler K, Urbanski J, Witek Z, Wołowicz M, Zachowicz J, Zarzycki T (2006) Basis for a valuation of the polish exclusive economic zone of the Baltic Sea: rationale and quest for tools. *Oceanologia* 48:145–167
- Verruijt A (1969) Elastic storage of aquifers. In: Dewiest RJM (ed) *W zbiorze: flow through porous media*. Academic Press, New York, pp 331–376

Ocean Acidification: Environmental Issue and Its Impact on Marine Life

Agnieszka Cichowska and Alicja Kosakowska

Abstract Concentration of carbon dioxide is rising with constantly progressing industrialization. The major sources of anthropogenic CO₂ are combustion of fossil fuels, transport and industrial processes. This gas is present not only in the atmosphere, but also in water. The oceans play an extremely important role in absorbing CO₂ from the atmosphere, and that process leads to a decrease in water pH, which causes changes in the environment and all the organisms present within. Acidification of the oceans is a process in which the pH value of water is reduced by increased partial pressure of CO₂ in the water. It is expected to observe a decrease in the pH of the open oceans by 0.35 units over the next hundred years. Reactions of marine organisms to ambient condition changes are specific for particular types or species. Effect of water acidification may affect organisms positively, negatively or may not have an impact at all. Organisms with calcareous shells or frustules are especially vulnerable to ocean acidification. Carbonic acid occurring as a result of the increasing CO₂ concentration in water will dissolve the shells built of calcium carbonate. This review focuses on the excessive amount of carbon dioxide in the atmosphere and the impact of this phenomenon on the marine ecosystems.

Keywords Ocean acidification • Carbon dioxide • Marine organisms • Phytoplankton

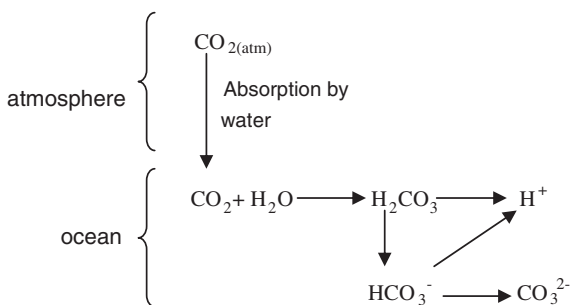
1 What is the Ocean Acidification

Sea water absorbs CO₂ from the atmosphere. Hence, the gas combined with water forms carbonic acid which dissociates into bicarbonate ion and hydrogen ion. Next, the bicarbonate ion dissociates into carbonate and hydrogen ion (Fig. 1).

A. Cichowska (✉) · A. Kosakowska
Polish Academy of Sciences, Marine Chemistry and Biochemistry Department,
Institute of Oceanology, Sopot, Poland
e-mail: acich@iopan.gda.pl

A. Kosakowska
e-mail: akosak@iopan.gda.pl

Fig. 1 Scheme of carbon dioxide absorption by the ocean water and the dissociation of carbonic acid



The excessive concentration of carbon dioxide in water reduces pH of water. This phenomenon is called ocean acidification and may result in serious consequences for the marine environment.

1.1 Causes of Ocean Acidification

The source of the problem originates from high and constantly increasing emission rate of carbon dioxide into the atmosphere. Acidification of the oceans is an ongoing problem. For over 800000 years, until the industrialization era, the ocean pH ranged from 8.2 to 8.3 (Zeebe and Ridgwell 2011). Just before the era of industrialization during the Holocene the carbon dioxide concentrations were relatively stable and amounted to from ~260 to ~280 ppmv, pCO₂ (partial pressure) (Zeebe 2012). First reports on the absorption of atmospheric CO₂ by the global ocean have been published by Revelle and Suess (1957), who suggested importance of the oceans in changing the concentration of CO₂ in the atmosphere. Since 1959, research is carried out at the top of the volcano Mauna Loa in Hawaii, which clearly shows an increase in the concentration of CO₂ in the atmosphere starting from late 1950s until today (Fig. 2). In May 2013, the concentration of carbon dioxide in the atmosphere amounted to 399.77 ppm.¹ Rising atmospheric carbon dioxide levels due to human activity have been shown to reduce the ocean pH by 0.1 units and are believed to reduce it even more in the future—by up to 0.4 pH units during the coming 100 years according to some recent estimates (IPCC 2007).

Anthropogenic effects on the dynamic increase of CO₂ in the atmosphere is mainly caused by fossil fuel burning, cement production, land use changes (e.g. deforestation) and transportation (Maina et al. 1986; Sabine et al. 2004). According to Schafer and Victor (1999), 13 % of carbon dioxide is released into the atmosphere by land transport while 3 % is emitted into the atmosphere by air transport (Vedanham and Oppenheimer 1998). It is estimated that from 1800 to 1994 the oceans absorbed $118 \pm 19 \times 10^9$ t of carbon. At this time, the emission

¹ www.esrl.noaa.gov/gmd/ccgg/trends/mlo.html.

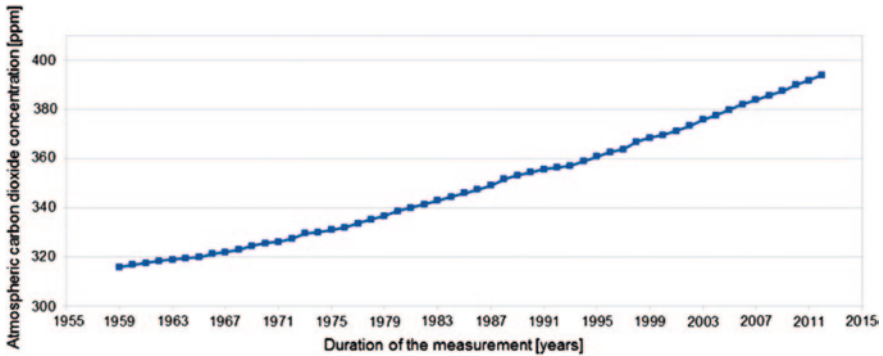


Fig. 2 Change in the concentration of carbon dioxide in the atmosphere, measured at the station Mauna Loa, Hawaii. Based on the data presented by <ftp.cmdl.noaa.gov>

of CO₂ to the atmosphere was $244 \pm 20 \times 10^9$ t of carbon. During the period 1980–1990, carbon dioxide emission from the fossil fuels burning and cement production amounted to nearly one-half of the carbon produced during the entire so-called anthropocene ($117 \pm 5 \times 10^9$ t). In this time, oceans have absorbed $37 \pm 8 \times 10^9$ t of carbon (Sabine et al. 2004).

The above data relate to the total value of the carbon dioxide emitted by humans and absorbed by the oceans. It is worth to consider the fact that the sea water and the oceans are intended as absorbers and emitters of carbon dioxide from and to the atmosphere.

2 Effect of Ocean Acidification on Living Organisms

The ocean acidification may influence living organisms in various ways. The ocean acidification causes distinct effects among organisms built of a limestone shell. As a result of lower pH, the aqueous dissolution of calcium carbonate occurs in seashells (Bednaršek et al. 2012) or planktonic shell organisms such as coccolithophores (Nimer et al. 1994; Krug 2009; Gao et al. 2012; Johnson and Carpenter 2012).

In response to elevated CO₂ and reduced pH, most of the test organisms show a reduction in the CaCO₃ concentration. This is the best documented and most frequently observed biological effect of seawater acidification (Committee on the Development of an Integrated Science Strategy for Ocean Acidification Monitoring et al. 2013). This lowered pH of water affects not only the organisms having a limestone shell, but also has an impact on phytoplankton physiology. Effect of low pH of water to the binding mechanism of inorganic carbon by phytoplankton and cyanobacteria cells is another example of the negative impact of the acidification of the oceans on marine organisms (Wu et al. 2010; Hopkinson et al. 2010; Yang and Gao 2012). Effect of water acidification on phytoplankton

Table 1 Effect of low pH of the sea and ocean on living organisms

Test organism	Classification	Low pH effect	References
Hydrolithon onkodes	Crustose coralline alga	Decrease in production of calcium carbonate (damage to the surface coating)	Johnson and Carpenter 2012
Limacina helicina antarctica	Pteropoda	Damage on the surface of a snail shell	Bednaršek et al. (2012)
Coccolithus braarudii	Coccolithophorid	Lower rate of growth and cell size	Krug (2009)
Pleurophysis carterae	Coccolithophorid	Contributing to growth and productivity (pH 8.1 and 9.3 cultures)	Moheimani (2005)
Emiliana huxleyi	Coccolithophorid	Slowdown in growth rate and productivity	Moheimani (2005), Nimer et al. (1994)
Phaeodactylum tricornutum	Diatoms	Reduced performance of mechanism of inorganic carbon binding	Wu et al. (2010)
Thalassiosira pseudonana	Diatoms		Yang and Gao (2012)
Stichococcus minor	Green algae	A wide tolerance range of pH from 5.0 to 9.5; however, it showed growth optimum at pH 8.2.	Moazami-Goudarzi and Colman (2012)
Stichococcus cylindricus			
Microcystis aeruginosa	Cyanobacteria	Decrease in cell growth	Wang et al. (2011)
Anabaena spiroides	Cyanobacteria		
Nodularia spumigena	Cyanobacteria	Decreasing rate of cell division, while increasing heterocyst production	Czerny et al. (2009)

biodiversity change was also observed (Biswas et al. 2011; Hama et al. 2012). Impact of acidification on marine life is described in Table 1.

2.1 Effect of Ocean Acidification on Coral Reefs

Coral reef is the most vulnerable ecosystem susceptible to ocean acidification. It is estimated that by mid-century there will be 10–50 % less reef-building organisms in relation to the pre-industrial amount (Kleypas and Yates 2009). Under the influence of low pH, the surface of coral composed of calcium carbonate

becomes blurred (Cerrano et al. 2013). This may affect their ability to function in the ecosystem. However, ocean acidification affects not only the reef. The decrease in production of calcium carbonate, combined with an increase in the dissolution of calcium carbonate, causes a decrease in biodiversity of coral reef, reduced ability to protect the coral shorelines, and lack of possibilities to create habitats for other organisms forming ecosystems, such as mangroves and seagrass (Kleypas and Yates 2009).

Many studies have been conducted on the effects of increased levels of carbon dioxide in the water and the reaction of the individual organisms. *Hydrolithon onkodes*, an important species that builds blocks of the coral reef, has been studied not only in terms of growth and the partial pressure of CO₂ in the environment, but also in correlation acidification and growth in temperature of the environment. Organisms comprising of calcium carbonate are sensitive to the increase of CO₂ in the environment. Carbon dioxide rising levels combined with higher average temperatures can lead to changes in calcareous shell. It has been shown that the influence of temperature and increased concentration of carbon dioxide is a non-linear relationship for the species of *H. onkodes* (Johnson and Carpenter 2012). That includes changing relationship between water temperature, CO₂ concentration and the impact on the shell limestone of *H. onkodes*. The lowest saturation of calcium carbonate as the mineral calcite (2.87 ± 0.28) was shown for high partial pressure ($847 \pm 102 \mu\text{atm}$.) at 26 °C, and pH of 7.76 ± 0.05 . The relationships between these factors have been studied for the temperature range from 26 to 29 °C, and partial pressure of CO₂ at 420, 530, 830 μatm . The same studies have shown increased susceptibility to grazing by sea urchins at high concentrations of in water pCO₂. It is one of the first indications of a specific chain reaction of changes in ocean temperature and coral ecosystems caused by acidification (Johnson and Carpenter 2012).

2.2 *How the Decrease in pH of Water Affects Planktonic Organisms*

The main source of organic matter in marine ecosystems is phytoplankton that occupies the upper layer water, where photosynthesis occurs. These single-celled organisms are an important component of the biological pump—the collection of processes that transport carbon from the euphotic zone to the deep ocean. Phytoplankton contributes to half of the primary production over the entire globe. Net primary production and carbon fixation mechanism during photosynthesis are the two mechanisms to convert atmospheric carbon dioxide into organic form in the ocean (O'Malley et al. 2010).

Zooplankton possessing shells is also affected by acidification of the oceans. Here, effects of low water pH are similar to those of coral reef where reducing of the calcium carbonate amount is observed. Adverse effects have been revealed for on snail shells (Bednaršek et al. 2012). The study was conducted for juvenile

forms of pteropod *Limacina helicina antarctica*, species common in the Southern Ocean. The experiment lasted 14 days under various CO₂ conditions affecting snail shells (375, 500, 750 and 1,200 ppm) (Bednaršek et al. 2012). Scanning electron microscopy image has showed severe damage to the surface of a snail shell when compared to the intact form grown under stable CO₂ concentration.

Coccolithophorids characteristic for their calcareous shells are the group of phytoplankton particularly highlighted by the acidification of the oceans.

The influence of elevated partial pressure of pCO₂ on *Coccolithus braarudii* compared with other species of Coccolithophores has been examined. Decrease in growth rate and cell size of *C. braarudii* has been observed with increased partial pressure of CO₂ (432, 732 and 1,225 μatm). Differences in sensitivity to changing levels of carbon dioxide in water were observed by comparing these results with other studied species such as *Emiliana huxleyi*, *Gephyrocapsa oceanic* and *Calcidiscus leptoporus*. It has been found that the sensitivity to changes in the environment depended on the species. It should be added that the negative impact on the shell limestone organisms is observed at the highest concentrations of CO₂ (Krug 2009). According to Moheimani (2005) the increase in carbon dioxide concentration in culture (pH 8.1 and 9.3) leads to an increase in the growth rate and productivity of *Pleurophysis carterae*, and causes a decrease in growth rate and productivity of *Emiliana huxleyi*.

The carbon dioxide concentration and pH of the aquatic environment have a significant impact on the growth of *Emiliana huxleyi*. A seemingly small change in the concentration of CO₂ in water can slow down or even completely inhibit the growth of the culture. Nimer et al. (1994) demonstrated that culture aeration of 0.1 % CO₂ (v/v) resulted in a reduction of cells density of 40 % compared to cultures aerated 0.03 % CO₂. Cultures aerated without CO₂ were similar in height to the original 0.03 % CO₂. Carbon dioxide concentration of 0.5 % completely stopped the growth of cultures (Nimer et al. 1994).

Changing the concentration of carbon dioxide in the water affects the change in phytoplankton species diversity. These results were obtained by examining the impact of ocean acidification on the biodiversity of Shimoda—marine phytoplankton station (Japan). Sample collected at the marine station was aerated for 15 days with known concentrations of CO₂ (400 ppm—control, 800 and 1,200 ppm). Microscopic observation showed that the initial phase of the experiment was dominated by diatoms and dinoflagellates, and later from day 8 to 15 dominated by haptophytes *Chrysochromulina* sp. and of the genus *Tetraselmis* sp. (green algae) (Hama et al. 2012).

Effect of change in species diversity was also noted in the area of Godavari River Estuary in India (Biswas et al. 2011). Two short-term bottle experiments (with and without nutrient addition) were conducted during the pre-monsoon season when the partial pressure of CO₂ in the surface water was low. In May ambient water pCO₂ was 156 μatm (control). Two other CO₂ levels (244 and 363 μatm pCO₂) were set in order to verify if phytoplankton production was limited by CO₂ supply. In June, the initial pCO₂ was 225 μatm pCO₂ (control). In addition, three CO₂ concentrations (643, 1,403 and 1,860 μatm CO₂) were tested.

It should be noted that phytoplankton samples were collected during a period of low nutrient salt concentrations, and the reactions of the test organisms may be different at other times of the year. The results indicate the joint impact of high CO₂ concentrations and low levels of nutrient salts in water. In the first experiment, the observed growth rate was 20 % higher for pressure of 244 μatm and 35 % at pressure of 363 μatm compared to the natural conditions. Increase in growth followed increase in partial pressure for both experiment settings. At the same time, the diversity of phytoplankton was studied in terms of the content of photosynthetic pigments. Diatoms were dominant, as evidenced by a higher ratio of fucoxanthin characteristic for these organisms, compared to zeaxanthin-characteristic pigment of cyanobacteria. The calculations also suggest that an inadequate concentration of nitrogen, phosphorus and silicon can lead to the inhibition of growth of the diatoms in the cyanobacterial competition regardless of the concentration of CO₂ in water (Biswas et al. 2011).

2.3 Ocean Acidification Effects on Carbon Concentrating Mechanism (CCMs)

Marine phytoplankton evolved mechanisms that support photosynthetic carbon (or CO₂) concentration. Carbon dioxide can enter into the chloroplast by diffusion or active transport. The latter is possible only for bicarbonate ions (Madsen and Bowes 1993).

Inorganic carbon concentration by single-celled organisms is an adaptation mechanism in response to low affinity of Rubisco to CO₂ substrate in the environment (Ghoshal and Goyal 2001). Rubisco, the ribulose-1, 5-biphosphate is an enzyme that actively participates in the fixation of photosynthetic carbon dioxide (Osafune et al. 1990). Carbon dioxide in its gaseous form is not readily absorbable in water, and the bicarbonate ion actively participates in transport to the chloroplast (Ghoshal and Goyal 2001). Carbonic anhydrase enzyme converts carbon dioxide into bicarbonate ions, and its transport to the membrane is affected by the pH of the environment (Ghoshal and Goyal 2001). Research conducted by Haglund et al. (1992) on *Tenuistipitata gracilaria* (Rhodophyta) showed the carbonic anhydrase activity regulates the transfer mechanism of inorganic carbon (as CO₂) into the cell. Ongoing ocean acidification may influence performance of inorganic carbon bond degradation mechanism. Because of the variety of phytoplankton species and their specific physiological responses, changes in their natural habitat are expected to affect the composition and amount of phytoplankton in the oceans (Falkowski and Oliver 2007; Wu et al. 2010).

Reduction of inorganic carbon accumulation efficiency is caused by pH lowering. The study conducted by Hopkinson et al. (2010) a phytoplankton sample collected from the Gulf of Alaska was treated with pH corresponding to high and low concentrations of pCO₂. The low concentration of CO₂ (109–168 atm) corresponds to a pH from 8.39 to 8.50, while the high concentration of carbon dioxide

(predicted to be reached in 100 years) was represented by 7.58 and pH 7.77 (concentration from 760 to 1,204 atm CO₂). Phytoplankton samples were tested under conditions of limited iron concentration with high CO₂ concentrations having positive effect on the growth of phytoplankton, while reducing the mechanism of binding of inorganic carbon (Hopkinson et al. 2010).

3 How the Acidification of Marine Water Affects Organisms Occurring in the Baltic Sea

The Baltic Sea is a specific and diverse sea, which, depending on the area of research, can emit or absorb carbon dioxide (Algesten et al. 2004; Kuss et al. 2006). It is still not certain whether the Baltic Sea is mainly emitting or absorbing carbon. According to Algesten et al. (2004) the Gulf of Bothnia emits into the atmosphere 37.2 g C/m²/year of carbon in the form of CO₂. The Baltic Proper (excluding the Gulf of Bothnia, the Gulf of Finland, the Gulf of Riga and the Danish Straits) absorbs 10.8 ± 1.1 g C/year/m² (Thomas and Shneider 1999), while Arkona Deep absorbs 36.0 g C/year/m² (Kuss et al. 2006). Kuliński and Pempkowiak (2011) reported that the emission of CO₂ into the atmosphere is 1.05 Tg C/year (2.7 g C/m²/year). These results depict the Baltic Sea as a weak source of CO₂ (Kuliński and Pempkowiak 2011). Additionally, the Baltic Sea is one of the sources of carbon for the North Sea. This inflow amounts to 0.63 ± 0.25 × 10¹² mol/year (Kuliński et al. 2011). Recent seasonal variability increase with the inclusion of eutrophication, makes the Baltic Sea both a sink and a source of CO₂. Modeling long-term variations of pH indicates an existence of stable conditions before industrialization and slight decrease due to increased atmospheric carbon dioxide concentrations during industrialization (Omstedt et al. 2009).

The carbon cycle in the marine environment depends on physical, chemical, and biological factors, and relies intensively on the activity of phytoplankton. Numerical models by Dzierzbicka-Głowacka et al. (2010) reflecting the phytoplankton, zooplankton and pelagic detritus concentration show the highest concentration of suspended organic carbon (POC) in May (870 mg C × m⁻³) and lowest in August (580 mg C × m⁻³). Seasonal variability of suspended organic carbon is associated with periods of maximum of dead organic matter and phytoplankton content (Dzierzbicka-Głowacka et al. 2010). Kuliński and Pempkowiak (2011) showed that the largest carbon supply in the Baltic Sea comes from river runoff that amounts to 10.90 Tg C/year (Tg = 10¹² g), including a 37.5 % organic carbon.

Monitoring studies 1972–2009 for the Baltic Sea showed the pH ranging from 9.2 to 7.4, with an average of 8.1. The values represent a significant downward trend, corresponding to the median annual change of 0.006 (Brutemark et al. 2011). It is difficult to determine unambiguously whether the acidification of the marine environment has a significant impact on the Baltic Sea phytoplankton.

Carbon dioxide is not the only factor reducing pH of the Baltic Sea water. Sulfur and nitrogen are other agents that contribute to aquatic environment acidification. Baltic Sea SO_x emission was 73.00 kt, while NO_x was equal to 81.00 kt. In the North Sea, these rates amounted to 173.00 and 191.91 kt, respectively. In the Baltic Sea the “acidifying agents” amounted to 4.48 and 1.77 for SO_x and NO_x, respectively (Potting et al. 1998).

Based on numerical models, Borges and Gypens (2010) suggested that in highly productive marine coastal environments, the impact of eutrophication and nutrient supply with runoff the rivers have a stronger impact on the carbon cycle than the acidification of surface waters through an intensive flow of carbon dioxide.

For years, the Baltic Sea has been examined in terms of planktonic organisms presence and phytoplankton seasonal variability. For spring and summer, downward trends were found for diatoms, while dinoflagellates generally showed an increase in the Baltic. Autumn diatoms increase was observed. Cyanobacteria dominate the central Baltic Sea mainly in summer months (Wasmund and Uhlig 2003; Wasmund et al. 2011). Spring blooms in the 1980s were dominated by dinoflagellates, (Wasmund et al. 2011). It is worth mentioning that the Baltic Sea has noted more instances of *Dactyliosolen fragilissimus*, diatom blooms which was first described by Łotocka (2006). Other bloom forming species were observed in the Baltic Sea: *Chaetoceros cf. lorenzianus* was found for the first time in the Gulf of Gdańsk in 2003 and in the Lithuanian coastal waters in 2005 (Kownacka et al. 2013).

Excessive algal growth can in turn cause problems especially in the coastal regions, e.g., Polish shoreline of the southern Baltic Sea, highly populated and tourists’ destinations such as Sopot, Gdynia. Research carried out for the area from 2004 to 2006 revealed several intense sunlight incidents, and strong southwest winds from May to August. Winds from the north would carry the algae mass along the coast (Filipkowska et al. 2009).

It is not clear how biodiversity of phytoplankton will change in the future, and it is essential to answer some of the emerging questions for important regions such as the Baltic Sea.

There are areas of the Baltic Sea where the acidification of the environment is not the cause of the increase of carbon dioxide but short-term local acidic runoff water from the rivers is responsible for the state of the aquatic environment. Studies on the pH changes in the environment led to fish (*Lota lota*), show that a longer period of time of low pH conditions was more harmful to the fish than the intense short-term disruption of the environment through acidification. This was tested in a situation where local river runoff caused rapid acidification of waters in which test on fish was performed. At pH as low as 5.3 and below these fish could survive successfully few weeks before hatching. The mass extinction of the larvae followed a month after hatching (Hudd and Kjellman 2002).

Frommel et al. (2013) studied the resistance of Baltic cod to water acidification. Spawning activity was tested at 380, 1,400, and 4,000 $\mu\text{atm pCO}_2$. The data indicated that the eggs and early larval stages of cod appear to be resistant to even

high levels of acidification of waters (3,200 μatm). No effects of acidification were found at successive development stages of Baltic cod. As suggested by Frommel et al. (2013) the species has adapted to low pH and high CO_2 concentrations occurring in the vicinity of spawning and growth areas.

In addition to research on acidification impact on fish in the Baltic Sea, various studies focusing on the effect of low pH on benthic organisms having calcareous shells have been performed.

In one of such studies, *Mytilus edulis* was treated for 40 days with different concentrations of pCO_2 in seawater (380, 1,120, 2,400 and 4,000 μatm pressure corresponding respectively to 39, 113, 243 and 405 Pa). Measured were both: the effect of changing conditions on the shell and the dry weight (without shell). With increasing concentration of CO_2 the shell length has been shown to decrease, while dry weight would increase in the same time. Length of the shell decreased of 7.4 ± 0.9 and 6.3 ± 0.3 mm under 1,120 and 4,000 pressure treated culture, respectively. This corresponds to a reduction in growth of 6–20 % relative to control sample. The dry weight increase was less observable as compared to the control. Initial mass (control 39 Pa) increased from 109 ± 19 mg to 319 ± 6.6 mg (Thomsen and Melzner 2010).

Phytoplankton as the base of the food web appears to be extremely important in the study of marine acidification. Unfortunately, there are very few reports on the effect of increased CO_2 concentrations in the water on the Baltic Sea phytoplankton organisms.

So far, research on the unicellular cell plankton organisms that occur in the Baltic Sea in relation to another areas of the globe was carried out. Studies concerning the Baltic Sea diatom *Phaeodactylum tricorutum* indicate the pH decreases due to the increase of CO_2 concentration to 101.3 Pa (1,000 ppmv), causing degradation of mechanism of inorganic carbon acquisition. Another studies of diatoms *Thalassiosira pseudonana* (South China Sea) also show adverse effects of high concentrations of carbon dioxide in water (culture test was carried out at 1,000 μatm pressure and at elevated light PAR—Photosynthetically Active Radiation). It has been shown that along with reducing the inorganic carbon binding, the intensity of lighting is not compatible with a high concentration of CO_2 (Yang and Gao 2012).

Although among examined plankton species the green algae did not show a significant presence in the Baltic Sea, there should be more information on how these organisms react to reduced pH in their natural environment. The species of *Stichococcus minor* and *Stichococcus cylindricus* (green algae) have been tested for tolerance to different pH levels in the environment. In the experiment conducted by Moazami-Goudarzi and Colman (2012) the pH of cultures was adjusted with an acid or base (without aeration). Both species showed a wide tolerance range of pH from 5.0 to 9.5, with growth optimum at pH 8.2. Both species, representatives of brackish water phytoplankton also showed high tolerances in terms of salinity.

Effect of seawater acidification on cyanobacteria is also poorly recognized. Few studies on the effects of low pH have been conducted. Studies on *Microcystis aeruginosa* and *Anabaena spiroides* treated by a pH of 5.5, 6.0 and 6.5 have shown that strongly acidic conditions slows the growth of cyanobacteria (Wang

et al. 2011). These results demonstrate differences in species tolerance for low pH. *M. aeruginosa* showed growth inhibition, but at the same time viability at pH 6.5. Only by lowering pH to 6.0 and 5.0 cell mortality was observed (Wang et al. 2011). Czerny et al. (2009) in their study on the effects of acidification on *Nodularia spumigena* has found lowering rate of cell division and increasing heterocyst production under low pH conditions. In the latest study, Unger et al. (2013) demonstrated that *N. spumigena* adapts to high concentrations of carbon dioxide in the water. For 15 days *N. spumigena* was grown under different conditions of CO₂ pressure (180, 380, and 780 ppm, corresponding to the state of the atmosphere in sequence: pre-industrial, present and future).

Ongoing research on ocean acidification and its impact on living organisms is on the top priority of the present-day scientific interests. It is important to study the issue extensively, especially for regions such as the Baltic Sea, where the data on the risk of low pH of the water are still little known.

References

- Algesten G, Wikner J, Sobek S, Tranvik LR, Jansson M (2004) Seasonal variation of CO₂ saturation in the Gulf of Bothnia: indications of marine net heterotrophy. *Global Biogeochem Cy* 18:GB4021
- Bednaršek N, Tarling GA, Bakker DCE, Fielding S, Jones EM, Venables HJ, Ward P, Kuzirian A, Lézé B, Feely HJ, Murphy EJ (2012) Extensive dissolution of live pteropods in the Southern Ocean. *Nat Geosci* 5:881–885
- Biswas H, Cros A, Yadav K, Ramana VV, Prasad VR, Acharyya T, Babu PVR (2011) The response of a natural phytoplankton community from the Godavari river estuary to increasing CO₂ concentration during the pre-monsoon period. *J Exp Mar Biol Ecol* 407:284–293
- Borges AV, Gypens N (2010) Carbonate chemistry in the coastal zone responds more strongly to eutrophication than to ocean acidification. *Limnol Oceanogr* 55(1):346–353
- Brutemark N, Engström-Öst J, Vehna A (2011) Long-term monitoring data reveal pH dynamics, trends and variability in the western Gulf of Finland. *Oceanol Hydrobiol St* 40(3):94–99
- Cerrano C, Cardini U, Bianchelli S, Corinaldesi C, Pusceddu A, Danovaro R (2013) Red coral extinction risk enhanced by ocean acidification. *Sci Rep* 3:1457
- Committee on the Development of an Integrated Science Strategy for Ocean Acidification Monitoring, Research, and Impacts Assessment, OSB, Division on Earth and Life Studies, National Research Council of the National Academies (2013) Ocean acidification, a natural strategy to meet challenges of a changing ocean. The National Academies Press Washington D.C. pp 171–182. http://www.nap.edu/openbook.php?record_id=12904&page=171
- Czerny J, Ramos JB, Riebesell U (2009) Influence of elevated CO₂ concentrations on cell division and nitrogen fixation rates in the bloom-forming cyanobacterium *Nodularia spumigena*. *Biogeosciences* 6(9):1865–1875
- Dzierzbicka-Głowacka L, Kuliński K, Maciejewska A, Jakacki J, Pempkowiak J (2010) Particulate organic carbon in the southern Baltic Sea: numerical simulations and experimental data. *Oceanologia* 52:621–648
- Falkowski PG, Oliver MJ (2007) Mix and match: how climate selects phytoplankton. *Nat Rev Microbiol* 5:813–819
- Filipkowska A, Lubecki L, Szymczak-żyła M, Łotocka M, Kowalewska G (2009) Factors affecting the occurrence of algae, on the Sopot beach (Baltic sea). *Oceanologia* 51(2):233–262
- Frommel AY, Schubert A, Piatkowski U, Clemmesen C (2013) Egg and early larval stages of Baltic cod, *Gadus morhua*, are robust to high levels of ocean acidification. *Mar Biol* 160:1825–1834

- Gao K, Helbling EW, Häder DP, Hutchins DA (2012) Responses of marine primary producers to interactions between ocean acidification, solar radiation, and warming. *Mar Ecol Prog Ser* 470:167–189
- Ghoshal D, Goyal A (2001) Carbon concentration mechanism(s) in unicellular green algae and cyanobacteria. *J Plant Biochem Biot* 10:83–90
- Haglund K, Björk M, Ramazanov Z, Garcla-Reina G, Pederson M (1992) Role of carbonic anhydrase in photosynthesis and inorganic-carbon assimilation in the red alga *Gracilaria tenuis-tipitata*. *Planta* 187:275–281
- Hama T, Kawashima S, Shimotori K, Satoh Y, Omori Y, Wada S, Taiki A, Hasegawa A, Midorikawa T, Ishii M, Saito S, Sasano D, Endo H, Nakayama T, Inouye I (2012) Effect of ocean acidification on coastal phytoplankton composition and accompanying organic nitrogen production. *J Oceanogr* 68:183–194
- Hopkinson BM, Yan X, Dalin S, McGinn PJ, Morel FMM (2010) The effect of CO₂ on the photosynthetic physiology of phytoplankton in the Gulf of Alaska. *Limnol Oceanogr* 55:2011–2024
- Hudd R, Kjellman J (2002) Bad matching between hatching and acidification: a pitfall for the burbot, *Lota lota*, off the river Kyrönjoki. *Baltic Sea Fish Res* 55:153–160
- IPCC (2007) Climate change 2007: the physical science basis. In: Solomon S, Qin D, Manning M, Chen Z, Marquis M, Averyt KB, Tignor M, Millers H (eds) Contribution of working group 1 to the fourth assessment report of the intergovernmental panel on climate change. Cambridge University Press, Cambridge, UK, and New York, 996 pp
- Johnson MD, Carpenter RC (2012) Ocean acidification and warming decrease calcification in the crustose coralline alga *Hydrolithon onkodes* and increase susceptibility to grazing. *J Exp Mar Biol Ecol* 434–435:94–101
- Kleypas J, Yates K (2009) Coral reefs and ocean acidification. *Oceanography* 22:108–117
- Kownacka J, Edler L, Gromisz S, Łotocka M, Olenina I, Ostrowska M, Piwosz K (2013) Non-indigenous species *Chaetoceros cf. lorenzianus* Grunow 1863—a new, predominant component of autumn phytoplankton in the southern Baltic Sea. *Estuar Coast Shelf Sci* 119:101–111
- Krug SA (2009) Coccolithophores in an acidifying ocean: from single strain to multiple species approaches. Dissertation, University of Kiel, pp 1–147. <http://d-nb.info/1019868767/34>
- Kuliński K, Pempkowiak J (2011) The carbon budget of the Baltic sea. *Biogeosciences* 8:3219–3230
- Kuliński K, She J, Pempkowiak J (2011) Short and medium term dynamics of the carbon exchange between the Baltic sea and the North sea. *Cont Shelf Res* 31:1611–1619
- Kuss J, Roeder W, Wlost KP, DeGrandpre KP (2006) Time-series of surface water CO₂ and oxygen measurements on a platform in the central Arkona sea (Baltic sea): seasonality of uptake and release. *Mar Chem* 101:220–232
- Łotocka M (2006) The first observed bloom of the diatom *Dactyliosolen fragilissimus* (Bergon) Hasle 1996 in the Gulf of Gdańsk. *Oceanologia* 48(3):447–452
- Madsen TV, Bowes G (1993) Carbon fixation and content rating mechanism. *J Aquat Plant Manage* 31:221–222
- Maina J, de Moel H, Zinke J, Madin J, McClanahan T, Vermaat E (1986) Human deforestation outweighs future climate change impacts of sedimentation on coral reefs. *Nat Commun* 4:1986
- Moazami-Goudarzi M, Colman B (2012) Changes in carbon uptake mechanisms in two green marine algae by reduced seawater pH. *J Exp Mar Biol Ecol* 413:94–99
- Moheimani DR (2005) The culture of coccolithophorid algae for carbon dioxide bioremediation. Dissertation, 1–266 Murdoch University. <http://researchrepository.murdoch.edu.au>
- Nimer NA, Brownee C, Merrenett MJ (1994) Carbon dioxide availability, intracellular pH and growth rate of the coccolithophore *Emiliania huxleyi*. *Mar Ecol Prog Ser* 109:257–262
- O'Malley RT, Behrenfeld MJ, Siegel DA, Maritorena S (2010) Global ocean phytoplankton in: State of the climate in 2009. *Bull. Amer. Meteor. Soc* 91(7):75–78
- Omstedt A, Gustafsson E, Wesslander K (2009) Modeling the uptake and release of carbon dioxide in the Baltic sea surface water. *Cont Shelf Res* 29:870–885

- Osafune T, Yokota A, Sumida S, Hase E (1990) Immunogold localization of ribulose-1,5-bisphosphate carboxylase with reference to pyrenoid morphology in chloroplasts of synchronized *Euglena gracilis* Cells. *Plant Physiol* 92:802–808
- Potting J, Scho W, Blok B, Hauschild M (1998) Comparison of the acidifying impact from emissions with different regional origin in life-cycle assessment. *J Hazard Mater* 61:155–162
- Revelle R, Suess HE (1957) Carbon dioxide exchange between atmosphere and ocean and the question of an increase of atmospheric CO₂, during the past decades. *Tellus* 9(1):18–27
- Sabine CL, Feely RA, Gruber NA, Key RM, Lee Kitack, Bullister JL, Wanninkhof R, Wong CS, Douglas WR, Wallace, Tilbrook B, Millero FJ, Peng TH, Kozyr A, Ono T, Rios AF (2004) The oceanic sink for anthropogenic CO₂. *Science* 305:367–371
- Schafer A, Victor DG (1999) Global passenger travel: implications for carbon dioxide emissions. *Energy* 24:657–679
- Thomas H, Shneider B (1999) The seasonal cycle of carbon dioxide in Baltic sea surface waters. *J Mar Sys* 22:53–67
- Thomsen J, Melzner F (2010) Moderate seawater acidification does not elicit long-term metabolic depression in the blue mussel *Mytilus edulis*. *Mar Biol* 157:2667–2676
- Unger J, Endres S, Wannicke N, Engel A, Voss A, Nausch G, Nausch M (2013) Response of *Nodularia spumigena* to pCO₂ part 3: turnover of phosphorus compounds. *Biogeosciences* 10:1483–1499
- Vedantham A, Oppenheimer M (1998) Long-term scenarios for aviation: demand and emissions of CO₂ and NO_x. *Energy Policy* 26(8):625–641
- Wang X, Chunbo H, Zhane F, Chuanping F, Yingnan Y (2011) Inhibition of the growth of two blue-green algae species (*Microcystis aeruginosa* and *Anabaena spiroides*) by acidification treatments using carbon dioxide. *Bioresour Technol* 102(10):5742–5748
- Wasmund N, Tuimala J, Suikkanen J, Vandepitte L, Kraberg A (2011) Long-term trends in phytoplankton composition in the western and central Baltic sea. *J Mar Sys* 87:145–159
- Wasmund N, Uhlig S (2003) Phytoplankton trends in the Baltic sea. *ICES J Mar Sc* 60:177–186
- Wu Y, Gao K, Riebesell U (2010) CO₂-induced seawater acidification affects physiological performance of the marine diatom *Phaeodactylum tricorutum*. *Biogeosciences* 7:2915–2923
- Yang G, Gao K (2012) Physiological responses of the marine diatom *Thalassiosira pseudonana* to increased pCO₂ and seawater acidity. *Mar Environ Res* 79:142–151
- Zeebe RE (2012) History of seawater carbonate chemistry, atmospheric CO₂, and ocean acidification. *Annu Rev of Earth Planet Sci* 40:141–165
- Zeebe RE, Ridgwell A (2011) Past changes of ocean carbonate chemistry. In: Gattuso JP, Hansson L (eds) *Ocean acidification*. Oxford University Press, Oxford, pp 21–40

Allelopathic Influence of Cyanobacteria *Microcystis aeruginosa* on Green Algae *Chlorella vulgaris*

Adam Żak and Alicja Kosakowska

Abstract Organic compounds not directly involved in the normal growth, development and reproduction of organism are called secondary metabolites. The growth and development of biological and agricultural systems could be affected by secondary metabolites with biological activity. This phenomenon is known as allelopathy. Allelochemicals could have influence on different physiological processes of target organism cells, which could lead to growth inhibition or even death. The goal of this work was to investigate allelopathic influence of cyanobacteria *Microcystis aeruginosa* on green algae *Chlorella vulgaris*. Both species occur in Baltic Sea; furthermore, *M. aeruginosa* could locally form toxic blooms (HABs) in coastal zone. Axenic cyanobacterial monocultures were cultivated in the flasks on liquid medium. After 30 days of growth cell-free solutions from cyanobacterial cultures were collected by filtering through the glass-fiber filters in sterile conditions and added to *Chlorella vulgaris* cultures. The influence of obtained extracellular secretion on growth of green microalgae was investigated after 3 and 7 days. In other experiment the influence of living cyanobacterial cells on growth of green algae was investigated (cocultures). In both experiments *M. aeruginosa* demonstrated allelopathic effects towards green algae.

Keywords Allelopathy • Cyanobacteria • Microalgae • Secondary metabolites
Biological activity

1 Introduction

Secondary metabolites are organic compounds not directly involved in the normal growth, development and reproduction of living organisms. Many of these compounds demonstrate biological activity and could affect the growth and

A. Żak (✉) · A. Kosakowska
Marine Chemistry and Biochemistry Department, Institute of Oceanology Polish Academy of Sciences, Powstańców Warszawy 55, 81–712 Sopot, Poland
e-mail: adamzak@iopan.gda.pl

development of biological systems. This process is observed worldwide and is known as allelopathy (Graneli et al. 2008).

This process can be defined as the direct or indirect effect of one species on another species, induced by organic compounds produced and released into the environment (Fergola et al. 2007). Allelopathy refers to inhibitory as well as stimulatory biochemical effects. The studies of biological active substances and allelopathy are important for several reasons. Cyanobacteria, green algae, diatoms and dinoflagellates are considered as sources of wide variety of biologically active, new substances with potential practical application in many branches of human industry, pharmacy and medicine. Allelopathic compounds isolated from phytoplankton include low molecular weight peptides, phenols, polysaccharides, fatty acids and alkaloids (Svircev et al. 2008). Allelochemicals potentially could be used as biodegradable, environment-friendly herbicides or biocontrol agents, because of their natural origin and short half lives in comparison to traditional, synthetic pesticides (Gantar et al. 2008; Qian et al. 2009). Crude cell extracts and identified compounds obtained from phytoplankton species demonstrated antibacterial activity against Gram-positive and Gram-negative bacteria. Also antifungal activity of allelochemicals has been reported. Some of bioactive compounds may be used as antiviral agents. Some of the isolated compounds have anti-inflammatory and antioxidant abilities. Finally, bioactive substances potentially could be used as anti-tumors in cancer treatment therapy (Tuney et al. 2006; Bhagavathy et al. 2011).

Allelopathy is not limited to terrestrial environment. Interactions caused by allelochemicals are widespread, occurring in all aquatic habitats and among aquatic producers belonging to different taxonomic groups (Cembella 2003; Gross 2003). In comparison to existing knowledge of allelopathy in terrestrial ecosystems, allelopathic interactions in aquatic environment are still not well recognized. Furthermore, more studies on allelopathy in aquatic environment have been carried out in fresh water habitats than in marine ecosystems.

Allelochemicals are potentially an important mediator of biological interactions between species, such as resource competition and predator-prey interactions. In aquatic environment, allelochemicals may function as agents capable of incapacitating or killing competitors. It is the chemical defence strategy and probably important adaptive factor. Species which produce bioactive compound or compounds harmful to other species could compete better and achieve dominance (Mulderij et al. 2005; Tillmann et al. 2008). Allelochemicals could be one of the factors promoting and maintaining algal and cyanobacterial blooms in marine and freshwater systems (Legrand et al. 2003). More detailed studies about allelopathy could give more information regarding successions in natural phytoplankton communities and harmful algal blooms (HAB) (Gantar et al. 2008). HAB's may lead to ecological, economical and medical problems due to changes in species composition, changes in food-chain, worsening of recreational waters and finally toxic blooms could be harmful for humans (Maso et al. 2006).

Allelochemicals could affect different physiological processes in living organisms. One allelopathic factor could have several modes of action and have influence on more than one process. The most common allelopathic mechanism observed is inhibition of photosynthesis and oxygen evolution. Usually direct

inhibition of photosystem II components (PSII). Allelochemicals could also affect ATP synthesis, could generate reactive oxygen species (ROS). There are reports of disruption of amino acids metabolism and influence on concentration of hormones (Weir et al. 2004). Allelopathic substances may cause growth rate inhibition of target species and in some situations cell lysis and death (Fistarol et al. 2004).

There are only single reports regarding allelopathy in the Baltic Sea concerning microalgae and cyanobacteria. The main goal of this study was to describe whether or not cyanobacteria *Microcystis aeruginosa* demonstrate allelopathic influence towards green algae *Chlorella vulgaris*. In order to accomplish the main goal, effects of living cyanobacterial cells and cell-free medium containing cyanobacterial secondary metabolites on green algae cultures were investigated.

2 Materials and Methods

2.1 Cyanobacterial and Microalgal Cultures

Cyanobacterial species *Microcystis aeruginosa* PCC7820 obtained from Pasteur Culture Collection of Cyanobacteria (Pasteur Institute, France) and green algae *Chlorella vulgaris* (A1-76, Culture Collection IO PAN, Sopot) isolated from the Baltic Sea, were used in these studies. Both organisms were grown on a liquid medium in the flasks (batch cultures), in 22 °C ± 2 at continuous light. Axenic *M. aeruginosa* strain was cultivated on ATCC 616 medium (616 Medium BG11 for blue green algae; <http://www.atcc.org/~media/157099A704B54A1DA8AF8ADDCE1BF2C8.ashx>). Axenic *C. vulgaris* strain was cultivated on BBM medium (Bold Basal Medium; Bischoff and Bold 1963). Cultures used as inocula in all experiments were in logarithmic phase of growth.

2.2 Influence of Cyanobacterial Metabolites on Growth of Green Algae

After 30 days of growth, a cell-free medium was obtained from *M. aeruginosa* cultures. Cell-free filtrates were collected by filtering aliquots of cyanobacterial cultures through the glass-fiber filters (GF/C Whatman) in sterile conditions. Filtrates with cyanobacterial extracellular secretion containing secondary metabolites were added to culture flasks with target species *C. vulgaris*. Total volume of medium in the flasks was 20 cm³ and inoculum of *C. vulgaris* was 10⁵ cells cm⁻³ and 10⁶ cells cm⁻³ in the other variant of the test. Cell-free filtrates were added to the flasks with green algae in two volumes: 1 and 5 cm³. Control samples were made by adding 5 cm³ of fresh medium to the batch cultures with target species. Experiments were carried out for 7 days. Samples were collected for measurements after 3 days and at the end of experiment. Seven independent experiments with three replicates were performed.

2.3 Influence of Cyanobacterial Living Cells on Growth of Green Algae

To examine the effect of living cyanobacterial cells on growth of target green algae, experiments with simultaneous growth were performed. Cyanobacteria *M. aeruginosa* and green algae *C. vulgaris* were cultivated as cocultures. Both organisms were grown together in the flasks on liquid BBM medium. Cyanobacterial and microalgal inocula were prepared in approximately 1:1 ratio. Flasks with green algae monoculture were used as control. Experiments were carried out for 7 days. After 3 days and at the end of experiments, samples were taken for further measurements. Six independent experiments with three replicates were performed.

2.4 Growth of *Chlorella vulgaris*

Growth of *C. vulgaris* was described applying cell number. Cells were counted with Bürker chamber and light microscope. Samples were diluted if needed to receive several cells in a single Bürker chamber square.

Cell viability was measured using cell staining (methylene blue). 35 μl of 0.1 % methylene blue water solution was added to 1 cm^3 of sample. After 30 min, the dye stained dead cells with blue color. Afterwards the viability was measured with Bürker chamber and light microscope by counting green living cells and marked blue dead cells.

2.5 Statistical Analysis

We calculated mean values and standard deviations from the different replicates per treatment ($n = 3$). The significance between variavnt and control was analyzed by Student's t test ($\alpha = 0.05$).

3 Results

3.1 Effect of *Microcystis aeruginosa* Extracellular Secretion on *Chlorella vulgaris* Cultures

The effects of *M. aeruginosa* cell-free filtrate on the growth of *C. vulgaris* are presented in Figs. 1 and 2 for 1 and 5 cm^3 volume of filtrate added respectively. Both figures present results obtained after 3 and 7 days of experiment (A and B, respectively). The initial density of *C. vulgaris* was 10^5 cells cm^{-3} or 10^6 cells cm^{-3} . For

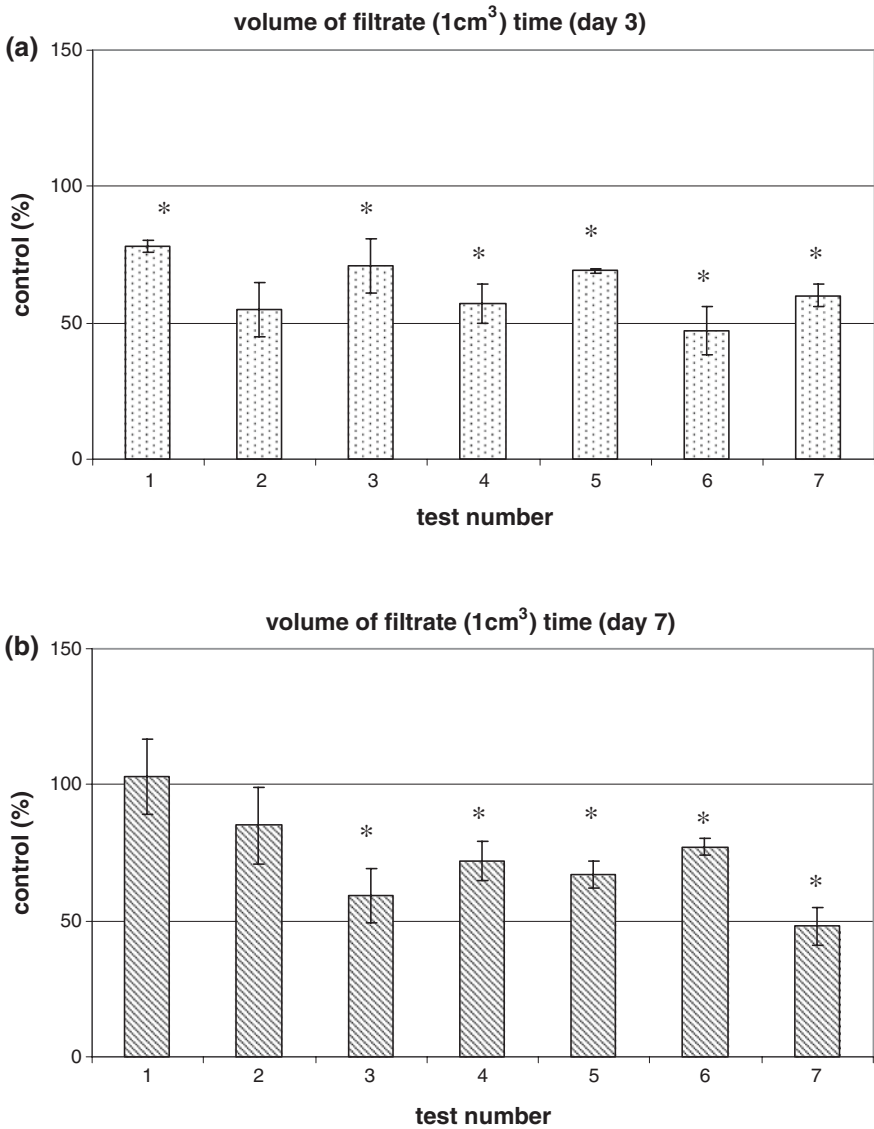


Fig. 1 The influence of *M. aeruginosa* cell-free filtrate (volume 1 cm³) on growth of *C. vulgaris* after: **a** 3 days, **b** 7 days, (1–7) experiment number. Data are given as mean cell number ± SD (n = 3). Asterisk statistical difference in comparison with control sample ($\alpha = 0.05$)

better comparison, results were presented as percentage of control. The most common effect of cyanobacterial metabolites observed in all tests was growth inhibition of target species cells, but slightly positive influence on growth was also observed in some cases. In a few samples, added filtrate had no influence on microalgae growth. After 3 days of the test *C. vulgaris* growth in variant with 1 cm³ volume

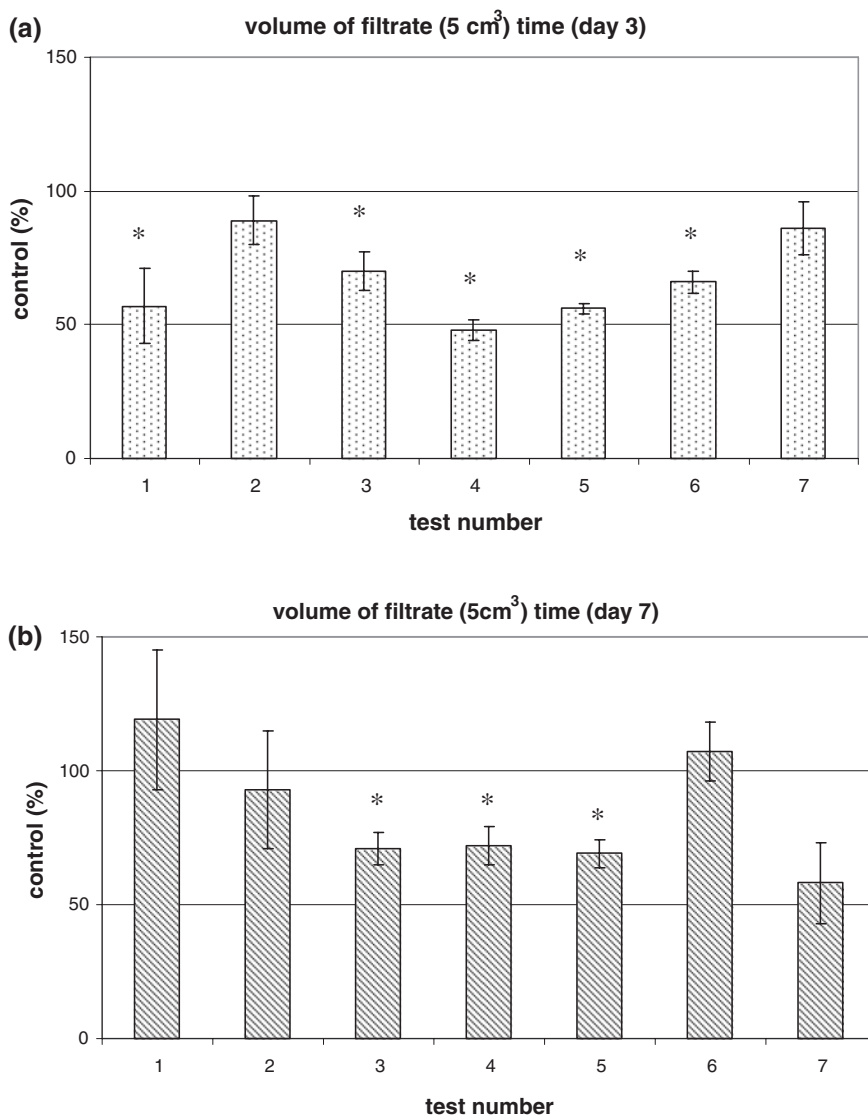


Fig. 2 The influence of *M. aeruginosa* cell-free filtrate (volume 5 cm³) on growth of *C. vulgaris* after: **a** 3 days, **b** 7 days, (1–7) experiment number. Data are given as mean cell number \pm SD (n = 3). Asterisk statistical difference in comparison with control sample ($\alpha = 0.05$)

of filtrate was inhibited from 22 % (no. 1) to 53 % (no. 6). In test no. 2 we noticed 45 % inhibition of growth; however this result was statistically insignificant, the overall trend was similar. After 7 days at the end of experiment, growth inhibition in flasks with 1 cm³ volume of filtrate ranged from 23 % (no. 6) to 52 % (no. 7).

In the test no. 2, growth was inhibited by 15 % but this result was statistically insignificant. In test no. 1 growth of *C. vulgaris* remained on control samples level (103 % of control). Similar results were obtained in second variant of experiment, with 5 cm³ volume of filtrate. After 3 days, growth stimulation was not observed. In tests number 2 and 7 the decrease in cells number was observed compared to control by 11 and 14 % but this results were not significant statistically. Growth inhibition after 3 days was noticed in 5 tests and ranged from 30 % (no. 3) to 52 % (no. 4). After 7 days slight positive effect was observed in test no. 1 (stimulation by 19 %) and test no. 6 (stimulation by 7 %), though both results were not significant. Although negative influence was observed in tests 2 and 7 (7 and 42 % reduction of growth) it was statistically insignificant. In three test (3, 4, 5) inhibition of growth by 28–31 % compared to the control samples was observed.

Summarizing, average influence of cell-free filtrate containing cyanobacterial extracellular secretion on green algae growth was negative. Mean inhibition of growth from all results ranged from 16 % after 7 days in variant with 5 cm³ volume of filtrate to 38 % after 3 days in variant with 1 cm³ volume of filtrate.

3.2 Viability of *C. vulgaris* Cells

The influence of *M. aeruginosa* metabolites on *C. vulgaris* viability was not observed in experiments with cell-free filtrates. Also in cocultures, negative effect on target cells viability was not reported. In experiments only single cells stained with dye were observed.

3.3 Effect of *Microcystis aeruginosa* Living Cells on *Chlorella vulgaris* Cultures

The influence of *M. aeruginosa* living cells on the growth of *C. vulgaris* (cocultures) is presented in Fig. 3. The initial density of target species was 10⁵ or 10⁶ cells cm⁻³. In the majority of cases, a negative impact of living cyanobacterial cells on the growth of green algae was observed. In cocultures, the observed influence of cyanobacteria on microalgae was similar as in experiments with cell-free filtrates. Moreover, stimulation of growth was not observed in cocultures, and results from only one test (no. 5) were statistically insignificant. After 3 days reduction of growth ranged from 27 % (no. 4) to 44 % (no. 2). Overall trend after 7 days was alike. Observed reduction of growth ranged from 19 % (no. 3) to 40 % (no. 2).

Average impact of cyanobacterial cells on *C. vulgaris* cells in cocultures was negative. Mean growth reduction of green algae cells in cocultures was 32 % after 3 days and 29 % after 7 days.

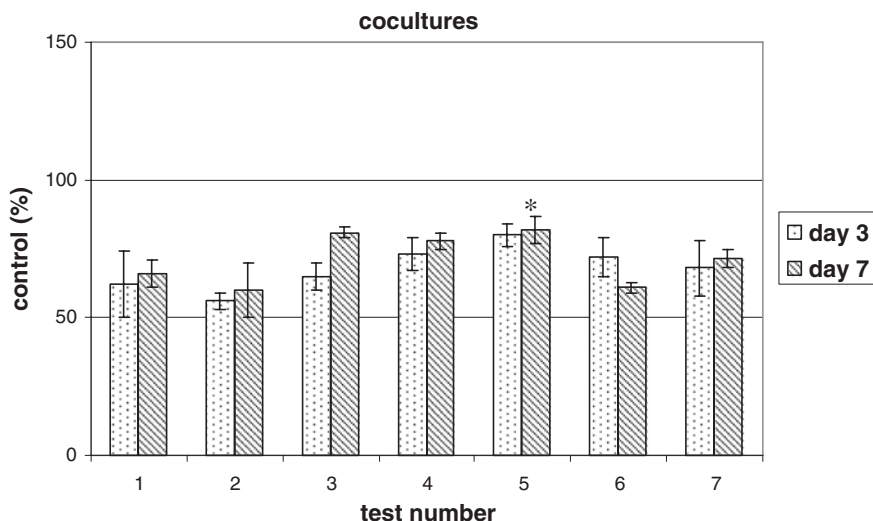


Fig. 3 The influence of *M. aeruginosa* living cells on growth of *C. vulgaris* after 3 and 7 days (cocultures), (1–6) experiment number. Data are given as mean cell number \pm SD ($n = 3$). Asterisk statistically insignificant in comparison with control sample ($\alpha = 0.05$)

4 Discussion

Cyanobacteria from *Microcystis* genera could produce hepatotoxins potentially harmful for animals and humans due to their negative influence on liver cells (Kaebernick and Neilan 2001). Several reports about negative influence of microcystins on phytoplankton species from different taxa have been found in the scientific literature. Hu et al. (2004, 2005) observed negative impact of microcystins on the cyanobacterium *Synechococcus elongatus*. Growth inhibition of target cyanobacteria and green algae, induced by toxins produced by *Microcystis* sp. was also noticed in experiments conducted by Singh et al. (2001) and Babica et al. (2007). Negative influence of microcystins and cell-free medium on target species dinoflagellate *Peridinium gatunense* was also described by Sukenik et al. (2002). In our experiments allelopathic influence of cyanobacteria *Microcystis aeruginosa* PCC7820 on green algae *Chlorella vulgaris* A1-76 was demonstrated. Allelopathic influence was observed in two kinds of experiments: with cell-free filtrates obtained from cyanobacterial cultures and cocultures. In the majority of results, growth inhibition of target species was noted. Similar negative effects were observed in the experiments with filtrate added in volume of 1 and 5 cm³. However, in a few tests a positive effect of cyanobacterial metabolites on growth of green algae was noticed it was statistically insignificant. Growth stimulation of target species (correlated with oxidative stress) induced by microcystins was

previously reported by Ou et al. (2005). It is possible that changes in bioactive compounds concentration in cyanobacterial cultures might induce different reactions of target species. Positive effects observed in our experiments were not statistically significant so we can treat them as “no influence” samples. On the other hand, positive influence of *M. aeruginosa* on *C. vulgaris* was not observed in cocultures experiments. Growth inhibition caused by living cyanobacterial cells was similar compared to experiments with cell-free filtrates containing cyanobacterial compounds. This effect was expected it to be clearly stronger as we described this trend in our previous experiments with influence of *Anabaena variabilis* and *Nodularia spumigena* on *Chlorella vulgaris* cells. Both tested cyanobacterial species caused reduction of target species in cocultures and in batch cultures. Negative influence on growth of target algae was stronger in cocultures than in experiments with cell-free filtrates (Žak et al. 2012). One of the reasons of this phenomenon could be continuous bioactive compounds production and release to culture medium. In this work, the observed impact of *M. aeruginosa* cells and cell-free filtrates on green algae cells was congruent (average growth reduction in cell-free filtrates by 28 % and in co-cultures by 31 %). In this work the influence of cyanobacterial metabolites on green algae viability or morphology was not observed. Similar observations were made in our previous work. It is possible that compounds produced by tested organisms do not cause cell death. Their negative influence on other organisms regardless of mode of action results in general inhibition of growth. As it was mentioned before, it is one of the most frequently observed allelopathic effects. Allelopathic effects described in this work could be induced by microcystins or other bioactive compounds produced by *M. aeruginosa*. According to the literature, most of allelochemicals are not identified and are referred to as unknown with influence on target organism description only. In order to investigate the type of bioactive compounds causing allelopathy and to explain the mechanisms of this influence and mode or modes of action of these compounds, more studies need to be done.

In conclusion, negative allelopathic effects of extracellular compounds produced by *M. aeruginosa* towards *C. vulgaris* were observed in this work. It is possible that allelopathy could be one of the factors allowing better competition in environment for species producing bioactive compounds.

Acknowledgments The study was partially supported by the Polish State Committee for Scientific Research (grant No. N N306 214137) and by the statutory programme of the Institute of Oceanology, PAS (grant No. II.3).

References

- Babica P, Hilscherová K, Bártová K, Bláha L, Maršálek B (2007) Effects of dissolved microcystins on growth of planktonic photoautotrophs. *Phycologia* 46:137–142
- Bhagavathy S, Sumathi P, Jancy Sherene Bell I (2011) Green algae *Chlorococcum humicola* – a new source of bioactive compounds with antimicrobial activity. *Asian Pac J Trop Biomed* S1–S7

- Bischoff HW, Bold HC (1963) Phycological studies IV. Some soil algae from enchanted rock and related algal species, vol 6318. University of Texas Publishing, pp 1–95
- Cembella A (2003) Chemical ecology of eukaryotic microalgae in marine ecosystems. *Phycologia* 42:420–447
- Fergola P, Cerasuolo M, Pollio A, Pinto G, DellaGreca M (2007) Allelopathy and competition between *Chlorella vulgaris* and *Pseudokirchneriella subcapitata*: experiments and mathematical model. *Ecol Model* 208:205–214
- Fistarol GO, Legrand C, Selander E, Hummert C, Stolte W, Graneli E (2004) Allelopathy in *Alexandrium* spp.: effect on a natural plankton community and algal monocultures. *Aquat Microb Ecol* 35:45–56
- Gantar M, Berry JP, Thomas S, Wang M, Perez R, Rein KS, King G (2008) Allelopathic activity among *Cyanobacteria* and microalgae isolated from Florida freshwater habitats. *FEMS Microbiol Ecol* 64(1):55–64
- Graneli E, Weberg M, Salomon PS (2008) Harmful algal blooms of allelopathic microalgal species: the role of Eutrophication. *Harmful Algae* 8:94–102
- Gross EM (2003) Allelopathy of aquatic autotrophs. *Crit Rev Plant Sci* 22:313–339
- Hu Z, Liu Y, Li D (2004) Physiological and biochemical analyses of microcystin-RR toxicity to the cyanobacterium *Synechococcus elongatus*. *Environ Toxicol* 19:571–577
- Hu Z, Liu Y, Li D, Dauta A (2005) Growth and antioxidant system of the cyanobacterium *Synechococcus elongatus* in response to microcystin-RR. *Hydrobiologia* 534:23–29
- Kaebnick M, Neilan BA (2001) Ecological and molecular investigations of cyanotoxin production. *FEMS Microbiol Ecol* 35:1–9
- Legrand C, Reigefors K, Fistarol GO, Graneli E (2003) Allelopathy in phytoplankton—biochemical, ecological and evolutionary aspects. *Phycologia* 42:406–419
- Maso M, Garces E (2006) Harmful microalgae blooms (HAB); problematic and conditions that induce them. *Mar Pollut Bull* 53:620–630
- Mulderij G, Mooij WM, Smolders AJP, Van Donk E (2005) Allelopathic inhibition of phytoplankton by exudates from *Stratiotes aloides*. *Aquat Bot* 82:284–296
- Ou D, Song L, Gan N, Chen W (2005) Effects of microcystins on and toxin degradation by *Poteriomonas* sp. *Environ Toxicol* 20:373–380
- Qian H, Xu X, Chen W, Jiang H, Jin Y, Liu W, Fu Z (2009) Allelochemical stress causes oxidative damage and inhibition of photosynthesis in *Chlorella vulgaris*. *Chemosphere*. doi:10.1016/j.chemosphere.2008.12.040
- Singh DP, Tyagi MB, Kumar A, Thakur JK, Kumar A (2001) Antialgal activity of a hepatotoxin-producing cyanobacterium, *Microcystis aeruginosa*. *World J Microbiol Biotechnol* 17:15–22
- Sukenik A, Eskhel R, Livne A, Hadas O, Rom M, Tchernov D, Vardi A, Kaplan A (2002) Inhibition of growth and photosynthesis of the dinoflagellate *Peridinium gatunense* by *Microcystis* sp. (cyanobacteria): a novel Allelopathic mechanism. *Limnol Oceanogr* 47(6):1656–1663
- Svircev Z, Cetojevic-Simin D, Simeunovic J, Karaman M, Stojanovic D (2008) Antibacterial, antifungal and cytotoxic activity of terrestrial cyanobacterial strains from Serbia. *Sci China Ser C Life Sci* 51(10):941–947
- Tillmann U, Alpermann T, John U, Cembella A (2008) Allelochemical interactions and short-term effects of the dinoflagellate *Alexandrium* on selected photoautotrophic and heterotrophic protists. *Harmful Algae* 7:52–64
- Tuney U, Cadirci HB, Unal D, Sukatar A (2006) Antimicrobial activities of the extracts of marine algae from the coast of Urla (Üzmir, Turkey) *Turk. J Biol* 30:171–175
- Weir TL, Park SW, Vivanco JM (2004) Biochemical and physiological mechanisms mediated by allelochemicals. *Curr Opin Plant Biol* 7:472–479
- Żak A, Musiewicz K, Kosakowska A (2012) Allelopathic activity of the Baltic cyanobacteria against microalgae. *Estuar Coast Shelf Sci*. doi:10.1016/j.ecss.2011.10.007